The Development of Vascularised 3D Tissue Engineering Constructs

Philip James Booth

Submitted in accordance with the requirements for the degree of Doctor of Philosophy

The University of Leeds

Faculty of Engineering

Institute of Medical and Biological Engineering

October 2024

Declaration

The candidate confirms that the work submitted is his own and that appropriate credit has been given where reference has been made to the work of others.

This copy has been supplied on the understanding that it is copyright material and that no quotation from the thesis may be published without proper acknowledgement. The right of Philip James Booth to be identified as Author of this work has been asserted by him in accordance with the Copyright, Designs and Patents Act 1988.

Acknowledgement

Firstly, I would like to say thank you to my supervisors Dr Xuebin Yang and Dr Robert Davies for your time and support during my PhD studies.

I would also like to express my thanks to the members of Oral Biology where this research was completed for your support during my time working in the lab. I'd like to express particular gratitude to Dr Sandeep Kumar, Dr Neelam Iqbal and Dr Tom Braxton for the banter in the lab that made the long weeks more enjoyable.

I'd also like to thank the EPSRC for funding my PhD and making it possible to pursue this research.

Finally, of everyone, I'd like to thank my family and friends the most. You have all been an ever-present source of encouragement and support throughout my life and studies and I wouldn't have made it without you. In particular, I would like to thank my wife, Laura. You have been by my side since starting my undergraduate degree and have made it possible for me to get this far.

Abstract

Despite significant advances in tissue engineering, the translation of these developments to clinical applications is limited. One of the major reasons that this is the case is that it is currently not possible to create engineered tissues which are vascularised suitable for transplantation. Vasculature is essential for the development of clinically relevant engineered tissues to facilitate the mass transport of oxygen and nutrients to cells within the tissue and removal of waste products. Furthermore, vasculature is essential for the integration of the tissue into the hosts circulatory system during transplantation to ensure the survival of the transplant. Current vascularisation strategies have been met with limited success with two of the key challenges being identifying an optimal cell source for the formation of vasculature and a scaffold material for supporting vascular growth.

This study set out to explore the potential of dental pulp stem cells (DPSCs) as an easily accessible adult mesenchymal stem cell with the potential for endothelial differentiation. Additionally, the self-assembling peptide P_{11}-4 was investigated as a possible scaffold material to support vascularisation due to its tuneable properties which allow it to be used in mimicking the extracellular matrix of several tissues.

DPSCs were induced to differentiate into an endothelial phenotype using endothelial cell culture media containing a number of essential growth factors required for endothelial cell function and survival. Endothelial differentiation was confirmed by the significant increase in the expression of endothelial markers CD31 and VEGFR2 at both the gene and protein expression level after 5 and 10 days of differentiation. Furthermore, differentiated cells demonstrated endothelial-like cell function during Matrigel tube formation assays, forming cellular networks comparable to those of human umbilical vein endothelial cells (HUVEC).

Optimised P_{11}-4 hydrogels were able to support HUVEC network formation in 3D culture, however endothelial-like cells derived from DPSCs did not interact with the gel in a comparable way.

This study provides evidence for the first time that P_{11}-4 possesses proangiogenic properties and has the capacity to support vascular like growth, though further modifications to the peptide are needed to improve its suitability for clinical applications. This research also confirms reports in other research that DPSCs have the potential to differentiate into endothelial-like cells, though improvements are needed to optimise their function for the creation of vascularised 3D tissue engineering constructs.

Table of Contents

List of Figures 11

List of Tables 15

Chapter 1 Literature Review 16

Introduction 16

Section 1: Vasculature and *in vivo* Vascular Development 18

1.1.1 *In vivo* vasculature 18

1.1.2 *In vivo* Vascular Development 19

1.1.3 Vasculogenesis 19

1.1.4 Angiogenesis 20

1.1.5 Endothelial Cell Activation and Tip/Stalk Cell Specialisation Through the VEGF and Notch Signalling Pathways 21

Section 2: Cells and Growth Factors in Vascular Engineering 25

1.2.1 Requirements of an *in vitro* engineered functional vascular network 26

1.2.2. Cells for vascular engineering 26

1.2.3. Endothelial progenitor cells (EPCs) 27

1.2.4. Autologous Adult Stem Cells 28

1.2.4.1 Bone marrow stem cells (BM-MSCs) and Adipose-derived stem cells (AD-MSCs) 28

1.2.4.2 Dental pulp stem cells (DPSCs) 30

1.2.5. Endothelial Differentiation of Stem Cells 32

1.2.5.1 VEGF in the Endothelial Differentiation of Stem Cells 33

1.2.5.2 Fibroblastic Growth Factor in the Endothelial Differentiation of Stem Cells 34

Section 3: Biomaterials in Vascular Engineering 36

1.3.1 Biomaterials in Vascular Engineering 37

1.3.2 Hydrogels 38

1.3.3 Natural Hydrogel Polymers 39

1.3.3.1 Fibrin 39

1.3.3.2 Collagen 40
1.3.4 Self-assembling Peptides 41
1.3.4.1 P_{11}-X Self-assembling Peptide Library 42
P_{11}-X library general structure 42
Concentration dependent self-assembly of P_{11}-X SAPs 44
pH triggered self-assembly of P_{11}-X SAPs 45
External Factors affecting self-assembly of P_{11}-X peptides 45
1.3.4.2 P_{11}-X Self-assembling Peptides in Tissue Engineering 47
1.3.4.3 P_{11}-4 in Tissue Engineering 48
2.0 Aims and Objectives 49
3. Materials and Methods 50
Materials 50
Consumables 50
Chemical reagents and kits 51
Equipment 52
Methods 53
3.1 Tissue Culture Methods 53
3.1.0 Standard practices and culture media 53
3.1.1 Recovery of cells after cryopreservation 54
3.1.2 Cell passage 54
3.1.3 Cell Counting 56
3.1.4 Cryopreservation and long-term storage 57
3.1.5 Endothelial differentiation of hDPSCs 57
3.1.6 Matrigel tube formation assays and analysis 58
3.2 Molecular Biology Methods 62
3.2.1 RNA extraction 62
3.2.2 RT-PCR 64
3.2.3 Quantitative Polymerase Chain Reaction (qPCR) 65
3.2.4 qPCR data analysis using the (delta-delta Ct method) 66
3.3 Fluorescent labelling and imaging methods 66
3.3.1 Immunofluorescent staining 66
3.3.2 Cell Viability/Live Cell Fluorescent Labelling 68

3.3.3 Confocal Microscopy and Image Analysis 69
3.3.4 Light Microscopy (Phase Contrast) 73
3.4 Hydrogel related methods 74
3.4.1 Preparation of pH indicator standard series in tissue culture media 74
3.4.2 P_{11}-4 Hydrogel Preparation 76
3.4.3 Rheological Analysis 76
3.4.4 2D P_{11}-4 hydrogel surface attachment 77
3.4.5 Fibronectin surface coating of P_{11}-4 hydrogels 77
3.4.6 Preparation of $P_{11\text{-}4}$ gels for 3D cell culture 78
3.4.7 Agarose encapsulated P_{11}-4 gels for 3D cell culture 78
3.4.8 Cytotoxicity testing of P_{11}-4 on HUVEC monolayers 79
3.5 Statistical Analysis 80
Chapter 4: Endothelial Differentiation of Dental Pulp Stem Cells 81
4.1 Introduction 81
4.2 Aims and Objectives 82
4.3 Results 83
4.3.1 Relative change in VEGFR2 and CD31 gene expression levels of hDPSCs after 5 and 10 days of endothelial differentiation 83
4.3.2 Effect of endothelial differentiation treatment on the expression of CD31 and VEGFR2 by DPSCs 85
4.3.3 Assessment of endothelial differentiated DPSCs to form vascular-like structures during Matrigel tube formation assays 89
4.3.4 Comparative analysis of the network forming ability of endothelial differentiated DPSCs 93
4.4 Discussion 95
4.4.1 Endothelial gene and protein expression after treatment with endothelial differentiation media 95
4.4.2 Endothelial differentiation of DPSCs results in cells with comparable endothelial cell function to HUVECs as measured by *in vitro* tube formation assay 100
4.5 Conclusion 102
4.6 Future Research 103

5.1 Introduction 104
5.2 Results 108
5.2.1 Rheological Characterisation of P_{11}-4 hydrogels at different concentrations 108
5.2.2 2D cell culture on 10 mg/mL P_{11}-4 gels 112
5.2.3 3D cell culture within 10 mg/mL P_{11}-4 gels 116
5.2.4 Effect of Fibronectin Coating on HUVEC Adhesion to P_{11}-4 Hydrogels 120
5.2.5 3D culture of HUVECs and DPSCs within agarose encapsulated P_{11}-4 hydrogels 121
5.2.6 Assessment of HUVEC Surface Adhesion After Exposure to P_{11}-4 125
5.2.7 2D culture of HUVECs on low concentration P_{11}-4 hydrogels 127
5.2.8 3D culture of HUVECs in 2.5 mg/mL P_{11}-4 hydrogels 129
5.2.9 3D culture of differentiated DPSCs in 2.5 mg/mL P_{11}-4 hydrogels 131
5.3 Discussion 133
5.3.2 Peptide concentration selection based on hydrogel stiffness .. 134
5.3.3 Biocompatibility of P_{11}-4 and Cell Attachment 136
5.3.4 Low P_{11}-4 peptide concentration facilitates HUVEC attachment and spreading 137
5.4 Conclusions and future work 140
Chapter 6: General Discussion 142
6.1 Dental Pulp Stem Cells for Vascular Engineering 142
6.2 Mechanical Sensitivity of P11-4 hydrogels 145
6.3 P_{11}-4 and the Creation of Vascularised Tissue Engineering Constructs 146
6.4 Lessons from P_{11}-4 Hydrogels 147
Chapter 7: Future Work 149
7.1 Improving Endothelial Differentiation of DPSCs and Analysis of Differentiation 149
7.2 Investigating Endothelial Cell Function on P_{11}-4 Hydrogels and P_{11}-X Design 150
7.3 Advancing P_{11}-4 Hydrogels as Tissue Engineering Scaffolds *in vitro* 151

Chapter 8: Conclusion 151
Chapter 9: References 152

List of Figures

Figure 1 – A) Phase contrast image example provided within the 'Angiogenesis Analyzer' plugin. B) Coloured schematic of network components measured by the 'Angiogenesis ~analyzer' plugin. A description of each component can be found in Table 5. 60
Figure 2 pH standards created using a-MEM between a pH range of 6.0 to 8.4. 75
Figure 3 - Fold change in expression of VEGFR2 and CD31 by DPSCs after 5 and 10 days of endothelial differentiation relative to untreated cells, normalised to GAPDH. Expression studies were performed with technical triplicates in each experiment and were repeated three times for each time point. Statistical analysis was performed using Student's t-test. NS – Non-Significant, *** = P< 0.001. Error bars represent mean ± standard deviation. 84
Figure 4 A) Representative images of VEGFR2 immunofluorescent staining after 5 and 10 days of endothelial differentiation. The images on the left show the staining of untreated control cells after 5 (top) and 10 (bottom) days and the images on the right show the same for differentiated cells. B) Graph showing the relative increase in corrected total cell fluorescence for VEGFR2 staining relative to controls after 5 and 10 days of endothelial differentiation. Error bars represent mean ± standard deviation. For each time point, experiments were performed with technical triplicates and experiments were repeated three times. Error bars represent mean ± standard deviation. Statistical analysis was performed using Students t-test. * = P < 0.05. 86
Figure 5 A) Representative images of CD31 immunofluorescent staining after 5 and 10 days of endothelial differentiation. The images on the left show the staining of untreated control cells after 5 (top) and 10 (bottom) days and the images on the right show the same for differentiated cells. B) Graph showing the relative increase in corrected total cell fluorescence for CD31 staining relative to controls after 5 and 10 days of endothelial differentiation. Error bars represent mean ± standard deviation. . For each time point, experiments were performed with technical triplicates and experiments were repeated three times. Error bars represent mean ± standard deviation. Statistical analysis was performed using Students t-test. *** = P < 0.001. 88
Figure 6 - Phase contrast images of Matrigel tube formation assays performed after 5 days of endothelial differentiation with HUVECs (left), Basal media (centre) and endothelial differentiation media (right) collected after 2, 4, 6 and 24 hours of culture. Each experiment was performed in triplicate using cells as described in Section 3.1.0. 90
Figure 7 Phase contrast images of Matrigel tube formation assays performed after 10 days of endothelial differentiation with HUVECs (left), Basal media (centre) and endothelial differentiation media (right) collected after 2, 4, 6 and

24 hours of culture. Each experiment was performed in triplicate using cells as explained in Section 3.1.0. 92
Figure 8 - Quantification of network formation in Matrigel tube formation assays comparing DPSCs differentiated for 5 or 10 days to HUVEC cells. Error bars represent standard deviation. Experiments were conducted in triplicate and were performed three times for each group as per Section 3.1.0. Statistical analysis was performed using GraphPad Prism as described in Section 3.5. ... 94
Figure 9 Amplitude sweep graphs obtained from 20, 10, 5 and 2.5 mg/mL P_{11-4} gels at 1 and 20 Hz. A shear strain rate of 0.1% was determined to be in the linear viscoelastic region (LVER) for the gels with a concentration of 20, 10 and 5 mg/mL. It was not possible to determine a LVER for the 2.5 mg/mL concentration gel due to wall slip. The amplitude sweeps were performed in triplicate for each concentration to determine the LVER. Error bars represent standard error of the mean. 109
Figure 10 Frequency sweeps performed on 20, 10, 5 and 2.5 mg/mL P_{11-4} gels at a strain rate of 0.1%. The storage modulus of the 20 mg/mL gel was found to be the highest. The storage modulus then reduced in a non-linear fashion as the gel concentration was reduced by 50%. Error bars represent the standard error of the mean. 111
Figure 11 - Maximum intensity Z-stack projection of 2D cell culture of HUVECs (left) and DPSCs (right) on the surface of 10 mg/mL P11-4 gels after 24 hours of culture. Live cells are stained green using Calcein AM. Dead cells stained red with Ethidium Homodimer-1 are difficult to identify due to the intense red fluorescent signal produced by P11-4. HUVECs display a non-adherent circular cell morphology (left: white arrow heads) whereas several DPSCs have attached to the gel and spread out on the surface of the gel (right: white arrows). Experiments were performed in biological triplicates with technical replicates. 112
Figure 12 – Graphs comparing the analysis of cell area, cell perimeter and circularity of HUVECs and DPSCs growing on 10 mg/mL P_{11}-4 gels. The graphs demonstrate the unattached cell phenotype of HUVECs having a cell area and perimeter which is significantly lower than DPSCs whilst having a circularity measure close to that of a perfect circle. Error bars represent standard deviation. Statistical analysis was performed using unpaired t-test. *** P-value <0.001. 113
Figure 13 Maximum intensity Z-stack projection of HUVECs (left) and DPSCs (right) growing on the surface of 10 mg/mL P11-4 gels after 48 hours of cell culture. HUVECs largely express a non-adherent cell morphology though processes emanating from cells (white arrows) may indicate attempts to interact with the surface of the gel. DPSCs were found to have attached to the

surface of the gel and spread. Experiments were performed in biological triplicates with technical replicates. 115
Figure 14 Z-stack montage of HUVECs (left) and DPSCs (right) cultured for 24 hours in 10 mg/mL P11-4 hydrogels. Samples were stained with Live/Dead staining prior to imaging which label viable cells as green and dead cells as red. Due to the fluorescent signal produced by P11-4 it is difficult to distinguish dead cells. Rows A, B and C correspond to the base of the gel, middle of the gel and top of the gel respectively. Images were captured at 10x magnification. Experiments were performed in biological triplicates with technical replicates. 117
Figure 15 Z-stack montage of HUVECs (left) and DPSCs (right) cultured for 48 hours in 10 mg/mL P11-4 hydrogels. Samples were stained with Live/Dead staining prior to imaging which label viable cells as green and dead cells as red. Due to the fluorescent signal produced by P11-4 it is difficult to distinguish dead cells. Rows A, B and C correspond to the base of the gel, middle of the gel and top of the gel respectively. Images were captured at 10x magnification. Experiments were performed in biological triplicates with technical replicates. 119
Figure 16 Maximum intensity Z-stack projections of HUVECs growing on P11-4 gels either uncoated (A) or coated with fibronectin (B). The cells cultured on the P11-4 gel without fibronectin maintained a non-adherent cell morphology whereas the HUVECs cultured on the fibronectin coated gel display a high degree of attachment and spreading. Experiments were performed in biological triplicates with technical replicates. 120
Figure 17 Z-stack montage of HUVECs (left) and DPSCs (right) growing within 10 mg/mL P11-4 gels encapsulated within 0.5% agarose gels for 24 hours. HUVECs show no obvious sign of attachment to the gel maintaining a rounded cell morphology whereas DPSCs display a high degree of attachment and spreading. Samples were stained with Live/Dead staining prior to imaging which label viable cells as green and dead cells as red. Due to the fluorescent signal produced by P11-4 it is difficult to distinguish dead cells. Rows A, B and C correspond to the base of the gel, middle of the gel and top of the gel respectively. Images were captured at 10x magnification. Experiments were performed in biological triplicates with technical replicates. 122
Figure 18 Z-stack montage of HUVECs (left) and DPSCs (right) growing within 10 mg/mL P11-4 gels encapsulated within 0.5% agarose gels for 7 days. HUVECs show no obvious sign of attachment to the gel maintaining a rounded cell morphology whereas DPSCs have proliferated within the gel to form a densely cellularised construct. Samples were stained with Live/Dead staining prior to imaging which label viable cells as green and dead cells as red. Due to the fluorescent signal produced by P11-4 it is difficult to distinguish dead cells.

Rows A, B and C correspond to the base of the gel, middle of the gel and top of the gel respectively. Images were captured at 10x magnification. Experiments were performed in biological triplicates with technical replicates. 124
Figure 19 Max intensity projections displaying confluent HUVEC monolayers treated with different concentrations of P11-4 gel. Treatment with 10 and 5 mg/mL concentration gels did not appear to impact the ability of HUVECs to adhere to the surface of tissue culture plastic. Treatment with 2.5 mg/mL however appears to alter the general arrangement of cells and some cells can be seen to be interacting directly with the gel (white arrows, D). Experiments were performed in biological triplicates with technical replicates. 126
Figure 20 Maximum intensity Z-stack projections of HUVECs (green) growing on 10 mg/mL (top), 5 mg/mL (centre) and 2.5 mg/mL (bottom) P11-4 gels after 24 hours of cell culture. HUVECs cultured on the surface of the 10 mg/mL and 5 mg/mL gels exhibit a non-adherent cell morphology whereas HUVECs growing on 2.5 mg/mL gels display a high degree of attachment and spreading on its surface. Experiments were performed in biological triplicates with technical replicates. 128
Figure 21 Z-stack montages of HUVECs cultured for 24h (left) and 48h (right) growing within 3D 2.5 mg/mL P11-4 gels. After 24h, HUVECs formed continuous cellular networks throughout the P11-4 gels. After 48h of culture, these structures had collapsed, similar to the process seen network collapse during Matrigel tube formation assays after 24 hours. Samples were stained with Live/Dead staining prior to imaging which label viable cells as green and dead cells as red. Due to the fluorescent signal produced by P11-4 it is difficult to distinguish dead cells. Rows A, B and C correspond to the base of the gel, middle of the gel and top of the gel respectively. Images were captured at 10x magnification. Experiments were performed in biological triplicates with technical replicates. 130
Figure 22 Z-stack montages of HUVECs (left), undifferentiated DPSCs (center) and DPSCs which had undergone 10 days of endothelial differentiation (right) growing in 3D 2.5 mg/mL P11-4 hydrogels for 24 hours. HUVECs formed attached to the gel and formed continuous cellular networks after this time period. Undifferentiated DPSCs interacted with the gel and were able to attach and spread on its surface and were arranged in a random fashion on the gel surface. Differentiated DPSCs demonstrated the same morphology and did not form networks. Samples were stained with Live/Dead staining prior to imaging which label viable cells as green and dead cells as red. Due to the fluorescent signal produced by P11-4 it is difficult to distinguish dead cells. Rows A, B and C correspond to the base of the gel, middle of the gel and top of the gel respectively. Experiments were performed in biological triplicates with technical replicates. 132

List of Tables

Table 1 Primary structure of two members of the P_{11}-X library, P_{11}-4 and P_{11}-8 . 43
Table 2 List of laboratory consumables used throughout this research 50
Table 3 List of chemical reagents and kits used throughout the research presented in this thesis 51
Table 4 List of equipment used to perform experiments in this study 52
Table 5 - Key of coloured components displayed in Figure 1.B. using the 'Angiogenesis Analyzer' plugin 60
Table 6 Measurements collected using the Angiogenesis Analyzer plugin and the rationale for each measurement 61
Table 7 Components and volumes used to prepare RNA-to-cDNA mixtures 64
Table 8 Components and volumes used to prepare qPCR reactions 65
Table 9 - Excitation and emission wavelengths used to image fluorophores in confocal microscopy 69
Table 10 Components of differentiation media used by research investigating the endothelial differentiation of DPSCs 98
Table 11 Examples of hydrogel stiffnesses that have been shown to support vascularisation in vitro and in vivo 106

Chapter 1 Literature Review

Introduction

The development of cell culture techniques at the beginning of the 20th century and the following century of improvements allows scientists from a wide range of fields to cultivate a diverse range of cell types outside of the body ranging from embryonic stem cells (Desai et al., 2015) to functional cardiomyocytes that can mimic the pulsatile behaviour of native cardiac tissue (Hayashi et al., 2017). This has allowed scientists to study biological processes at a molecular level as well as providing a platform to produce therapeutic tools such as vaccine development (Kumar et al., 2021). In addition to its many other uses, the ability to culture cells in the laboratory as well as the clinical need for cell-based therapies has also led to the creation of the multidisciplinary field of tissue engineering (TE) and regenerative medicine.

TE integrates many branches of biology, chemistry and physics with the overarching goal of fabricating transplantable tissues and organs to repair or replace those damaged or diseased in patients. To do this, many strategies have been developed which often require the combination of both the cellular components of the required tissue or organ and also biocompatible materials which mimic the extracellular matrix (ECM) to act as a scaffold (Sohn et al., 2020).

Despite many advances in TE, the ability to fabricate tissues of a clinically relevant size still, for the most part, eludes scientists as it is not currently possible to vascularise engineered tissues adequately to provide oxygen and nutrients to cells beyond a diffusion limit of approximately 250 μm in cell-rich tissues (Vajda et al., 2021). Through employing equipment and methods such as bioreactors, it has been possible to create tissues of a thickness greater than 250 μm (Gensler et al., 2024), however, due to the lack of vasculature, the majority of cells perish after transplantation due to the inability to join the grafted tissue to the host's vasculature and nourish the cells (Lim et al., 2022).

As such, the development of techniques to incorporate vasculature within engineered tissues will be necessary for their translation to the clinic (Song et al., 2018).

Section 1: Vasculature and *in vivo* Vascular Development

1.1.1 *In vivo* vasculature

The cardiovascular system (CVS) has a hierarchal structure of blood vessels composed of afferent and efferent blood vessels. The afferent portion of the CVS is formed from arteries that carry oxygenated blood away from the heart to the body, arterioles that modulate blood flow into capillary beds and capillary beds which are the site of mass transport for the exchange of gas, nutrients and metabolic waste products. The efferent portion of the CVS then transports deoxygenated blood and waste products back towards the heart via venules which increase in size and transition to veins for recirculation (Slowey and Nyhan, 2022).

Each of these different vessels is essential for the correct functioning of the cardiovascular system and much research has been focussed on fabricating replacement vessels for grafts such as those used in coronary bypass surgery (Desai et al., 2011). However, in the pursuit of creating engineered tissues of a clinically relevant size, capillaries are perhaps the most important for two key reasons. Firstly, as the site at which mass transport occurs, the inclusion of capillaries in a vascularised construct is essential as without them tissues cannot be grown to a clinically relevant size as outlined above. Secondly, capillaries are the precursor to all other blood vessels in the body (Alberts et al., 2002) and therefore if capillary beds can be grown into engineered tissues, methodologies could be developed to form the other necessary vessels of the vascular tree with arterioles and venules being of particular importance to allow the joining of the graft-host vasculature.

1.1.2 *In vivo* Vascular Development

Two processes exist by which vasculature develops in the body, vasculogenesis and angiogenesis (Naito et al., 2020). Vasculogenesis is the *de novo* formation of blood vessels from precursor cells which happens almost entirely in the early embryo and establishes a network of blood vessels to support the growth of the embryo (Goldie et al., 2008). Once this early network has been established, angiogenesis is the process which leads to the expansion of the length and number of blood vessels (from existing vasculature) to adequately supply the growing tissue with oxygen and nutrients (Carmeliet, 2003).

1.1.3 Vasculogenesis

Vasculogenesis occurs approximately 18 days after conception during the process of gastrulation (Wang and Zhao, 2010) which establishes the three germ layers, the ectoderm, mesoderm and endoderm which go on to differentiate into the different tissue types of the body (Ferretti and Hadjantonakis, 2019).

After the establishment of the three germ layers, a portion of mesodermal cells differentiate into hemangioblasts which are a precursor cell to both endothelial cell and haemopoietic cell lineages (Cao and Yao, 2011). These hemangioblasts then aggregate to form hemangioblastic aggregates which, after exposure to growth factors secreted by surrounding cells, differentiate into blood island aggregates (Traore and George, 2017). Within these blood island aggregates, two distinct cell populations exist; endothelial precursor cells (EPCs) occur at the outer extremities of the aggregates which give rise to endothelial cells and haemopoietic cells exist in the centre which give rise to blood cells (Traore and George, 2017). As blood islands mature during the differentiation of these cells, they anastomose and form the primary capillary plexus, a simple network of capillaries from which almost every blood vessel of the adult body can be traced back to (Traore and George, 2017).

1.1.4 Angiogenesis

To keep up with the energetic demands of the growing embryo and in all tissues during development and growth, the primary capillary network needs to expand to ensure that all cells are within approximately 200 µm of a capillary (Rouwkema and Khademhosseini, 2016). Two variations of angiogenesis occur to achieve this; intussusceptive angiogenesis where a pillar of endothelial cells is inserted to split the vessel(Mentzer and Konerding, 2014) and sprouting angiogenesis where cells in the wall of a blood vessel invade the surrounding tissue to create new vasculature(Ribatti and Crivellato, 2012) which is more well researched and understood.

Several growth factors and signalling pathways are implicated in sprouting angiogenesis and will be discussed further in section 1.1.5., however, two of the most well understood are the hypoxia-inducible factor (HIF) and vascular endothelial growth factor (VEGF) signalling pathways.

HIF is a family of transcription factors with the two most predominant HIF-α isoforms being HIF-1α and HIF-2α which dimerise with HIF-1β to exert their effect on angiogenesis (Semenza, 2012; Semenza, 2022; Yuan et al., 2023). HIF-1β is constitutively expressed by cells whilst HIF-α is continuously produced by cells at low levels and is degraded rapidly in the presence of adequate oxygen supply (normoxia) through its oxygen-dependent degradation domains (ODD) (Forristal et al., 2010).

Under normoxic conditions, proline residues (Pro402 or Pro564) in the ODD are hydroxylated by members of the prolyl hydroxylase domain (PHD) enzyme family which increases the affinity of the HIF-α subunit to the binding domain of the von Hippel-Lindau tumour suppressor (pVHL) (Gorres and Raines, 2010). Upon binding to pVHL, the HIF-α molecule is ubiquitinated which targets it for proteasomal degradation (Cockman et al., 2000). The tight regulation of this system prevents the overexpression of pro-angiogenic genes which in turn prevents the overgrowth of vasculature.

When cells experience hypoxic conditions such as when they exist beyond the diffusion limit of oxygen, the activity of PHD enzymes is inhibited as O_2 is required as a co-substrate which leads to the accumulation of HIF-α (Schofield and Ratcliffe, 2005). After accumulating, HIF-α is translocated to the nucleus where it dimerises with HIF-β which subsequently binds to hypoxia-responsive elements (HRE) on DNA leading to the transcription of over 100 genes implicated in the cellular response to hypoxia (Samanta et al., 2017). Out of these genes, the upregulation of VEGF is one of the greatest drivers of neovascularisation through the establishment of a diffusion gradient in tissues between cells experiencing hypoxia and surrounding vasculature (Vempati et al., 2014). The diffusion of VEGF leads to vascularisation through activation of endothelial cells in the wall of surrounding vessels (Shibuya and Claesson-Welsh, 2006a) which initiates the process of tip and stalk cell specialisation. After tip and stalk cell selection, VEGF also provides a path for the tip endothelial cells to follow towards the region of hypoxia.

1.1.5 Endothelial Cell Activation and Tip/Stalk Cell Specialisation Through the VEGF and Notch Signalling Pathways

There are two key signalling pathways responsible for normal sprouting angiogenesis with the first being the VEGF signalling pathway. The VEGF signalling pathway consists of three tyrosine kinase receptors (VEGF receptor-1, -2 and -3) and six growth factors (VEGF- A – E and placental growth factor (P1GF))(Apte et al., 2019). VEGFR-3 is primarily involved in blood vessel development during embryonic growth and in lymphatic endothelial cells(Shibuya and Claesson-Welsh, 2006b) whereas the ligand/receptor combination of VEGFR-2 and VEGF-A is the most important in the pro-angiogenic response to hypoxia (Wang et al., 2020a). The VEGFR-1 receptor has a relatively poorly understood role in angiogenesis though it is believed that due to its high affinity for VEGF-A and its low level of kinase activity, that it dampens the

response to pro-angiogenic signalling by limiting the amount of available VEGF binding to VEGFR-2(Shibuya, 2006; Cudmore et al., 2012).

The second pathway key to normal angiogenesis is the Notch signalling pathway. Unlike the VEGF signalling pathway, the Notch signalling is activated by ligands presented on neighbouring cells and functions as a contact-dependent signalling mechanism that regulates cell fate in many tissues (Shaya et al., 2017; Zhou et al., 2022). The Notch signalling pathway is composed of four Notch receptors (Notch 1-4) and five Notch transmembrane ligands (Delta-like ligand 1,2,3 and 4 (Dll1-Dll4), Jagged-1 and Jagged-2)(Bray, 2006; Zhou et al., 2022).

The interplay of these two pathways results in normal angiogenesis through activation of endothelial cells in quiescent vessels and directing these cells to specialise as either tip cells or stalk cells(Blanco and Gerhardt, 2013). Tip cells are the leading cells in angiogenesis and follow cues to migrate through tissues towards the site of hypoxia whereas the stalk cells follow the tip cell forming neo-vasculature(Blanco and Gerhardt, 2013).

The exact mechanism by which VEGF/Notch signalling leads to tip/stalk cell selection and angiogenesis is still unclear due to the intricate regulatory effects each pathway has on the other. However, in knockout studies it has been demonstrated that both are essential and inhibition of either one results in aberrant angiogenesis. It has been found that the homozygous knockout of either VEGF-A (Ferrara et al., 1996) or the VEGFRs (Baldwin et al., 2004) involved in the VEGF signalling pathway leads to embryonic lethality which is also true for members of the Notch signalling pathway such as Notch1 (Huppert et al., 2000; Ng et al., 2021) and Dll4 (Gale et al., 2004). This demonstrates that not only are both pathways essential for angiogenesis but that these signalling molecules are particularly essential.

The regulation of both signalling pathways has also been demonstrated to be key for normal angiogenesis in studies where either pathway is manipulated using pharmacological methods. Under normal circumstances, exposing endothelial cells in vessels to VEGF-A results in the formation of tip cells along the vessel

wall with extended filipodia. However, by sequestering VEGF-A through the use of soluble VEGFR-1 (sVEGFR-1) (Gerhardt et al., 2003) or by blocking VEGF-A/VEGFR-2 signalling through antibody inhibition of VEGFR-2 (Budd et al., 2009), filipodia do not extend from the tip cells which prevent the cell's migration along VEGF-A gradients. Whilst this demonstrates that activation of the VEGF signalling pathway through VEGF-A/VEGFR-2 binding gives rise to tip cells, the reason why all endothelial cells exposed to VEGF-A do not become tip cells is not explained using only the VEGF in isolation.

If all cells exposed to VEGF-A became tip cells, each endothelial cell along the wall of a vessel would migrate towards hypoxic signals independently resulting in the breakdown of the original vessel rather than the formation of a new one. By ensuring that tip cells are interspaced at intervals along the vessel wall the number of new vascular sprouts directed towards the hypoxic tissue is limited which is achieved through Notch signalling.

Through inhibition or overactivation of the Notch pathway, the ratio of tip to stalk cells can be modified as demonstrated through the neutralisation of Notch signalling through inhibition of Dll4 (Hellström et al., 2007). When Dll4 activity is lowered using anti-Dll4 antibodies, the number of endothelial cells that acquire a tip cell phenotype is greatly increased, demonstrated by a greater number of cells possessing filipodia along with an increase in capillary network density due to the number of sprouts emanating from each blood vessel (Lobov et al., 2007). Conversely, if Notch signalling is increased through administering synthetic Jagged-1, the number of cells possessing filipodia is reduced along with the number of branches produced by vessels (Hellström et al., 2007).

Whilst both signalling pathways have been shown to be essential in tip/stalk cell selection, the reasons why a particular cell is initiated to become either remains unclear. One potential explanation is that neighbouring cells naturally have small differences in the number of VEGFRs that they possess and that cells with more VEGFR-2 or a higher ratio of VEGFR-2 to VEGFR-1 have a natural advantage to become tip cells due to increased VEGF signalling. This has been demonstrated in studies using genetically modified endothelial cells to either overexpress

VEGFR-2 or under-express VEGFR-1 with cells possessing either of these traits having a substantially increased chance of becoming a tip cell (Jakobsson et al., 2010).

The proposed model of tip cell selection is that endothelial cells with a greater number of VEGFR-2 are more strongly stimulated by VEGF-A resulting in increased activation of both the VEGFR-2 and Dll4 promoters. With this, VEGFR-2 production is increased in the cell leading to ever increasing VEGF activity whilst at the same time, increasing Dll4 production causes lateral inhibition of neighbouring cells via Notch1 and the Notch signalling pathway. The activation of Notch signalling in the neighbouring cells activates the VEGFR-1 promoter leading to an increase in VEGFR-1 expression and therefore, lower stimulation by VEGF-A, thereby reinforcing its phenotype as a stalk cell.

In addition to suppressing tip cell activity in neighbouring cells, activation of the tip cells also promotes filipodia development and the upregulation of necessary proteins such as metalloproteinases which allow the tip cell to degrade extracellular matrix facilitating migration of the tip cell towards the hypoxic signal region (Sounni et al., 2011).

After the establishment of the endothelial tip and stalk cells, the tip cell begins to migrate through the surrounding tissue towards the site of hypoxia. As this occurs, the stalk cells follow the path of tip cells and form new blood vessel in its wake through the process of tubulogenesis (Xu and Cleaver, 2011).

Section 2: Cells and Growth Factors in Vascular Engineering

1.2.1 Requirements of an *in vitro* engineered functional vascular network

As shown in Section 1.1, the *in vivo* processes of vasculogenesis and angiogenesis are highly complex and rely on the precise control of numerous cell signalling pathways. As such, to create vascularised tissue engineering constructs of a clinically relevant size for transplantation *in vitro*, it will be necessary to establish a platform which mimics the *in vivo* microenvironment of native tissue including the presence of endothelial or endothelial-like cells, a supply of necessary growth factors and a material that mimics the properties of soft tissue (Kaully et al., 2009).

Two main approaches have currently been employed to obtain an *in vitro* model of vasculogenesis with the aim of developing vascularised tissue engineering constructs. The first is direct patterning in which a vascular network is physically fabricated into a 3D tissue construct through a range of methods such as by producing a scaffold with hollow networks that are then seeded with vascular cells (Skylar-Scott et al., 2017) or by 3D printing a construct using bioinks containing cells which map out a vascular network (Cohen et al., 2023). The second approach, cell-directed vascularisation, relies on providing vascular cells with a suitable scaffold that mimics natural ECM and the spontaneous formation of vascular structures comparable to *in vivo* vasculogenesis. As this research is concerned with cell-directed vascular engineering, this is the only method to be discussed in detail.

1.2.2. Cells for vascular engineering

Beginning in the mid-1900s, many attempts to isolate endothelial cells were made with the first successfully identified population of human endothelial cells grown using an explant culture technique from human umbilical veins (Jaffe et al., 1973). Since then, endothelial cells have been cultured from a variety of sources including the aorta (Wang et al., 2016), pulmonary vasculature (Liu et al., 2021) and cerebral vasculature (Assmann et al., 2017) allowing the study of the different phenotypes each have. Whilst this has provided a detailed

understanding of the biology of different endothelial cell populations, the use of endothelial cells isolated from patients for personal, vascularised engineered tissue has practical difficulties with the primary one being that the proliferative capacity of mature endothelial cells *ex vivo* is limited (Medina et al., 2013).

As such, to obtain autologous cells to create vascularised tissue engineering constructs, the cells which currently have the highest potential for use currently are endothelial progenitor cells (EPCs) and autologous adult stem cells.

1.2.3. Endothelial progenitor cells (EPCs)

EPCs are bone marrow-derived cells present in circulating blood that were first isolated in 1997 (Asahara et al., 1997). In the body, EPCs have been found to attach to injured blood vessels and differentiate into endothelial cells to repair the damaged endothelium (Pyšná et al., 2019) and have also been implicated in the process of tumour vascularisation and progression (Feng et al., 2020; Doppelt-Flikshtain et al., 2023).

Due to their presence in peripheral blood, it has long been the aim of researchers to utilise EPCs as a source of endothelial cells for cell therapy treatments and tissue engineering due to being harvested in a relatively non-invasive manner e.g. standard blood collection (Chopra et al., 2018). Several groups have attempted this however the yield of colony forming cells is low with most methods which limits their use in tissue engineering. One group developed a novel method for obtaining a higher yield of EPCs using small volumes of diluted whole blood that behaved like endothelial cells in tube formation assays and expressed the correct endothelial cell markers (Kang et al., 2013). However, the work performed by Kang et al. (2013) was conducted using umbilical cord blood and as such the technique may not be applicable to use in older patients. The reason for this is that the percentage of EPCs present in umbilical cord blood ranges from 0.2 to 1% whereas this falls off to 0.002 to 0.01% in circulating blood (Qin et al., 2017). Therefore, even with an efficient method of isolation, the volume of blood required to obtain a sufficient number of EPCs in some patients could be massive for use in translatable tissue engineering.

Whilst EPCs do show potential for use in tissue engineering, the development of better isolation techniques and the ability to select subpopulations of cells with the greatest regenerative potential are required before they are able to be used widely for vascular engineering.

1.2.4. Autologous Adult Stem Cells

1.2.4.1 Bone marrow stem cells (BM-MSCs) and Adipose-derived stem cells (AD-MSCs)

Somatic stem cells are unspecialised cells found in many tissues of the body with stem traits such as being able to self-replicate and being able to differentiate into some or all of the specialised cells of their resident tissue (Goodell et al., 2015). Adipose-derived (AD-MSCs) and bone marrow-mesenchymal stem cells (BM-MSCs) are two of the most widely researched somatic stem cell populations in vascular engineering, and tissue engineering as a whole.

Unlike EPCs, both AD-MSCs and BM-MSCs can be collected from patients in sufficient numbers for tissue engineering research (Marion and Mao, 2006) and are able to differentiate down an endothelial cell lineage. In 2005, it was reported that treatment of AD-MSCs with VEGF promoted the expression of endothelial cell markers (CD31 and VEGFR2) indicating that AD-MSCs are capable of differentiating into endothelial-like cells (ELCs) (Cao et al., 2005)

Furthermore, it has also been demonstrated that ELCs derived from AD-MSCs display endothelial cell-like behaviour both *in vitro* and *in vivo (Cheng et al., 2018; Arderiu et al., 2019)*. The Matrigel tube formation assay is a widely used method of measuring vasculogenesis and angiogenesis in endothelial cell research as it allows the direct observation of a population of cells to form vasculature like structures (Auerbach et al., 2003). In numerous studies, AD-MSC-derived endothelial cells have been demonstrated to assemble into vascular-like networks in the Matrigel tube formation assay resembling those formed by human umbilical vein endothelial cells (HUVECs) (Zhang et al., 2011; Arderiu et al., 2019).

Similar results have also been found when AD-MSC derived ELCs have been tested in *in vivo* models. Cheng (2018) used endothelial cells derived from AD-MSCs using lentiviral transfection in a hind limb ischaemic mouse model (Cheng et al., 2018). It was found that ELCs derived from AD-MSCs expressed endothelial cell markers at a much higher level than uninduced AD-MSCs, however, the expression level was not as high as HUVECs which were used as a control (Cheng et al., 2018). Nevertheless, after transplantation into the ischaemic tissue of nude mice, the perfusion rate and total vessel density of the newly formed vasculature in the tissue by the ELCs were at a similar level to that of the HUVEC control group (Cheng et al., 2018).

Similar results are also found with ELCs derived from BM-MSCs. In several studies, after endothelial induction, BM-MSCs expressed endothelial cell markers such as CD31 and VEGFR2 (Janeczek Portalska et al., 2012). Furthermore, BM-MSC derived endothelial cells are also able to form vascular-like networks in Matrigel tube formation assays *in vitro* and vascularise tissues after transplantation into mouse ischaemic hindlimb models (Yao et al., 2020).

Although BM-MSCs and AD-MSCs hold great promise for tissue engineering, a disadvantage to their use is the invasive manner in which they are obtained. BM-MSCs can be obtained from a number of procedures such as bone marrow aspiration from the iliac crest (Cavallo et al., 2023) or the femoral head after total hip replacement surgery (Wagenbrenner et al., 2020) which both carry risks of postoperative complications. Furthermore, it has been demonstrated that different methods of bone marrow extraction can lead to diverse differentiation potentials of isolated BM-MSC populations (Herrmann et al., 2019) which may cause variation in the successful use of BM-MSCs to derive ECs.

As such, although both of these stem cells have the potential to be used in vascular engineering, other stem cell sources exist in the body which may have the potential for endothelial differentiation such as dental pulp stem cells (DPSCs).

1.2.4.2 Dental pulp stem cells (DPSCs)

DPSCs are an adult stem cell population that was first described in 2000 (Gronthos et al., 2000). Since then, interest has grown in their potential application in tissue engineering due to them possessing mesenchymal stem cell properties and because they are convenient to harvest in routine tooth extraction. Similar to BM-MSCs and AD-MSCs, DPSCs are multipotent and are able to differentiate into several cell types such as odontoblasts (Luo et al., 2023), neuronal cells (Gao et al., 2022) and adipocytes (Garcia-Urkia et al., 2022). Furthermore, it has been demonstrated that DPSCs have a higher proliferation rate than BM-MSCs (Gronthos et al., 2000) and also have a higher number of stem cells in comparable populations (Alge et al., 2010) making them a promising candidate for tissue engineering.

While much of the research carried out on DPSCs has centred around their use in hard tissue engineering due to their capacity to differentiate into osteoblasts (Maity et al., 2022) and chondrocytes (Salvador-Clavell et al., 2021), there is an ever-growing body of evidence for their potential use in vascular engineering.

Stem cells can have pro-angiogenic effects through two processes; either paracrine signalling which promotes the formation of new blood vessels (Kinnaird et al., 2004) or by differentiating into endothelial cells themselves to form vasculature as discussed earlier regarding BM-MSCs (Yao et al., 2020) and AD-MSCs (Arderiu et al., 2019).

DPSCs have been shown to secrete a wide range of pro-angiogenic growth factors including VEGF and fibroblastic growth factor (FGF) which increase the network-forming capabilities of HUVECs in Matrigel tube formation assays and vascularisation *in vivo* (Hilkens et al., 2014). Interestingly, DPSCs have been found to secrete more of these pro-angiogenic molecules than BM-MSCs and AD-MSCs in culture (Matsumura-Kawashima et al., 2021a). As such, it is possible that DPSCs may increase the vascularisation of scaffolds by providing GF signalling to endothelial cells *in situ* or may cause the differentiation of sub-populations of DPSCs into endothelial cells by the secretion of these factors.

In addition to their pro-angiogenic paracrine signalling, DPSCs have also been shown to differentiate into ELCs. One of the earliest studies to demonstrate this found that whilst attempting to study osteogenic differentiation in DPSCs, some of the cells expressed VEGFR2 and 30% of the cells expressed endothelial cell-specific markers such as CD31 and vWF (d'Aquino et al., 2007). When these cells were transplanted into rats, it was also found that the bone produced by the osteogenic population of DPSCs contained vasculature originating from DPSCs demonstrating their ability to differentiate into functional endothelial cells. Interestingly, the media used to grow and differentiate the cells in the study did not contain VEGF, which is the most common growth factor used in the differentiation of MSCs into endothelial cells leading the authors to attribute the endothelial differentiation of the cells to the interplay between VEGFR-2-expressing cells and the secretion of growth factors by other cells in the population (d'Aquino et al., 2007).

Investigations as to the angiogenic potential of DPSCs for use in tissue engineering have also been conducted. Marchionni (2009) induced the endothelial differentiation of DPSCs using 50ng/mL of VEGF (the medium was changed every two days for 7 days in total) (Marchionni et al., 2009). This work showed that DPSCs were found to constitutively express VEGFR-1 and VEGFR-2 with the expression of both being significantly increased after endothelial induction. Matrigel tube formation assays confirmed DPSCs treated with VEGF formed vascular-like structures whereas uninduced cells formed aggregates instead.

With several such studies demonstrating that DPSCs have the potential to differentiate into endothelial cells based on cell surface markers and function, determining how to differentiate DPSCs into endothelial cells is of great importance.

1.2.5. Endothelial Differentiation of Stem Cells

Stem cells differentiate down different cell lineage pathways due to the result of one or more of many stimuli such as local growth factor exposure acting on the cell (Wang, 2021). These signals result in the modulation of the expression of one or a multitude of different genes which, via altered protein expression and subsequent signalling, result in a terminal cell type such as the endothelial cell (Ruijtenberg and van den Heuvel, 2016). Through the careful control of such processes, cell biologists are able to control the desired differentiation pathway of stem cells to obtain specific cell types.

One of the most frequently employed methods of controlling differentiation is through the administration of growth factors (GFs) to cell culture media (Salerno et al., 2023). GFs are signalling proteins secreted by cells which are important in the regulation of several cell processes including differentiation and cell survival (Rodrigues et al., 2010). GFs work by binding to cell surface receptors on target cells triggering a signalling cascade that results in modulation of the cell's gene expression (Miller and Lappin, 2022).

Several GFs and signalling pathways have been implicated in the process of endothelial differentiation, however, delineating how each specifically results in endothelial specialisation is difficult due to the crosstalk between several signalling pathways and GFs. As such, a definitive and direct process by which to differentiate stem cells into endothelial cells still does not exist though two key GFs, VEGF and basic fibroblastic growth factor (bFGF), have been identified as being able to aid in the differentiation of a range of stem cells into an endothelial lineage which are discussed below.

1.2.5.1 VEGF in the Endothelial Differentiation of Stem Cells

One of the first publications to examine the *in vitro* endothelial differentiation of adult MSCs utilised BM-MSCs. In this work, the only GF administered to cells was VEGF at a dose of 50 ng/mL which was selected based on previous work investigating the differentiation and maturation of EPCs (Gehling et al., 2000; Quirici et al., 2001). In this study, BM-MSCs differentiated into ELCs which were positive for endothelial cell surface markers and were also able to form vascular-like structures in tube formation assays.

Following this, several other groups have successfully differentiated endothelial cells from other MSCs such as AD-MSCs (Cao et al., 2005) and stem cells from exfoliated deciduous teeth (SHED) (Sakai et al., 2010) using VEGF treatment in isolation. Although it has been proved possible to derive endothelial cells from treatment with VEGF alone, researchers often also include other GFs such as fibroblast growth factors (FGFs) which have been shown to be key in vascular development (Yu et al., 2017).

Interestingly, some research has questioned the necessity of VEGF inclusion for the endothelial differentiation of stem cells. Ning (2009) investigated the effect of different GFs on the endothelial differentiation of AD-MSCs and found that VEGF was not necessary for endothelial differentiation but that bFGF was (Ning et al., 2009). To assess this, AD-MSCs were grown in culture media with different combinations of GFs included or omitted. The results showed that the omission of VEGF did not have a significant effect on differentiation but that the exclusion of bFGF and its subsequent blockade with an FGFR1 inhibitor did. However, the study did not also assess whether inhibition of endogenous VEGF signalling altered differentiation in the same way as bFGF and therefore VEGF secreted by AD-MSCs in culture may have still resulted in VEGF signalling.

It is also interesting to note that the use of VEGF is not specific to the endothelial differentiation of stem cells and is also used in several other differentiation protocols such as in the osteoblastic differentiation of BM-MSCs (Joensuu et al., 2015) and that the VEGF signalling is important for the odontogenic

differentiation of DPSCs (Janebodin et al., 2021). The fact that VEGF plays a role in the differentiation of stem cells into several cell lineages highlights the complexity of the signalling pathways used in cell specialisation processes and the need for further research to ascertain the optimum protocols to control them.

1.2.5.2 Fibroblastic Growth Factor in the Endothelial Differentiation of Stem Cells

The fibroblastic growth factor (FGF) family is a group of 18 FGF ligands and four transmembrane tyrosine kinase receptors (FGFR1-4) which control many cellular processes such as proliferation, migration and differentiation (Beenken and Mohammadi, 2009). Activation of the FGF signalling pathway occurs after one of the FGF ligands binds to FGFR causing the receptor to dimerise and the transphosphorylation of tyrosine residues on the cytoplasmic domain of the receptor (Wesche et al., 2011). These phosphorylated residues act as docking sites for signalling molecules which initiate several different signalling cascades such as mitogen-activated protein kinase/extracellular signal-regulated kinase (MAPK/ERK) (Böttcher and Niehrs, 2005)and PI3/AKT (Geary and Labonne, 2018), both of which have been implicated in the endothelial differentiation of stem cells (Shin et al., 2016; Liu et al., 2017) .

Early studies highlighted the importance of FGF/FGFR signalling in regard to vascular function in mouse models where it was found that disruption of FGF-2 signalling led to abnormal vascular development in the yolk sack and poor embryonic development (Leconte et al., 1998). Deng (1994) also investigated the importance of FGF signalling in embryonic vascular development through the blocking of FGF-2 signalling via disruption to FGFR1. In this study, transgenic mouse embryos expressing a truncated version of FGFR1 were found to form abnormal yolk sack vasculature and displayed abnormal embryonic growth leading to death in many cases (Deng et al., 1994).

As the FGF family were found to be crucial to vascular development, members of the FGF family have been investigated *in vitro* to assess their role in the endothelial differentiation of stem cells.

As discussed in section 2.5.1, one such study found that contrary to popular belief, FGF2 is essential for the endothelial differentiation of AD-MSCs and that VEGF is not and that removal of FGF2 from growth media or the blocking of FGFR1 almost entirely eliminates endothelial differentiation (Ning et al., 2009).

FGF-2 has also been demonstrated as a potent inducer of endothelial differentiation in induced pluripotent stem cells (iPSCs) (Harding et al., 2017; Ream et al., 2024). One particular study investigated the affect binding of FGF-2 or different synthetic FGFR agonists have on stem cell fate and the induction of endothelial differentiation specifically (Edman et al., 2024). This study showed that activation of FGFR signalling induced the endothelial differentiation of iPSCs with approximately 60% becoming endothelial-like and 40% differentiating into mesenchymal lineages. However, when stimulation of the FGF receptor was not induced, only 40% of cells differentiated into endothelial cells. It is interesting that such a high proportion of cells still differentiated into endothelial cells without treatment. The study authors attributed this to the release of FGF-2 by cells in culture which supports the notion that the necessity for the inclusion of some GFs in differentiation media may be dependent on the GFs naturally secreted by the cell population.

Section 3: Biomaterials in Vascular Engineering

1.3.1 Biomaterials in Vascular Engineering

Biomaterials are a wide-ranging group of materials that are biocompatible and are used in medicine and tissue engineering in a variety of different roles. These biomaterials may be acellular or used in conjunction with tissue culture methods to form cellularised materials and may be produced from either natural or synthetic sources or a combination of both. The selection of a suitable material is dependent on the requirements of the tissue being repaired.

One of the key considerations that need to be made when selecting a biomaterial for a tissue engineering application is the mechanical properties of the material and how it compares to the tissue being targeted (Jammalamadaka and Tappa, 2018; Jang et al., 2023). Vascularised tissues in the human body range from the strongest, cortical bone with a Young's modulus of >15 GPa (Bittner-Frank et al., 2024) to some of the softest tissues such as neural tissue having a Young's modulus of <1 KPa (Canovic et al., 2016). As such, many different materials have been studied for their ability to support vascularisation in tissue engineering such as β-tricalcium phosphate in bone tissue engineering (Xu et al., 2022) and silk for soft tissue engineering (Qian et al., 2020).

Although it is likely to be necessary to use specific materials to create tissue engineering constructs for some tissues such as bone, hydrogels are a group of biomaterials that may offer a base platform for the creation of vasculature that can be combined with other materials to create vascularised tissue for many applications.

1.3.2 Hydrogels

Hydrogels are materials formed from three-dimensional networks of cross-linked polymer chains that are able to absorb aqueous solutions and are typically >98% W/V (Lee and Kim, 2018). The physical properties of hydrogels such as stiffness can commonly be tuned by altering polymer concentration, the amount of cross-linking within the material and the gelation speed at which the hydrogel forms (Tan et al., 2018; Xue et al., 2022). By modifying the physical properties of hydrogels such as stiffness it is possible to generate tissue engineering scaffolds that have material properties comparable to that of *in vivo* tissue. In addition to mechanical properties, the alteration of concentration, cross-linking and gelation speed are also able to be used to modify other physical properties of the resulting hydrogel such as porosity and pore size (Chavda and Patel, 2011).

Hydrogels can be produced using a range of natural polymers such as collagen (Pien et al., 2021) and chitosan (Pita-López et al., 2021), synthetic polymers such as poly(ethylene glycol) (PEG) (Ju et al., 2023) or a mixture of synthetic and natural polymers in composite hydrogels (Gaona et al., 2023). The choice of whether to use natural, synthetic or a composite of polymers for a particular application in tissue engineering is influenced by many factors and each has advantages and disadvantages in its own right. Natural polymers such as collagen have the advantage of being biocompatible and possess cell binding domains that facilitate cell attachment and growth (Davidenko et al., 2016). However, collagen has source and batch variability (Rýglová et al., 2023) and pure collagen hydrogels often have poor mechanical properties and a limited range of tunability (Dong and Lv, 2016).

Synthetic polymers such as rationally designed self-assembling peptides (SAPs) on the other hand can be designed and tuned to have specific mechanical properties, are highly reproducible (Chen and Zou, 2019) but can suffer from issues with cellular attachment and toxicity (Yamada et al., 2021).

In vascular engineering, many natural and synthetic hydrogels are being explored as possible scaffold materials to facilitate vascularisation in tissue engineering.

1.3.3 Natural Hydrogel Polymers

Many natural proteins such as collagen and fibrin, have been used as hydrogels to promote and support vasculogenesis and angiogenesis *in vitro* (Elomaa et al., 2022; Wein et al., 2024). While it has been demonstrated that endothelial cells can vascularise a multitude of different natural biomaterials, the American Heart Association recommends either fibrin or collagen I to be used in 3D models of vasculogenesis and angiogenesis as both proteins are abundant in the body and therefore are able to replicate the ECM more closely than non-human natural hydrogels such as alginate (Simons et al., 2015).

1.3.3.1 Fibrin

Fibrin is an insoluble protein formed by the cleavage of fibrinogen by thrombin which assembles into fibrous 3D networks essential to the coagulation pathway and thrombus formation after injury to blood vessels (Weisel and Litvinov, 2017). In addition to aiding in blood clotting in wounds, fibrin has also been shown to upregulate angiogenic sprouting in the wound bed via several mechanisms such as αvβ3 integrin signalling (Hadjipanayi et al., 2015) demonstrating its pro-angiogenic properties in tissue repair and vascularisation.

Fibrin has been explored as a hydrogel polymer for use in tissue engineering. Different concentrations of fibrinogen and thrombin have been used to produce gels with stiffnesses ranging from 0.058kPa to 4kPa (Duong et al., 2009; Brown and Barker, 2014). These fibrin scaffolds have been used in a wide range of applications such as in the repair of critical-sized bone defects (Shi et al., 2021) and as an injectable cell carrier to repair cardiac tissue damage after myocardial infarction (Christman et al., 2004). In vascular tissue engineering, fibrin gels have been demonstrated to support the growth of blood vessels both *in vitro (Wein et al., 2024)* and *in vivo* where vascularisation of fibrin gels prior to implantation leads to anastomosis with the host vasculature resulting in a greater recovery after hind limb ischaemia (Friend et al., 2024).

Whilst fibrin has the potential to be used in vascular tissue engineering, two primary issues exist with its use. Firstly, altering the concentration of thrombin,

fibrinogen or both changes the angiogenic properties of the resulting hydrogel with higher-stiffness gels demonstrating low vascular sprout numbers and abnormally dense branching (Stéphanou et al., 2007). Secondly, hydrogel shrinkage is also problematic when fibrin is used as a tissue engineering scaffold. Fibrin shrinkage occurs as a result of the fibrinolytic enzymes secreted by cultured cells which leads to a non-specific decrease in hydrogel size and volume as the number of cells within it increases (Janmey et al., 2009). This may be controlled through the inclusion of inhibitors that prevent fibrinolytic degradation such as aprotinin (Sacchi et al., 2014), however, this has also been found to have an inhibitory effect on vasculogenesis and angiogenesis (Mühleder et al., 2018). As such, whilst it is possible to create pro-angiogenic tissue engineering scaffolds with a range of stiffnesses using fibrin, their usefulness as a material for the creation of 3D vascularised tissue is limited.

1.3.3.2 Collagen

Collagens are one of the most abundant proteins in the body with at least 16 being present in humans (Deshmukh et al., 2016). Of these, type I collagen is the most abundant member of the collagen family accounting for approximately 90% of collagen in tissues (Naomi et al., 2021). Collagen has been used in the production of tissue engineering scaffolds for many different applications due to the fact that it is non-immunogenic and contains cell binding domains (Davidenko et al., 2016). Furthermore, as collagen is abundant in the ECM, endothelial cells possess enzymes such as matrix metalloproteinases (MMPs) (Wang and Khalil, 2018) for its degradation which facilitates angiogenesis making collagen a suitable hydrogel material for vascular engineering.

Type 1 collagen is a triple-helical protein formed from 67 nm banded fibrils which repeat to produce fibrils with a length of approximately 300nm (Shoulders and Raines, 2009). In neutral pH conditions, collagen fibrils self-assemble into fibres that have a diameter of 12-120 nm which crosslink to form a hydrogel network when exposed to water (Ricard-Blum, 2011).

In tissue engineering, collagen hydrogels have been demonstrated to support the development of vasculature both *in vitro* (Elomaa et al., 2022) and *in vivo* (Kuo et al., 2015). However, similarly to other naturally derived hydrogels, challenges with the use of collagen exist in tissue engineering applications.

Much like fibrin, the mechanical properties of collagen can be modified by varying the concentration of collagen used in the gel (Sohutskay et al., 2020), however, this also alters the ability of endothelial cells to form vascular structures within it (Yamamura et al., 2007). Collagen also suffers from rapid degradation and shrinkage due to proteolytic degradation meaning that the long-term stability of engineered tissue using collagen scaffolds may be poor (Nicodemus and Bryant, 2008). Furthermore, unlike fibrinogen which is able to be derived from human plasma for use in medicine and tissue engineering (Sanz-Horta et al., 2023), collagen is most commonly obtained from animal sources such as bovine or porcine tissue which have been shown to induce an immune response (Alijotas-Reig et al., 2013) *in vivo* and also show batch variability (Rýglová et al., 2023).

1.3.4 Self-assembling Peptides

Self-assembling peptides (SAPs) are a class of synthetic peptide molecules which are able to assemble into 3D networks without the need for external factors such as enzymes (Whitesides and Boncheva, 2002). SAPs were first described in the early 1990's (Burdick et al., 1992) and have since become widely studied with potential clinical applications ranging from drug delivery (Wang et al., 2017) to tissue engineering scaffolds (Gelain et al., 2021).

SAPs are short peptide chains which self-assemble into several different hierarchical nanostructures such as α-helices and β-sheets (Habibi et al., 2016). The assembly of SAPs in solution can be triggered by one or several stimuli depending on the peptide such as a change in pH (Aggeli et al., 2003), temperature (Huang et al., 2014) or the concentration of SAP monomers (Zhang et al., 2017).

SAPs are well suited for use in tissue engineering as they can be chemically modified to display a range of biologically active molecules such as cell binding domains (Liu and Hudalla, 2019) and GFs (Santhini et al., 2022). Many different SAPs exist and several have been shown to have low immunogenicity and toxicity and can support the growth and differentiation of cells as well as support vascularisation (Lu and Wang, 2018; Tran et al., 2020a). One such peptide is RADA16, a 16 amino acid peptide which self-assembles into nanofiber hydrogels (Yokoi et al., 2005) producing fibres 10- 20 nm in thickness (Dzierżyńska et al., 2023). This SAP has been shown to support vascularisation *in vitro* and *in vivo* (Tran et al., 2020a) however, it has also been shown that RADA16 degrades rapidly through the action of enzymes secreted by cells (Yu et al., 2024) and therefore its use may be limited in some applications.

Several other SAPs exist such as KLD-12 and Fmoc-SAPs which have been demonstrated to have low toxicity and support cell growth (Sun et al., 2010; Ramirez-Labrada et al., 2024). However, their use in tissue engineering applications outside of the laboratory is limited due to currently being unapproved by regulatory bodies.

1.3.4.1 P_{11}-X Self-assembling Peptide Library

P_{11}-X library general structure

The P_{11}-X library of SAPs consists of peptides that are 11 amino acids in length which, apart from the aromatic residues tryptophan and phenylalanine, have an alternating pattern of polar and non-polar residues which allows them to adopt a β-sheet structure (Aggeli et al., 2001).

An example of two members of the P_{11}-X library, P_{11}-4 and P_{11}-8 can be found below in Table 1. As can be seen, the primary structure of both members is identical apart from the selection of the residues at position 5 and 7 (highlighted red). The selection of residues at these positions dictates the net charge of the peptide and the pH at which a particular P_{11}-X member will be in a monomeric

state (Aggeli et al., 2003). The responsiveness of P_{11}-X peptides to pH and the triggering of self-assembly by pH change will be discussed below.

The hydrophobic tryptophan and phenylalanine aromatic core of the P_{11}-X library (highlighted in blue) is positioned at the centre of the peptide chain to facilitate self-assembly through π-π stacking interactions between different peptide monomers in solution (Aggeli et al., 2003).

Table 1 Primary structure of two members of the P_{11}-X library, P_{11}-4 and P_{11}-8

Peptide	Primary Structure	Net Charge at pH 7.4
P_{11}-4	CH_3CO-Gln-Gln-Arg-Phe-Glu-Trp-Glu-Phe-Glu-Gln-Gln-NH_2	-2
P_{11}-8	CH_3CO-Gln-Gln-Arg-Phe-Orn-Trp-Orn-Phe-Glu-Gln-Gln-NH_2	+2

Concentration dependent self-assembly of P_{11}-X SAPs

The self-assembly of the P_{11}-X family occurs in a hierarchal manner and is both concentration and pH dependent. In concentration dependent assembly of P_{11}-X peptides, a critical concentration (C^*_{tape}) of peptide in solution must be reached to initiate the one dimensional self-assembly of peptide monomers (Davies et al., 2006). Prior to this concentration, P_{11}-X monomers exist as random coil conformations in dilute solutions. As the concentration of peptide increases, the random coil structure of monomers in solution transition to a β-strand conformation once the peptide conformation transition energy (the amount of thermal energy required within the system to adopt a β-strand conformation, described by the energetic parameter $\varepsilon_{trans}K_BT$) is overcome (Aggeli et al., 2003; Davies et al., 2006).

Once the peptide concentration is greater than C^*_{tape}, monomers are able to assume a β-strand conformation. Once this occurs, they are able to align with each other and assemble into tape structures through hydrophobic interactions, complementary hydrogen bonding and coulombic interactions between the amino acid residues of the peptide backbone (Aggeli et al., 2003; Davies et al., 2006).

After the formation of P_{11}-X peptide tapes, if present at a great enough concentration (C^*_{ribbon}), tapes stack into pairs with each other through hydrophobic interactions, hydrogen bonding and π-π stacking which are called peptide ribbons (Aggeli et al., 2003; Davies et al., 2006). If the concentration of the peptide is great enough to overcome the energy threshold to form fibrils (C^*_{fibril}), ribbons stack to form fibrils which then interact to form fibres if the energy threshold for fibre formation (C^*_{fibre}) is overcome (Aggeli et al., 2003; Davies et al., 2006). At a sufficient concentration (C^*_{gel}), the P_{11}-X fibres arrange in solution to form anisotropic gel (Aggeli et al., 2003; Davies et al., 2006).

pH triggered self-assembly of P_{11}-X SAPs

Modulating the pH of solutions of P_{11}-X peptides can also be used to trigger self-assembly and the disassembly of hydrogels. When self-assembly of P_{11}-X peptides is triggered using pH rather than concentration, the assembly of the peptide occurs through the same hierarchal order of structures with the energy required to form each being influenced by direct electrostatic forces between polar residues in the primary structure of the peptide (Davies et al., 2006).

Using P_{11}-4 as an example, when present in a solution of pH ≥8, the glutamic acid residues at positions 5, 7 and 9 are negatively charged and the repulsive forces between these residues on different peptide monomers prevent β-sheet assembly causing the P_{11}-4 peptides to remain in a monomeric state (Davies et al., 2006; Carrick et al., 2007).

As the pH is lowered (pH <8), the glutamate residues on some peptides begin to gradually become protonated due to the P_{11}-4 molecule being a polyelectrolyte (Davies et al., 2006; Carrick et al., 2007). This changes the charge of the P_{11}-4 molecule, the amount of intermolecular interactions between monomers and the energy parameters required for the assembly of monomers into peptide tapes as well as the energy required to assemble into higher order structures (ribbons, fibrils and fibers) (Davies et al., 2006; Carrick et al., 2007). As the pH is lowered further towards being neutral, more glutamic acid residues become protonated which increases the number of interactions between peptides leading to the assembly of a self-supporting hydrogel at a physiological pH (Davies et al., 2006; Carrick et al., 2007).

External Factors affecting self-assembly of P_{11}-X peptides

In addition to pH, other external stimuli such as temperature and the ionic strength of a solution can alter the assembly of P_{11}-X peptides. Temperature has two primary effects on the self-assembly of the P_{11}-X peptides. Firstly, as temperature changes, so does the rate of protonation/deprotonation or polar amino acids (Fazary et al., 2006) which may impact assembly. Secondly, an increase in temperature increases molecular vibration which can beak hydrogen

bonds to break leading to weakened to completely disassembled gels. However, after cooling, hydrogen bonds are able to reform and self-assembly reoccurs (Carrick et al., 2007).

The ionic strength of P_{11}-X peptide solutions is also able to alter the assembly of P_{11}-X peptide solutions due to interfering with electrostatic interactions between peptide monomers. Koch et al. (2018) studied the affect that different buffer compositions and ion type had on the mechanical properties of different members of the P_{11}-X library (Koch, Müller, et al., 2018). In this work it was demonstrated that when P_{11}-4 and P_{11}-8 hydrogels were formed in buffers containing divalent ions (Mg^{2+} and SO_4^{2-}), the stiffness of the material was almost doubled in comparison to those formed in buffers containing monovalent ions (Na^+ and Cl^-). Additionally, the group also studied the mechanical properties of P_{11}-4 and P_{11}-8 hydrogels when formed in two biologically relevant buffers, artificial saliva and the tissue culture media DMEM (Koch, Müller, et al., 2018). It was shown that in the negatively charged peptide P_{11}-4, the stiffness of the material increased in the artificial saliva group when compared to DMEM but its brittleness also increased as measured by yield point. In the negatively charged peptide P_{11}-8, the opposite was true with a significant increase in stiffness being demonstrated when the gel was formed in DMEM with a modest decrease in brittleness (Koch, Müller, et al., 2018).

The change in ionic composition of buffers used to create P_{11}-X is believed to either enhance or reduce certain mechanical properties of hydrogels through screening of electrostatic interactions which can alter the C* that is required for self-assembly (Davies et al., 2006). The screening of electrostatic interactions has been demonstrated as being responsible for this by investigating β-sheet formation by P_{11}-4 in pure water and water containing 130 mM NaCl (Carrick et al., 2007). In pure water, the structures formed by P_{11}-4 had an almost entirely β-sheet conformation in a pH range of 2-7. When pH increased beyond 7, disassembly of P_{11}-4 began with complete monomerization of the peptide occurring around pH 9 (Carrick et al., 2007). However, when the same experiment was conducted in water containing 130 mM NaCl, β-sheet assembly

reached a maximum of 80% which was maintained between a pH range of 2-11. After this point, disassembly began occurring with full monomerization of the peptide occurring by approximately pH 13 (Carrick et al., 2007). The protonation/deprotonation of P_{11}-4 amino acid residues was also investigated under these conditions and it was found that the rate of protonation did not change, implying that the observed affect was caused by shielding of electrostatic interactions by ions in the buffer (Carrick et al., 2007).

As such, the selection of buffer used to prepare P_{11}-X SAPs can be made to influence the mechanical properties of the resultant hydrogel, however, this may also alter the secondary structures formed within resulting hydrogels as demonstrated above by its effect on β-sheet formation.

1.3.4.2 P_{11}-X Self-assembling Peptides in Tissue Engineering

The physical properties of the hydrogels formed by members of the P_{11}-X library family have led to them being explored in tissue engineering. Depending on the particular P_{11}-X peptide used, gels have been produced formed from fibres with a range of thicknesses such as 32 ± 6.6 nm in P_{11}-4 and 37 ± 6.6 nm in P_{11}- 8 (Koch, Müller, et al., 2018). The thickness of these fibres is greater than those produced by other SAP hydrogels such as RADA16 (Dzierżyńska et al., 2023) and therefore more closely resemble those of collagen fibrils.

Furthermore, much like collagen, the stiffness of P_{11}-X hydrogels can be tuned by changing the concentration of P_{11}-X peptide. For instance, in P_{11}-4 it is possible to create hydrogels with a range of stiffnesses from < 1kPa (El-Sayed et al., 2020) to >10 kPa (Koch, Müller, et al., 2018) and in P_{11}-8, hydrogels can be produced with a wide range of stiffnesses from 31-120 kPa (Koch, Müller, et al., 2018). As such, by using members of the P_{11}-4 library, it is possible to mimic the stiffness of a much greater range of tissues than when using other hydrogel materials such as collagen which often have a limited stiffness range from 0.1 to 10 kPa without the utilisation of extra processing methods (Diamantides et al., 2022).

In addition to favourable mechanical properties, P_{11}-X library members such as P_{11}-4 and P_{11}-8 have both been found to be non-cytotoxic in cell culture (Guilliatt, 2013) and are also able to be modified with bioactive molecules such as glycosaminoglycans (Barco et al., 2018) and fibronectin (Koch, Wolff, et al., 2018a). As such, the P_{11}-X family of SAPs have many desirable qualities for the creation of tissue engineering scaffolds.

1.3.4.3 P_{11}-4 in Tissue Engineering

Of particular interest in the P_{11}-X library is P_{11}-4. This member of the P_{11}-X family is perhaps one of the most well explored in tissue engineering with a large proportion of this work being conducted in hard tissues. In particular, P_{11}-4 has been explored in dentistry where it has been demonstrated to be an effective treatment for dental caries (Bröseler et al., 2020; Keeper et al., 2023) and has also been demonstrated to improve periodontal tissue regeneration in an *in vivo* model of periodontal disease (El-Sayed et al., 2020). Furthermore, P_{11}-4 has also been explored in bone tissue regeneration where treatment with the peptide significantly increased bone regeneration in a rat cranial defect model (Saha et al., 2019). However, applications in other tissues are limited, though studies have demonstrated that fibroblasts are able to attach and spread on the surface of the gel (Koch, Wolff, et al., 2018a).

Whilst it has been demonstrated that P_{11}-4 has a proven safety record in both *in vitro* and *in vivo* studies, and has suitable mechanical properties for use in vascular tissue engineering, it is yet to be investigated whether the material is able to support vascularisation and the development of a 3D vascularised tissue engineering construct. As such, in this research, dental pulp stem cells will be used as a stem cell source from which to derive endothelial cells by differentiation which will then be explored to test the feasibility of creating 3D vascularised constructs using patient cells and P_{11}-4 as a hydrogel scaffold material.

2.0 Aims and Objectives

The primary aims of this research are to determine whether DPSCs are capable of differentiating into endothelial-like cells and to use these cells to create a vascularised 3D tissue engineering construct using P_{11}-4. These aims will be pursued by completing the following objectives:

- Investigate the expression of the endothelial cell marker genes *VEGFR2* and *CD31* in DPSCs after the induction of endothelial differentiation
- Determine whether a change in expression of *VEGFR2* and *CD31* leads to an increase in the production of the protein product of each gene
- Assess the functionality of differentiated DPSCs regarding their ability to form vascular-like networks using Matrigel tube formation assays
- Select an appropriate concentration at which to make P_{11}-4 hydrogel scaffolds and optimise for endothelial cell attachment
- Modify the surface of P_{11}-4 with extracellular matrix proteins if required to improve cellular attachment
- Assess whether differentiated DPSCs and/or HUVECs are able to form vasculature within 3D P_{11}-4 hydrogels

3. Materials and Methods

Materials

Consumables

Many laboratory consumables were used throughout this research, a list of which can be found below in Table 2.

Table 2 List of laboratory consumables used throughout this research

Item	Catalogue Number	Supplier
13 mm Cover slips	631-1578	VWR Collection
Cell culture flasks (T25, T75, T175)	F22112, F22114, 156380	Nunc
Cryovials (2 mL)	431386	Corning
Eppendorf centrifuge tubes (0.5 mL, 1.5 mL, 2.0 mL)	T8911, T9661, T2795	Sigma-Aldrich
Falcon tubes (15 mL, 50 mL)	339650, 339652	Thermo Fisher Scientific
Microscope slides	3800050	Leica Biosystems
PCR plate seals	AB0558	Thermo Fisher Scientific
PCR Plates (96 well; light cycler type)	1402-9909	Starlab
PCR tubes (0.2 mL)	TF10201	Bio-Rad
u-Slide 15 well 3D	81506	Ibidi
Well plates (12 well, 24 well, 96 well)	3512, 3527, 3598	Corning

Chemical reagents and kits

Throughout this research a number of chemical reagents and kits were used to perform experiments, a list of which can be found below in Table 3.

Table 3 List of chemical reagents and kits used throughout the research presented in this thesis

Reagent/Kit	Catalogue Number	Supplier
Alpha Modification - Minimum Essential Medium Eagle	M4526-500ML	Sigma Life Science
Anti-CD31 Antibody	66065-2-Ig	Proteintech
Anti-VEGFR2 Antibody	26415-1-AP	Proteintech
Bovine Serum Albumin	A2934	Sigma-Aldrich
Corning Matrigel Growth Factor Reduced Basement Membrane Matrix	354230	Corning
DMSO	D2650	Sigma-Aldrich
Endothelial Cell Basal Medium plus Supplement Pack	C-22210	Promo Cell
Fibronectin	F4759-1MG	Sigma Life Science
Foetsal bovine serum	F7524-500ML	Sigma Life Science
Goat anti-Mouse Alexa Fluor 488	1032-30	SouthernBiotech
Goat anti-Rabbit Alexa Fluor 594	A-11012	Invitrogen
High Capacity RNA-to-cDNA kit	4387406	Applied Biosystems
Hyclone HyPure water	SH40003.01	Cytiva
L-Glutamine solution	G7513-100ML	Sigma Life Science
P_{11}-4	-	Credentis AG
Penicillin-Streptomycin solution	P4333	Sigma Life Science
Phosphate-buffered saline (PBS)	21-040-CV	Corning
ProLong Gold Antifade mountant	P36931	Invitrogen
Rnase-Free Dnase kit	79254	Qiagen
Rneasy Mini Kit	74104	Qiagen
SeaKem LE Agarose	50004	Cambrex
TaqMan CD31 Gene Expression Assay	Hs01065282_m1	Thermo Fisher Scientific

TaqMan Fast Advanced Master Mix	4444557	Thermo Fisher Scientific
TaqMan GAPDH Gene Expression Assay	Hs02786624_g1	Thermo Fisher Scientific
TaqMan VEGFR2 Gene Expression Assay	Hs00911700_m1	Thermo Fisher Scientific
Triton X-100	HFH10	Thermo Fisher Scientific
Trypan Blue solution	T8154	Sigma-Aldrich
Trypsin-EDTA solution	T4049-500ML	Sigma Life Science
Viability/Cytotoxicity Assay Kit (Live/Dead)	30002-T	Biotium

Equipment

Throughout the research presented in this thesis various equipment was required to perform experimental work. A list of equipment used to perform experiments can be found below in Table 4.

Table 4 List of equipment used to perform experiments in this study

Equipment	Model	Manufacturer
Cell Culture Incubator	MCO-20AIC	Sanyo
Confocal Scanning Laser Microscope	DM6	Leica
LightCycler® 480	Roche LC480	Roche Life Science
Inverted Light Microscope	Axio Vert.A1	Zeiss
Mr Frosty™ Freezing Container	11315674	Thermo Fisher Scientific
NanoDrop™ 2000 Spectrophotometer	ND-2000	Thermo Fisher Scientific
pH Meter	FE20	Metler Toledo
Rheometer	MCR 302	Anton Paar

Methods

3.1 Tissue Culture Methods

3.1.0 Standard practices and culture media

All cells were incubated at 37°C with 5% CO_2 and approximately 90% humidity within a cell culture incubator (MCO-20AIC, Sanyo). All work that involved the use of cells was performed in a class II laminar flow hood using aseptic technique.

Ethical approval for acquiring and performing experimental work on human Dental Pulp Stem Cells (DPSCs) was obtained from the Dental Research Ethical Committee (DREC) prior to commencing work **(REF: 240919/PB/284).** DPSCs from three patients were obtained from the Department of Oral Biology biobank (under ethical approval by the DREC) at passage 0 and were cultured in Minimum Essential Medium Eagle – Alpha Modification (M4526, Sigma-Aldrich) with 10% foetal bovine serum, 1% (v/v) 200 mM L-Glutamine, 1% (v/v) Penicillin-Streptomycin (10,000 units penicillin and 10 mg streptomycin/mL, P0781, Sigma-Aldrich) henceforth referred to as α-MEM.

DPSCs from three patients were used in the development of methodologies used in this work. However, in experimental work used to obtain data, DPSCs from a sole patient (Biobank REF: 030612/21C) were used. All experiments were performed in technical triplicates and were repeated three times unless otherwise stated. No characterisation of patient cells were performed unless outlined in experimental data.

Commercially available Human umbilical vein endothelial cells (HUVECs) pooled from multiple donors were purchased from PromoCell (C-12203, PromoCell) and cultured in Endothelial Basal Medium + supplement pack (C-22110, PromoCell) plus 1% (v/v) Penicillin-Streptomycin (10,000 units penicillin and 10 mg streptomycin/mL, P0781, Sigma-Aldrich) referred to henceforth as endothelial culture medium. HUVECs were used experimentally between passages 3-7.

3.1.1 Recovery of cells after cryopreservation

Rationale

Both HUVECs and DPSCs are primary cell lines which are collected from human tissues. As such, they have a limited number of population doublings that they can withstand before experiencing genotypic/phenotypic changes or senescence that may interfere with experiments. It is therefore essential to cryopreserve cells at low passage numbers to be used for future experimental work. When required, cells can then be brought out of cryopreservation and recovered using the below method.

Method

In order to recover cells, they were removed from liquid nitrogen storage and transported to the tissue culture room on dry ice to prevent premature thawing. Cells were then defrosted for 2 minutes in a water bath heated to 37°C. The cells were transferred from cryovials to a T25 tissue culture flask containing pre-warmed culture media. DPSCs were cultured in α-MEM and HUVECs were cultured in endothelial culture media. A full description of the tissue culture media is found in Section 3.1.0.

After 24 hours of incubation, tissue culture media was aspirated from flasks to remove dimethyl sulfoxide (DMSO) contained in cryopreservation media and replaced with fresh media warmed to 37°C. Cells were then cultured until reaching approximately 80% confluence prior to passaging.

3.1.2 Cell passage

Rationale

Once cells become confluent (cells cover the entire surface area of culture vessel) it is possible that they may exhibit behaviours such as contact inhibition where cells stop dividing or in cells such as DPSCs, may spontaneously differentiate. Whilst 100% cell confluence is often used during differentiation protocols, in general cell culture where the expansion of cells is desired cell

populations are split into empty vessels to ensure that cell growth is not inhibited.

To split cells, they must first be detached from culture vessels. In this study, 0.25% Trypsin-EDTA was used to enzymatically digest proteins securing cells to each other and culture vessels which was then inhibited using tissue culture media containing FCS to prevent enzymatic damage to cells. After detachment and trypsin neutralisation, cells are then collected into a pellet using a centrifuge at 1200 RPM for 5 minutes so that the trypsin containing media can be removed and the cells can be diluted into a known volume of fresh tissue culture media so that they can be split accurately.

It is possible to split cells into a ratio such as 1:3 (e.g. 1 T25 flask split into 3 T25 flasks) or cells may be counted and seeded into empty flasks at a specific density. In this research, cells were counted using the method in Section 3.1.3 and seeded at a 5,000 cells/cm^2.

Method

Once confluent, tissue culture media was aspirated from flasks and the cells were washed with 1xPBS (free of Ca^{2}+ or Mg^{2+}) to remove residual tissue culture media. PBS was then aspirated and replaced with 1 mL of 0.25% Trypsin-EDTA in flasks with a volume <= 75 mL or 2 mL of 0.25% Trypsin-EDTA for flasks with a volume greater than this. The flask was then tilted in multiple directions to ensure even coverage of cells and moved to a cell culture incubator for 2 minutes for cellular detachment. Cell detachment was visualised using a phase contrast microscope and once approximately 80% of the cells had detached from the tissue culture plastic, the trypsin was inhibited by adding α-MEM to the flask at a ratio of 3:1 relative to the volume of trypsin in the flask. The cell suspension was then moved to a falcon tube of appropriate volume for centrifugation.

Cells were centrifuged at 1200 RPM for 5 minutes. The supernatant was removed and discarded with great care being taken not to disturb the cell pellet at the bottom of the tube. Cells were then resuspended in 10 mL of fresh tissue culture

media and 45 µL of the suspension was aliquoted into a 1 mL Eppendorf tube for cell counting.

3.1.3 Cell Counting

Rationale

For many experimental procedures requiring cells it is necessary to know the number of cells being used. To determine this, cells are suspended in a known volume of tissue culture media and counted using a haemocytometer which allows the calculation of cell concentration and total cell number using Equation 1 below. A dye such as trypan blue is also added to the cell suspension counted which is unable to pass through intact cell membranes. As such, dead cells are stained (blue when using trypan blue) and can be disregarded from the final cell count. The volume of dye is accounted for in the equation for calculating total cell number (Equation 1) so that it does not distort the result.

Method

5 µL of trypan blue was added to the cell suspension obtained in Section 3.1.2 and mixed thoroughly ensuring that no bubbles were produced. 10 µL of this mixture was loaded onto a haemocytometer and cells were counted in each corner square of the chamber. The total number of cells collected from the flask was calculated using the following formula:

$$Total\ cell\ number = Average\ number\ of\ cells\ per\ quadrant\ x\ 1.1\ (dilution\ factor)\ x\ 10^4\ x\ total\ volume\ of\ cell\ suspension$$

Equation 1 – Calculation of total cell number obtained from a tissue culture flask

3.1.4 Cryopreservation and long-term storage

Rationale

As discussed in Section 3.1.1, cryopreservation is essential in tissue culture so that primary cells may be maintained at a low passage number for experimental work. During the freezing process of cryopreservation, there is a risk of ice crystal formation within the cell which could damage the cell membrane and render the cell unviable. As such, cells are suspended in a cryopreservation media containing a cryoprotectant such as DMSO which inhibits the formation of ice crystals. In addition to using a cryoprotectant to protect cells from ice crystal formation, cells are frozen in a container containing isopropanol which allows for a cooling rate of 1°C/minute to reduce ice crystal formation.

The correct cryopreservation of cells and storage in liquid nitrogen makes it possible to store cells for several years if not indefinitely depending on the cell type.

Method

For cryopreservation, the number of cells within a suspension was determined using the method outlined in Section 3.1.3 followed by centrifugation of the suspension at 1200 RPM for 5 minutes to pellet the cells. The media was then aspirated and an appropriate volume of cryopreservation media (α-MEM, 70% FCS, 10% DMSO) was used to create a cell suspension at a concentration of 1 x 10^6 cells/mL. 1 mL aliquots were then dispensed into labelled cryostorage Eppendorf tubes and frozen in a Mr Frosty™ box containing isopropyl alcohol at -80°C overnight. The cells were then transferred to liquid nitrogen storage the following day on dry ice to prevent thawing.

3.1.5 Endothelial differentiation of hDPSCs

Rationale

To derive endothelial cells from DPSCs, endothelial culture media was used to induce differentiation as it contains many essential growth factors and additives necessary for endothelial cell function and survival.

Method

DPSCs were seeded in T25 tissue culture flasks at a density of 10,000 cells/cm^2 and allowed to reach approximately 100% confluency. Once confluent, old tissue culture media was removed and replaced with 5 mL endothelial culture medium. DPSCs were allowed to differentiate for 5 or 10 days depending on experimental conditions. Tissue culture media was replaced every 24 hours for the duration of the differentiation time. Control DPSCs were prepared in the same way for each sample however α-MEM was used as culture media rather than endothelial media.

3.1.6 Matrigel tube formation assays and analysis

Rationale

Matrigel is a basement membrane extract that forms a stable gel after polymerisation that is rich in several ECM proteins that support cell growth. The assay is widely used in the development of anti-angiogenic therapeutics to measure the ability of endothelial cells to form networks similar to *in vivo* vascularisation after treatment. Furthermore, the assay is also used in research concerning the endothelial differentiation of stem cells to measure the functionality of differentiated cells. In this research, the Matrigel tube formation assay was employed to investigate whether cells derived from DPSCs displayed an endothelial cell phenotype after both 5 days and 10 days of endothelial differentiation.

Method

Prior to performing the tube formation assay protocol, angiogenesis slides (μ-Slide 15 well 3D, 81506, Ibidi) were stored at 4°C along with 10 μL pipette tips. Matrigel aliquots were defrosted overnight at 4°C prior to the beginning of the procedure. It is recommended that materials used in the preparation of Matrigel tube formation assays are kept below 10°C (Kane et al., 2018).

Matrigel aliquots were transferred to a laminar flow hood in a sterile freezer block and angiogenesis slides were placed on top of a chilled sterile metal block in the

laminar flow hood to maintain a temperature below 13°C. 10 µL of Matrigel was added to the inner well of each large well on the slide. If bubbles were formed during pipetting, these were carefully lanced with a sterile needle. After loading wells, the angiogenesis slide was transferred to a tissue culture incubator set to 37°C to allow gel polymerisation for a minimum of 30 minutes.

Whilst the Matrigel gels were polymerising, cells were detached from their flasks and counted using the method described in Section 3.1.3. Cell suspensions were prepared from these at a concentration of 2.5×10^5/mL. The angiogenesis slides were placed back into the laminar flow hood and 50 µL of cell suspension was carefully added to the wells of the slide. The samples were then moved back to a tissue culture incubator.

Cells were imaged after 2, 4, 6 and 24 hours of incubation using a light microscope (Axio Vert.A1, Zeiss) and phase contrast microscopy as described in Section 3.3.4 and analysed using the Angiogenesis Analyzer plugin for ImageJ (Carpentier et al., 2020).

Tube Formation Image Analysis

Images from the 6-hour time point were loaded into the 'Angiogenesis Analyzer' to quantify formed networks. The image in Figure 1A show an example of tube formation analysis using the example HUVEC phase contrast image provided within the plugin. The image in Figure 1B demonstrates the different parameters measured by the plugin. A description of the highlighted and numbered parameters can be found in Table 5.

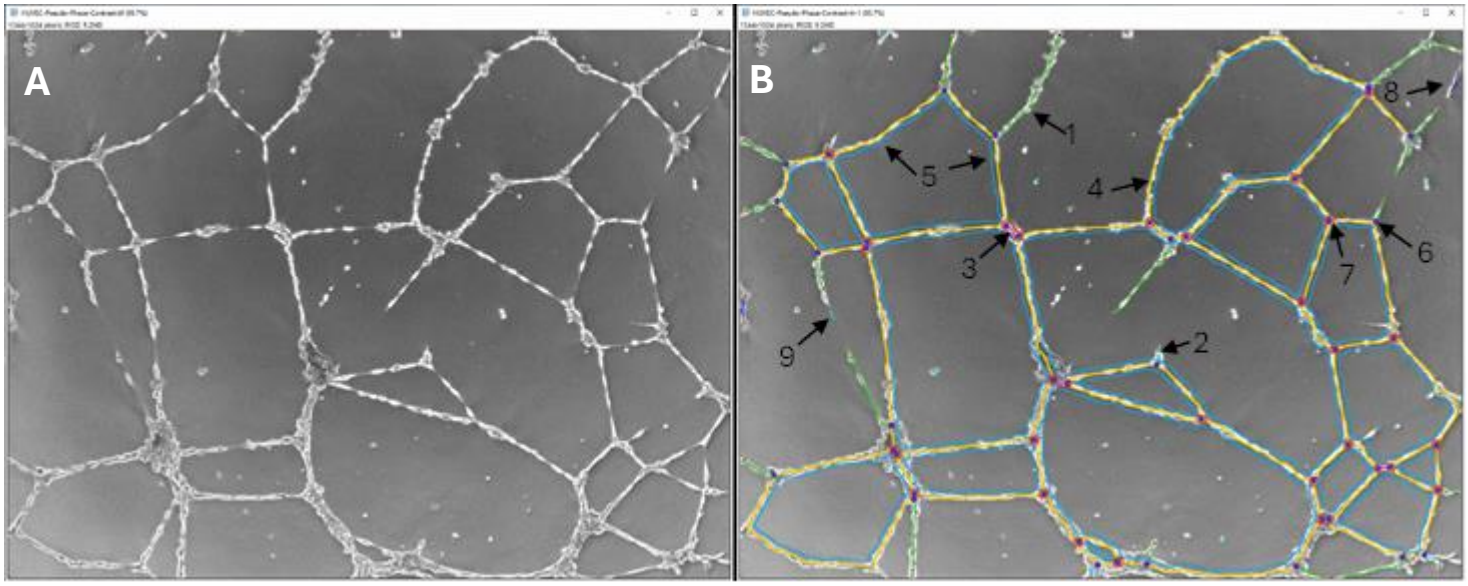

Figure 1 – A) Phase contrast image example provided within the 'Angiogenesis Analyzer' plugin. B) Coloured schematic of network components measured by the 'Angiogenesis analyzer' plugin. A description of each component can be found in Table 5.

Table 5 - Key of coloured components displayed in Figure 1.B. using the 'Angiogenesis Analyzer' plugin

Colour	Component
Green	Branches (1)
Cyan	Twigs (2)
Magenta	Segments (3)
Orange/Yellow	Master Segments (4)
Sky Blue	Meshes (5)
Red surrounded by blue	Nodes surrounded by junctions (6)
Junctions surrounded by red	Master Junctions (7)
Blue	Isolated elements (8)
Cyan	Small isolated elements (9)

For each image, the above parameters were used by the plugin to quantify the cellular networks including measurements such as Total Network Length and the Total Mesh Area. A full list of measurements used to compare the networks formed by HUVECs and DPSCs can be found in Table 6.

Table 6 Measurements collected using the Angiogenesis Analyzer plugin and the rationale for each measurement

Measurement	Description	Rationale for Use
Total Network Length	Sum of the length of all parameters detected in a tube formation assay	Used to compare the length of each network. More complex networks have a greater number of individual tubes formed.
Number of Junctions	Sum of the total number of junctions detected in the tubular network.	Used to compare the complexity of a tube formation network. A greater number of junctions indicates a more complex and branched network.
Branching Interval	Average distance between junctions	Used to compare the complexity of networks between samples. As the branching interval decreases, the complexity of the network increases.
Total Mesh Area	Sum of the total area enclosed by meshes	Used in conjunction with number of meshes and mesh size to compare the formation of closed networks.
Number of Meshes	Total number of meshes within the cellular network	Used to compare the formation of complete networks between experiments.
Mean Mesh Size	Average size of meshes formed withing cellular network	Used to compare whether the average size of meshes between samples is different.

Tube formations and analyses were performed in technical triplicate and repeated three time for each cell population. Statistical analysis of results was performed as per Section 3.5.

3.2 Molecular Biology Methods

Rationale

The molecular biology methods used in this research were performed to measure the expression of the endothelial marker genes *VEGFR2* and *CD31*. To analyse gene expression, it is first necessary to extract mRNA from cell samples. In the case of this research, DPSC cells treated with endothelial cell culture media were compared to control DPSCs after 5 and 10 days of treatment. This allowed the comparison of the endothelial gene expression of these cells to monitor endothelial differentiation at a genetic level.

Once extracted, it is necessary to perform reverse transcription PCR (RT-PCR) to convert the mRNA of expressed genes to cDNA. cDNA is used for qPCR in the investigation of gene expression as it is more stable than mRNA both in terms of storage and also when exposed to temperatures used in the execution of qPCR.

Finally, quantitative PCR (qPCR) is used to measure the number of cDNA copies which are replicate during each cycle of the experiment. Fluorescent probes are used in qPCR which bind the target cDNA being investigated which allows the amplification of target genes to be measured. Once the fluorescent intensity measured is greater than the threshold of detection (cycle threshold, Ct), the Ct of control and treatment samples can be measured to compare the gene expression between groups relative to a housekeeping gene.

Below are the different methods used to first extract mRNA from samples, transcribe the mRNA to cDNA and to perform qPCR and analyse the expression of the target genes investigated in this research.

Methods

3.2.1 RNA extraction

To extract RNA for downstream qPCR, an RNeasy Mini Kit (74104, Qiagen) was used as per the manufacturer's instructions. To do this, 1 x 10^6 cells were collected per sample as per the procedures outlined above. After collecting

cells, the pellet was washed with 1x PBS and centrifuged. This process was then repeated twice to ensure all tissue culture media was removed from cells.

Once washed, the PBS was carefully removed without disturbing the pellet. 350µL of RLT buffer was added to each sample and mixed thoroughly by pipetting. An equal volume of 70% ethanol was then added to the sample and mixed thoroughly again by pipetting. The entire 700 µL of lysate was transferred to a RNeasy Mini RNA extraction column in a 2 mL collection tube and centrifuged for 15s at 10,000 x g. The flow-through was discarded and 350 µL RW1 buffer was added to the column and again centrifuged at 10,000 x g, discarding the flow-through afterwards.

On-column DNA digestion was performed using an RNase-Free DNase set (79254, Qiagen) as per the manufacturer's instructions. 80 µL of DNase solution (10µL DNase stock + 70 µL buffer RDD) was added to the column membrane and incubated for 15 minutes at room temperature.

Following DNA digestion, 350 µL RW1 buffer was added to the column and centrifuged for 10,000 x g for 15s, discarding the flow-through once this step was completed. 500 µL RPE buffer was added to the column and centrifuged for 15s at 10,000 x g, following which the flow-through was discarded. A further 500 µL of RPE buffer was added to the column and centrifuged for 2 minutes at 10,000 x g.

The spin column was moved to a fresh 2 mL collection tube and centrifuged for 1 minute at 10,000 x g to dry the column. Finally, the spin column was moved to a new 1.5 mL nuclease free Eppendorf tube. 30 µL of nuclease free water was added carefully to the spin column membrane and RNA was eluted by centrifugation for 1 minute at 10,000 x g and kept on ice.

The concentration and purity of the RNA was quantified using a NanoDrop 2000 spectrophotometer (Thermo Scientific) set to measure RNA. The measurement was taken by adding 1.5 µL of RNA sample to the sensor of the spectrophotometer and the 260/280 ratio and RNA concentration was recorded.

3.2.2 RT-PCR

cDNA was produced for qPCR using a High-Capacity RNA-to-cDNA kit (4387406, Applied Biosystems). The components of the kit were thawed on ice and preparations were made according to the manufacturer's instructions recreated in Table 7 giving a final volume of 20 µL for each sample in 200 µL PCR tubes. All samples were prepared on ice.

Table 7 Components and volumes used to prepare RNA-to-cDNA mixtures

Component	Volume
RT Buffer	10 µL
Enzyme Mix	1 µL
RNA sample	Up to 9 µL (maximum of 2 µg RNA)
Nuclease Free Water	Amount required to make final reaction volume 20 µL.

Once prepared, samples were mixed by inverting the reaction tube and then they were briefly centrifuged to collect the mixture at the bottom of the tube. The RNA-to-cDNA reaction was performed using a thermocycler set at 26°C for 60 minutes followed by 5 minutes at 95°C to inactivate the enzyme and terminate the reaction. Once finished, samples were held at 4°C and then moved to storage at -20°C until required to perform qPCR.

3.2.3 Quantitative Polymerase Chain Reaction (qPCR)

qPCR was performed using TaqMan gene expression assays for the genes of interest CD31 (Hs01065282_m1, Thermo Fisher Scientific) and VEGFR2 (Hs00911700_m1, Thermo Fisher Scientific) plus GAPDH (Hs02786624_g1, Thermo Fisher Scientific) as a housekeeping gene. All reactions were performed using a Roche LC480 Light Cycler using the Light Cycler 480 software. Each reaction was performed in triplicate within white 96 well PCR plates each with a volume of 20 µL. The reaction mixtures were made as per the manufacturer's instructions outlined in Table 8.

Table 8 Components and volumes used to prepare qPCR reactions

Component	Volume
Master Mix	10 µL
Nuclease Free Water	8 µL
cDNA Sample	1 µL cDNA sample at a concentration of 40 ng/µL
TaqMan gene expression assay	1 µL

After mixing reagents thoroughly on ice, 20 µL of each sample was transferred to a recorded well in the PCR plate. The plate was sealed and centrifuged for 10s to ensure that all samples were collected at the bottom of wells. The plate was then transferred to the light cycler and the following program was ran:

1. Pre-incubation cycle, 95°C for 10 minutes
2. 45 amplification cycles, each cycle was composed of incubation at 95°C for 5s then 65°C for 1 minute
3. Final cooling cycle for 4°C for 30s

3.2.4 qPCR data analysis using the (delta-delta Ct method)

Ct data obtained from qPCR was analysed using the delta-delta Ct method as described by (Schmittgen and Livak, 2008) This method was used to determine if a change in endothelial gene expression (*CD31* and *VEGFR2*) had occurred in DPSCs that had undergone endothelial differentiation for 5 and 10 days.

$$\text{Fold change in gene expression} = 2^{-\Delta\Delta Ct}$$

3.3 Fluorescent labelling and imaging methods

3.3.1 Immunofluorescent staining

Rationale

Immunofluorescent staining is a method used to visualise target molecules within or on the surface of cells such as proteins. In this research, immunofluorescent labelling was used to visualise and quantify the expression of VEGFR and CD31 in control and differentiated cells.

Immunofluorescent labelling can be performed in two ways, direct immunofluorescent labelling and indirect immunofluorescent labelling. In direct immunofluorescent labelling, a fluorophore is bound to an antigen specific antibody which is then used to detect a target. In this study, indirect immunofluorescent labelling was performed which uses a primary antibody to bind the target antigen and then a secondary antibody bound to a fluorophore which is used to detect the primary antibody.

In both types of labelling and in between each antibody treatment a blocking solution is incubated with the sample being labelled. The blocking solution is prepared using a protein source such as bovine serum albumin (BSA) and Triton X-100 which binds hydrophobic sites on the sample which may cause non-specific staining if left untreated. Following staining with primary and antibodies,

the sample is then counterstained with DAPI so that the nucleus can be visualised during imaging.

Method

To prepare cells for immunofluorescent staining, cells were collected, counted and then seeded onto 10 mm coverslips in 12 well plates at a density of 10,000 cells/cm^2 and incubated for 24 hours. This seeding density had been determined as optimal in previous experiments as it ensured cells were dispersed enough to accurately measure after staining.

After incubation, tissue culture media was aspirated and discarded and cells were carefully washed three times in PBS to remove tissue culture media. The PBS was then replaced with 500 µL 4% neutral buffered formalin and incubated for 10 minutes at room temperature for cell fixation.

Cells were then gently washed three times with 1× PBS for 5 minutes to remove excess formalin. The samples were then blocked in 500 µL of blocking solution (3% BSA, 0.3% Triton X-100, 1×PBS) for 1 hour at room temperature. Primary antibodies directed against VEGFR2 (1:300, rabbit polyclonal, 26415-1-AP, Proteintech) and CD31 (1:150, mouse monoclonal, 66065-2-Ig, Proteintech) were prepared individually in blocking solution. Blocking solution was removed from fixed cells and replaced with 500 µL of the required primary antibody solution and incubated overnight at 4°C in a humidified container.

After incubation, the primary antibody solution was removed from the wells and the cells were gently washed three times for 5 minutes in 0.1% PBS-Tween. Goat anti-mouse Alexa Fluor 488 (1:500, 1032-30, SouthernBiotech) and goat anti-rabbit Alexa Fluor 594 (1:500, A-11012, Invitrogen) were prepared in the dark in blocking solution. 0.1% PBS-Tween was removed from the cells and replaced with 500 µL of the necessary secondary antibody solution and incubated for 1 hour in the dark.

After incubation the slides were washed three times with 0.1% PBS-Tween to remove excess secondary antibodies and the samples were mounted onto

microscope slides using ProLong™ Gold Antifade mountant (P36931, Invitrogen) and stored at 4°C until visualisation with confocal microscopy.

3.3.2 Cell Viability/Live Cell Fluorescent Labelling

Rationale

Fluorescent labelling of live cells is a technique that can be used for two purposes. Primarily the Live/Dead assay is used as a method to quantify the number of living versus dead cells within a sample as a measure of cell viability. Further to this purpose, as living cells are stained but unharmed during the labelling protocol the Live/Dead assay can also be used to visualise the growth of living cells as it was in this study.

The stains used within the Live/Dead assay are Calcein-AM (excitation/emission 494/517 nm), a membrane permeant stain and Ethidium Homodimer III (EthD-III) (excitation/emission 532/625 nm), a membrane impermeant dye which stain living and dead cells respectively. After treatment, Calcein-AM passes the cell membrane and is hydrolysed into the fluorescent green calcein molecule which is then able to be visualised. As the conversion of Calcein-AM to calcein requires enzymatic action, only living cells are stained. EthD-III on the other hand is unable to pass through the cell membrane of living cells and is therefore only able to act upon dead cells. The EthD-III molecule is positively charged and binds to DNA allowing the nuclei of dead cells to be visualised.

Method

To stain cells growing on the surface or within P_{11}-4 gels a live/dead cell cytotoxicity assay kit (30002, Biotium) was used. Reagents were prepared as per the manufacturer's instructions to create a staining solution with a final concentration of 2 μM calcein AM and 4μM ethidium homodimer-III in tissue culture containing no FCS. This was achieved by adding 20 μL of 2 mM ethidium homodimer III and 5 μL of 4 mM calcein AM to 10 mL α-MEM.

To stain cells, media was carefully removed from wells containing gels and the gels were washed once with 1× PBS. During all procedures, liquids were pipetted down the walls of wells to minimise disruption of the P_{11}-4 gels. PBS was removed and replaced with 500 µL of live/dead staining solution and incubated in a tissue culture incubator for 45 minutes. After this time, the intensity of fluorescence was observed using a fluorescent microscope (Axio Vert.A1, Zeiss). If fluorescence was visible live/dead staining solution was removed and the gels were washed gently twice in 1× PBS.

The gels were then imaged using confocal microscopy as per Section 3.3.3.

3.3.3 Confocal Microscopy and Image Analysis

Confocal imaging was performed using a Leica DM6 confocal microscope and its associated Leica Application Suite (LAS) software. Prior to acquisition, the appropriate excitation/emission wavelengths for each fluorophore used was selected within the LAS. A list of excitation/emission wavelengths can be found in Table 9.

Table 9 - Excitation and emission wavelengths used to image fluorophores in confocal microscopy

Fluorophore	Excitation Wavelength (nm)	Emission Wavelength (nm)
DAPI	359	461
AlexaFluor 488	490	520
AlexaFluor 594	590	617
Calcein Green	490	520
Ethidium Homodimer	532	625

Image acquisition

Image acquisition was initiated by loading the sample onto the microscope and adjusting the Z-position to bring the sample into focus. The Z-position was then adjusted to locate the deepest visible plane of the sample which was selected as the lower boundary for the Z-stack within the LAS. The Z-position was then raised to locate the uppermost visible region of the sample which was selected as the upper boundary of the Z-stack.

After defining the Z-stack boundaries, the Z-stack was browsed in 'Saturation Indication' mode to ensure that pixels were not oversaturated within the Z-stack. In this imaging mode, blue pixels represent saturated areas which were used to set the laser intensity to ensure that only a minimal amount of pixels throughout the sample were saturated.

After setting the correct intensity, no further modifications were made to imaging parameters to ensure that all samples were imaged using the same settings and were therefore comparable during analysis.

The defined Z-stack was then imaged using the 'System Optimised' option within the LAS to partition the Z-stack into the optimal number of Z-Steps and define Z-step size. Line-sequential imaging was performed to ensure that no crosstalk between the excitation/emission wavelengths of each fluorophore occurred.

The same process was then repeated for each sample and image stacks were exported for analysis in ImageJ.

Processing and Analysis of Fluorescent Images

Corrected Total Cellular Fluorescence (CTCF)

Z-stack image sequences of CD31 and VEGFR2 staining were imported into ImageJ. Stacks were split into separate colour channels and the required channels were isolated depending on experimental conditions (Red: VEGFR2, Green: CD31 and Blue: DAPI).

Cell counting was performed using the DAPI channel. To do this, a maximum intensity Z-stack projection of the blue channel was created and the number of

cell nuclei were counted and used to infer the number of cells present in the sample.

To calculate CTCF, a Z-projection of the appropriate colour channel was created using the 'Sum Slice' option in ImageJ. By creating a Z-projection in this way, the pixel value of each slice is summed together which allows the total fluorescence value of each pixel within the Z-stack to be calculated.

Automatic thresholding was then performed to distinguish cells from background fluorescence. The thresholding algorithm to be used for each colour channel was selected by processing positive and negative control samples using all automated thresholding methods available within ImageJ and choosing the one which segmented the images into signal/background without the need for manual input. The optimal thresholding algorithm to be applied to VEGFR2 images was Triangle thresholding and Huang thresholding for CD31 images.

After selecting regions of interest using thresholding, the thresholding layer was used to create a binary image mask to direct the 'Set Measurements' tool within ImageJ to measure the correct regions of the cells. Additionally, three measurements of the background fluorescent intensity not selected for by the thresholding algorithm were taken at random using the circle tool to calculate an average background grey value for each image.

For each image, the area, integrated density and mean grey value of the total fluorescence was collected using the 'Measure' tool within ImageJ and exported. These were then used to calculate CTCF using Equation 2.

$$\begin{aligned}&Corrected\ Total\ Cell\ Fluorescence\\&= Integrated\ Density\\&- (area\ of\ selected\ cell\ x\ average\ mean\ gray\ value\ of\ backgroung)\end{aligned}$$

Equation 2 – Formula used to calculate Corrected Total Cell Fluorescence (CTCF)

The result of this was then divided by the total number of cells within each sample to give the average corrected total cell fluorescence.

For each experiment, samples were created in technical triplicates and each experiment was repeated three times. Three randomly selected fields of view from each sample were imaged and analysed to measure protein expression. Statistical analysis of the results was performed in GraphPad prism as per Section 3.5.

Live/Dead Image Processing

To process images of Live/Dead staining within gels, Z-stack sequences were collected for each sample using the method outlined above and imported into ImageJ. 2D samples were processed by creating a maximum intensity Z-stack projection of the image stack.

For 3D image sequences, the bottom and upper most Z-stack slices with visible cells were used to illustrate the top and bottom regions of a sample. The Z-stack slice which fell in the middle of these two layers was then used to represent the centre of the stack. These images were then assembled into a montage to demonstrate cellular behaviour throughout the 3D sample.

Cellular Morphology Characterisation

To analyse cell area, perimeter and circularity of HUVECs and DPSCs growing on 2D 10 mg/mL P_{11}-4 gels, image stacks of samples were loaded into ImageJ. Maximum intensity Z-stack projections were created and the resulting image was split into separate colour channels and the green channel (Calcein AM) was selected. Thresholding was then performed on this channel using the Huang thresholding algorithm to create a binary mask of the selected cells. The 'Analyse Particles' tool was then used to measure cell area, cell perimeter and cell circularity. Three images from each repeat of experiments (9 images in total) were analysed for HUVECs and DPSCs. Statistical analysis was then performed on data using GraphPad Prism as per Section 3.5.

3.3.4 Light Microscopy (Phase Contrast)

Rationale

Phase contrast microscopy is a light microscopy technique used in live cell imaging which allows visualisation of cells without first needing to stain them (Yin et al., 2012). This is possible through the use of optical components within the microscope; the annular diaphragm within the condenser and the phase plate within the objective. The annular diaphragm focusses direct light from the source of illumination into a cone of light which interacts with all sections of the sample with the same intensity, however, light passing through different sections of the sample are diffracted by slightly different amounts dependent on the part of the material (Sanderson and Hospital, 2002). Diffracted light and direct light which has not interacted with the cellular component of the sample pass through the objective where it then reaches the phase plate. The phase plate is a circular disk which attenuates the direct light so that its intensity is matched to the diffracted light and also alters the phase of direct light by one quarter of a wavelength relative to the diffracted light. The difference in phase of the light results in interference which in positive phase contrast, as used here, results in thicker sections of a sample being visualised as darker sections on a light background (Sanderson and Hospital, 2002).

Method

Samples were loaded onto the microscope (AxioVert.A1, Zeiss) and illuminated. Images were collected using the microscope's associated imaging software ZEISS ZEN. Images were saved and analysed in ImageJ as outline in Section 3.1.6.

3.4 Hydrogel related methods

3.4.1 Preparation of pH indicator standard series in tissue culture media

Rationale

In the process of creating P_{11}-4 hydrogels, the pH of the peptide solution must be switched between basic and neutral conditions to initiate self-assembly. Due to being required to maintain solutions in a sterile state for cell culture experiments, it was not possible to directly measure the pH of the solution. To overcome this challenge, a series of pH standards were created with both α-MEM and endothelial cell culture media. Both tissue culture media were suitable for use in this way as both contain phenol red, a pH indicator that changes colour from yellow bellow pH 6.8 to dark purple above pH 8.2. As such, by comparing the colour of P_{11}-4 solutions to the pH standards it was possible to determine the approximate pH of the solution. In experiments where cells were added to or encapsulated within P_{11}-4 gels, cells were added to gels when the pH had been reduced to between 7.6-7.0 to prevent cells being exposed to extreme conditions which could result in alkali shock.

Method

For each indicator, 2 mL of tissue culture media was added to a 5mL sterile bijoux glass vial. 1M NaOH or 1M HCl was then added dropwise to the media until the desired pH was achieved whilst measuring the pH of the solution with a pH meter (FiveEasy FE20, Metler Toledo). Standards were created between a pH range from 6.0 to 8.4, an example of which created using α-MEM is shown in Figure 2 below.

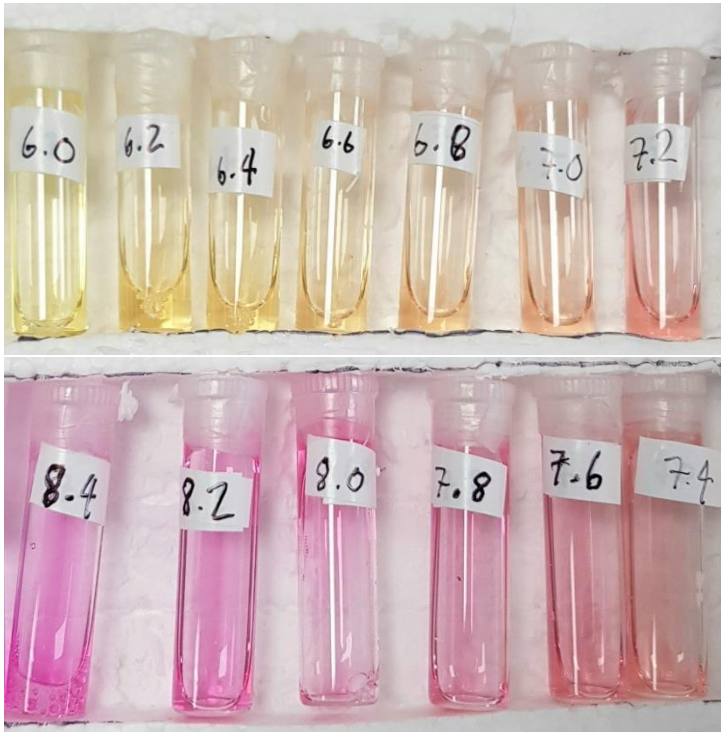

Figure 2 pH standards created using a-MEM between a pH range of 6.0 to 8.4

3.4.2 P_{11}-4 Hydrogel Preparation

Lyophilised peptide was weighed out into sterile Eppendorf tubes or sterile Bijou glass vials at the necessary mass for the final concentration and volume required. 90% of the final volume worth of tissue culture media was added to the peptide and microlitre volumes of 1M NaOH were added to the solution until a suitable level of alkalinity was achieved to monomerise the P_{11}-4 powder using the pH standards created in Section 3.4.1 (tissue culture media dark purple = pH >8.2). The solution was then gently mixed by pipetting the solution carefully using a P1000 and filtered 1000µl pipette tip to fully suspend the P_{11}-4. Microlitre volumes of 1M HCl were then added to the solution until a pH of 7.0 was achieved. The necessary volume of media to achieve the final volume was added to the solution required whilst adjusting pH to maintain the culture media at a pH of 7.0.

3.4.3 Rheological Analysis

Rationale

Rheology is a method commonly used to measure the stiffness of hydrogels. Rheology was performed in this study so that a gel concentration of P_{11}-4 could be selected which would have appropriate material properties for use as a scaffold material with HUVECs and endothelial cells differentiated from DPSCs.

Method

All rheological measurements were performed using an Anton Paar MCR 302 rheometer using a cone-plate with geometry (diameter: 50mm, cone angle: 1^0, gap: 0.05mm). All tests were performed at 37°C using a solvent trap to prevent evaporation of samples.

Amplitude sweeps were performed at a shear strain of 0.01-100%. Two amplitude sweeps were performed for each concentration sample (1 Hz and 20 Hz). Using the data collected from this, a shear strain level was selected at a point where storage modulus (G') and loss modulus (G'') were independent of strain amplitude at each frequency.

Frequency sweeps were carried out for each sample between 1 Hz and 20 Hz using the strain rate obtained from amplitude sweep analysis.

RheoCompas software was used to control and obtain raw data from the rheometer which was exported into Origin Pro for plotting.

3.4.4 2D P_{11}-4 hydrogel surface attachment

To create gels for 2D attachment experiments, P_{11}-4 hydrogels were prepared as in Section 3.4.2. 300 µL of the gel mixture (2.5, 5.0, 10 or 20 mg/mL) was added to the wells of a 12 well plate and allowed to equilibrate in a tissue culture incubator for at least 60 minutes prior to the addition of cells.

Cells were collected as per Section 3.1.2 and diluted to a concentration of 1×10^6 in 1 mL of tissue culture media. The cell suspension was then gently added to the well containing the gel taking great care not to disrupt the surface of the gel. The samples were then moved to a tissue culture incubator and maintained for as long as the experiment was set to run after which point the cells were stained using the Live Cell Labelling protocol found in Section 3.3.2.

3.4.5 Fibronectin surface coating of P_{11}-4 hydrogels

Rationale

Fibronectin is an ECM protein that is commonly used in tissue engineering to improve cellular attachment to materials. In this study, P_{11}-4 hydrogels were coated with fibronectin in an attempt to improve the attachment of HUVECs to the material.

Method

10 mg/mL P_{11}-4 gels were prepared as in Section 3.4.2. 300 µL of gel was aliquoted into 12-well plates and allowed to equilibrate for 60 minutes in a tissue culture incubator. 300 µL of fibronectin from foetal bovine serum (300 µg/mL in 1× PBS, F4759, Sigma) was then added to the surface of the gels and incubated for 2 hours to allow fibronectin to adsorb onto the surface of P_{11}-4 gels. The fibronectin solution was then carefully removed from the gels which were then washed twice for 5 minutes with 1× PBS.

HUVECs were collected and prepared at a concentration of 1 x 10^5 in 2 mL of endothelial culture media as per 3.1.2. The PBS was then removed from the P_{11}-4 gels and 1 mL of HUVEC containing media was added carefully to the surface of the gels. The samples were incubated for 24 hours in a tissue culture incubator prior to staining and imaging as per Sections 3.3.2 and 3.3.3.

3.4.6 Preparation of $P_{11\text{-}4}$ gels for 3D cell culture

For 3D cell culture, P_{11}-4 gels were prepared in the same way as described in Section 3.4.2, however, the final 10% of tissue culture media volume contained cells that had been counted and resuspended in the required volume of media. The cells were mixed into the gel mixture thoroughly by pipetting and 300 µL of the mixture was pipetted into the wells of a 12-well plate. The gels were allowed to equilibrate for 60 minutes after which point 1 mL of tissue culture media was added to the well, being careful not to disrupt the surface of the gel.

The gels were incubated for the length of the experiment and then stained using the live/dead staining protocol in Section 3.3.2.

3.4.7 Agarose encapsulated P_{11}-4 gels for 3D cell culture

To protect P_{11}-4 gels from shear forces created during the changing of media during tissue culture, P_{11}-4 gels were encapsulated within agarose to allow cells to be cultured within P_{11}-4 gels for 7 days. To do this, a 2x strength (1% (w/v)) solution of agarose (SeaKem LE Agarose, 50004, Lonza) was created in 1× PBS and heated to 80°C, the solution was mixed periodically to ensure full dissolution

of the agarose into the PBS. The solution was then autoclaved and diluted to a working concentration of 0.5% (w/v) by adding 20 mL of sterile 1× PBS to the solution in a tissue culture hood. The solution was then held at 60°C in a water bath.

To prepare the moulds 500 µL of 0.5% agarose solution was added to the wells of a 12-well plate. A 6 mm diameter disc of sterile silicone with a depth of 3 mm was then added to the agarose. The agarose was allowed to cool to room temperature in a tissue culture hood. During this time, light pressure was applied to the silicone disc using sterile forceps to ensure it remained in the agarose as it set. Once set, the plates were incubated for 30 minutes at 37°C in a tissue culture incubator.

P_{11}-4 containing cells was prepared as in Section 3.4.6. The plates containing agarose moulds were moved to a tissue culture hood and the silicone discs were removed using sterile tweezers. 80 µL of P_{11}-4 containing cells was pipetted into the agarose mould and the plates were returned to the tissue culture incubator for 60 minutes to allow the P_{11}-4 to equilibrate. 100 µL of 0.5% agarose solution at 40°C was then applied carefully to the outer edge of the agarose mould which then covered the P_{11}-4 gels. The agarose was allowed to cool for 10 minutes to allow gelation and then 1.2mL of tissue culture media was applied to the gel.

The samples were incubated for the required time depending on experimental conditions with the tissue culture media being replaced 24 hours after creation and then every 48 hours after that. Samples were then stained and visualised using live/dead staining as in Section 3.3.2.

3.4.8 Cytotoxicity testing of P_{11}-4 on HUVEC monolayers

HUVECs were seeded onto 96-well plates at a density of $1x10^5$ and cultured until reaching approximately 80% confluency. Culture media was then removed and replaced with different concentrations of P_{11}-4 gel with either 10, 5 or 2.5 mg/mL hydrogels being used. The volume of gel applied was changed for each sample to ensure that the same mass of peptide (0.625mg) was added to each well. To do this, 62.5 µL of 10 mg/mL, 125 µL of 5 mg/mL and 250 µL of 2.5 mg/mL gels

were added to their respective wells. The gels were allowed to equilibrate for 30 minutes and then the tissue culture media was added to each well to achieve a final volume of 250 μL. The samples were then incubated for 24 hours and visualised after live/dead staining as per Section 3.3.2.

3.5 Statistical Analysis

Numerical data are presented as mean ± standard deviation. Statistical analysis was performed in GraphPad Prism (Version 6). In analyses where data from two groups were compared, unpaired Students *t*-test was performed. In analyses comparing more than two groups, one-way analysis of variance (ANOVA) was performed with Tukey's multiple comparison test.

Chapter 4: Endothelial Differentiation of Dental Pulp Stem Cells

4.1 Introduction

The successful development of transplantable tissue engineering therapies is currently hindered by being unable to effectively create vasculature in engineered tissues (Zhao et al., 2022; Li et al., 2024; Iqbal et al., 2024). Vascularisation is essential to ensure the delivery of oxygen and nutrients during *in vitro* culture and to integrate with the hosts vasculature after transplantation (Rademakers et al., 2019). Without proper vascular integration, cells within the implanted tissue are prone to ischemia and subsequent cell death, compromising the therapeutic outcome (Shahin et al., 2020).

As discussed in Section 1.2.2 and 1.2.3 respectively, the use of autologous endothelial cells and EPCs presents practical limitations, particularly with respect to availability and scalability. Therefore, adult stem cells have emerged as a promising alternative for generating vascular networks in tissue engineering applications. Among the various adult stem cell populations, BM-MSCs and AD-MSCs have shown the ability to differentiate into endothelial-like cells and form vasculature both *in vitro* and *in vivo* (Section 1.2.4.1).

In addition to these well-studied stem cell sources, DPSCs offer another viable option for vascularisation strategies. DPSCs have demonstrated the capacity to differentiate into endothelial-like cells and secrete higher levels of pro-angiogenic growth factors compared to other stem cell types, suggesting their potential as an effective cell source for generating vascularised tissue constructs (section 2.4.2).

The research presented in this chapter focuses on the endothelial differentiation of DPSCs and the evaluation of their capacity to function as endothelial cells. This investigation aims to assess whether DPSCs can serve as a suitable cell

source for creating vascularised tissue engineering constructs, providing a basis for future clinical applications.

4.2 Aims and Objectives

The aim of this chapter was to determine the endothelial differentiation potential of DPSCs using commercially available endothelial cell culture media. To achieve this the specific objectives were to:

1. Determine what affect the treatment of DPSCs with endothelial cell culture media had on the expression of two endothelial marker genes (CD31 and VEGFR2) over different time periods *in vitro*.
2. Assess whether differential expression of endothelial genes translates to changes in protein abundance using immunolocalisation studies.
3. Assess whether differences in endothelial gene and protein expression correlated with the ability of differentiated DPSCs to form vascular-like structures during Matrigel tube formation assays.

4.3 Results

4.3.1 Relative change in VEGFR2 and CD31 gene expression levels of hDPSCs after 5 and 10 days of endothelial differentiation

The fold change in *VEGFR2* (red) and *CD31* (green) gene expression, relative to untreated cells after 5 and 10 days of endothelial differentiation are displayed in Figure 3. The results show that after 5 days of endothelial differentiation, *VEGFR2* mRNA levels are increased by an average of 103 ± 54-fold relative to the untreated control and that *CD31* mRNA expression is increased by 124 ± 44.4-fold compared with the untreated control.

After 10 days of endothelial differentiation, the expression of *VEGFR2* mRNA was found to be increased by 192 ± 16-fold relative to the untreated control DPSCs which is significantly ($P<0.001$) higher than the relative expression of *VEGFR2* after 5 days of differentiation. After 10 days of endothelial differentiation there is a 142 ± 13-fold increase in *CD31* expression relative to the untreated control, however, the increase in *CD31* expression is not significantly higher than the expression of *CD31* after 5 days.

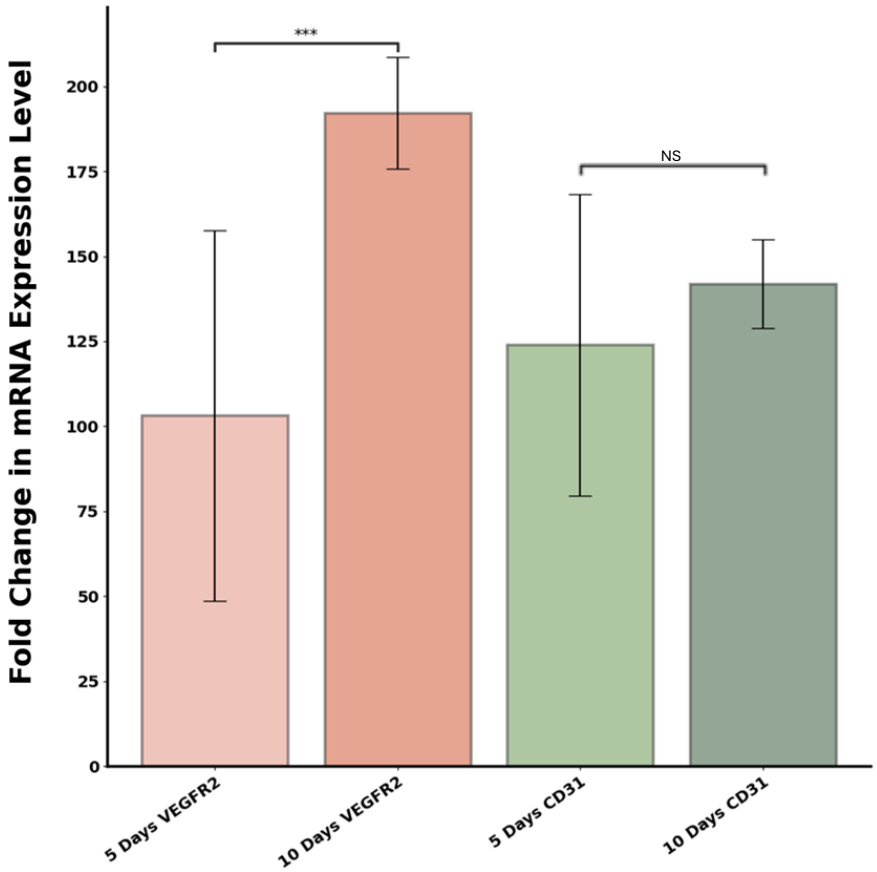

*Figure 3 - Fold change in expression of VEGFR2 and CD31 by DPSCs after 5 and 10 days of endothelial differentiation relative to untreated cells, normalised to GAPDH. Expression studies were performed with technical triplicates in each experiment and were repeated three times for each time point. Statistical analysis was performed using Student's t-test. NS – non-significant, *** = P< 0.001. Error bars represent mean ± standard deviation.*

4.3.2 Effect of endothelial differentiation treatment on the expression of CD31 and VEGFR2 by DPSCs

To determine whether an increase in the expression of *CD31* and *VEGFR2* mRNA correlated with an increased CD31 and VEGFR2 protein expression, immunofluorescent labelling of both proteins was performed after 5 and 10 days of treatment.

Figure 4-A shows representative images for VEGFR2 antibody staining after 5 days and 10 days of endothelial differentiation. The images show that after 5 days of differentiation, DPSCs that received treatment with endothelial media had more intense VEGFR2 (red) labelling than control cells at the same time point. After 10 days of treatment, the same trend is seen that cells exposed to endothelial cell culture media demonstrate much more intense labelling than that of the control cells. In both time points, weak labelling can be detected on control cells. It is unclear whether this is true labelling of weakly expressed VEGFR2 or whether this is nonspecific background labelling.

The graph in Figure 4-B displays the increase in corrected total cell fluorescence (CTCF) of VEGFR2 labelling in DPSCs differentiated using endothelial cell culture media for 5 or 10 days relative to untreated control DPSCs. As indicated, after 5 days of differentiation DPSCs show an increase of 49% in expression relative to controls. After 10 days, the increase in CTCF is 165% relative to controls which is significantly higher ($P<0.05$) than the increase seen after 5 days of differentiation.

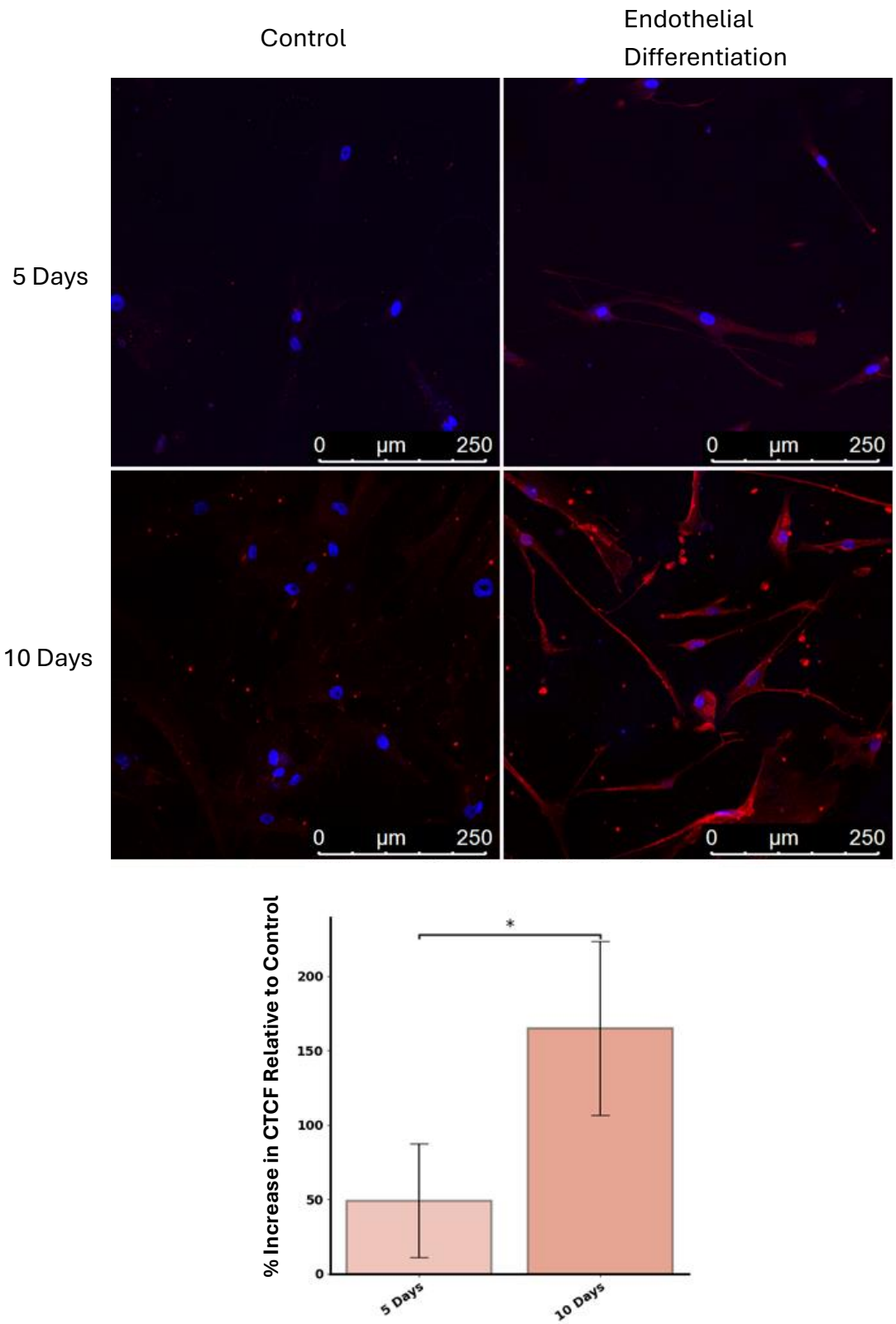

*Figure 4 A) Representative images of VEGFR2 immunofluorescent staining after 5 and 10 days of endothelial differentiation. The images on the left show the staining of untreated control cells after 5 (top) and 10 (bottom) days and the images on the right show the same for differentiated cells. B) Graph showing the relative increase in corrected total cell fluorescence for VEGFR2 staining relative to controls after 5 and 10 days of endothelial differentiation. For each time point, experiments were performed with technical triplicates and experiments were repeated three times. Error bars represent mean ± standard deviation. Statistical analysis was performed using Students t-test. * = $P < 0.05$.*

In addition to VEGFR2, immunofluorescent localisation of CD31 was also performed after 5 and 10 days of endothelial differentiation, the results of which are displayed in Figure 5-A and Figure 5-B. As shown, after 5 days of endothelial differentiation treated cells exhibit a much higher level of CD31 labelling than control cells with all cells being positively labelled for CD31. The same trend is also true for DPSCs that underwent 10 days of endothelial differentiation which have a much greater degree of positive labelling for CD31 relative to control cells. It is unclear whether the faint staining of control cells in both the 5- and 10-day control group is positive labelling or background.

The CTCF of differentiated cells relative to control DPSCs was also calculated for CD31 labelling after 5 and 10 days of differentiation, the graph of which can be found in Figure 5-B. It was found that after 5 days of differentiation DPSCs have a 44% increase in CTCF relative to control cells and that after 10 days of differentiation the CTCF for endothelial differentiated cells was significantly increased ($P<0.01$) to 422% relative to controls.

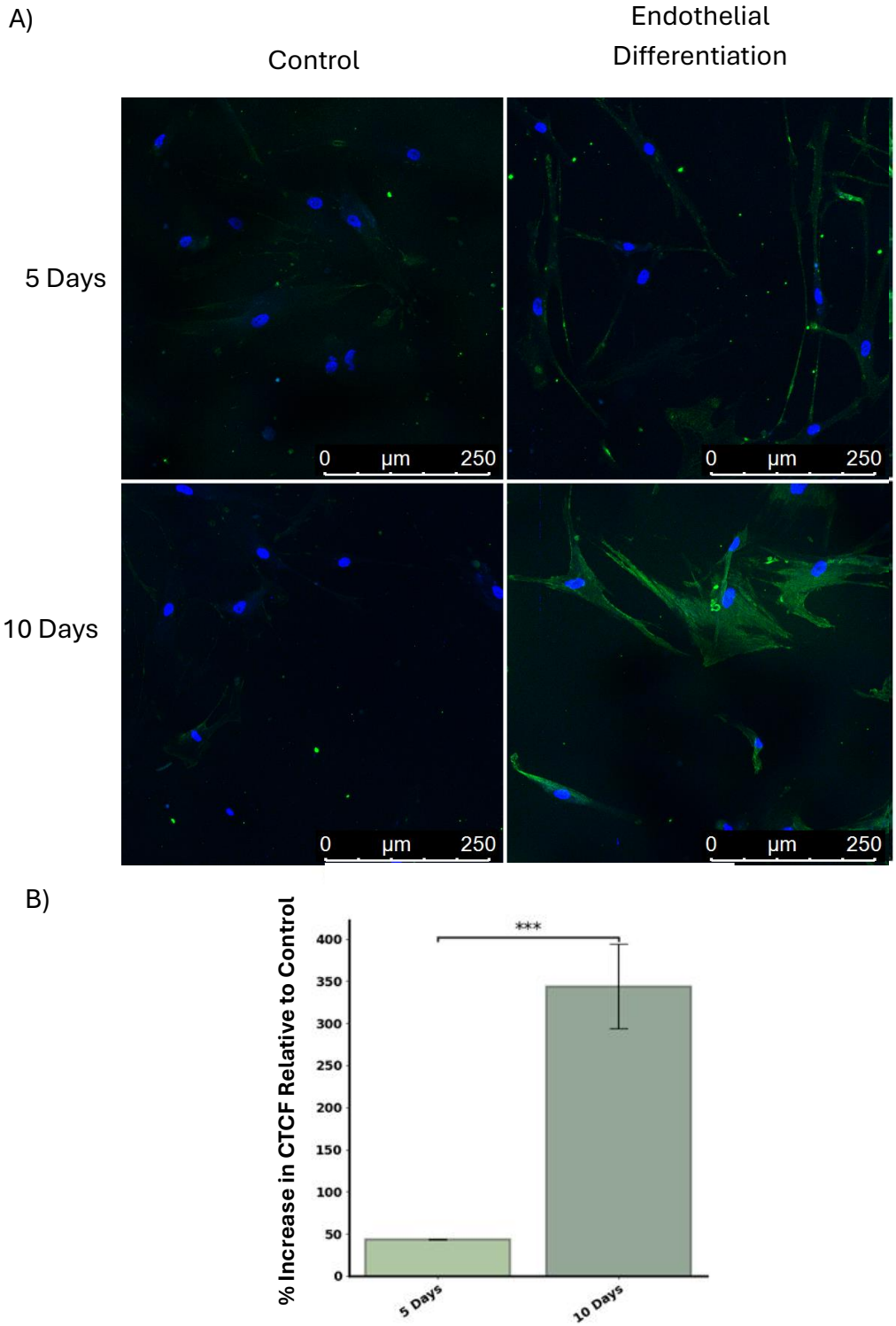

*Figure 5 A) Representative images of CD31 immunofluorescent staining after 5 and 10 days of endothelial differentiation. The images on the left show the staining of untreated control cells after 5 (top) and 10 (bottom) days and the images on the right show the same for differentiated cells. B) Graph showing the relative increase in corrected total cell fluorescence for CD31 staining relative to controls after 5 and 10 days of endothelial differentiation. For each time point, experiments were performed with technical triplicates and experiments were repeated three times. Error bars represent mean ± standard deviation. Statistical analysis was performed using Students t-test. *** = P < 0.001.*

4.3.3 Assessment of endothelial differentiated DPSCs to form vascular-like structures during Matrigel tube formation assays

To investigate whether increased endothelial gene and protein expression correlates with an increase in endothelial-like cell behaviour, Matrigel tube formation assays were performed on differentiated and undifferentiated cells after 5 and 10 days of cell culture.

After being subject to their respective culture conditions, DPSCs were seeded onto Matrigel and imaged at time intervals of 2-, 4-, 6-, and 24-hours post-seeding. Human Umbilical Vein Endothelial Cells (HUVECs) served as the control group to validate endothelial tube formation. Phase contrast microscopy was used to collect images of the tube formation assays as described in Section 3.3.4.

Figure 6 shows representative images obtained from tube formation assays conducted on HUVECs (left), DPSCs cultured in basal media (centre), and DPSCs cultured in endothelial differentiation media (right) following a 5-day culture period.

After 2 hours of incubation, DPSCs cultured in basal media were able to migrate on the surface of the Matrigel and largely formed irregular aggregates of cells with little structural organisation. Endothelial differentiated DPSCs on the other hand formed well organised cellular networks which resembled those formed by HUVECs.

When imaged after both 4 and 6 hours, the same pattern existed with the organisation of untreated DPSCs tending to form disorganised aggregates of cells and endothelial differentiated cells maintaining an organised branched network similar to those produced by HUVEC cells.

After 24-hours, DPSCs cultured in endothelial media formed dense clusters of cells at various regions along the perimeter of the culture vessel walls which were interconnected by a thick cord of cells. This contrasted with HUVECs which retained a network, although this network was more sparse than at previous time

points. DPSCs cultured in basal media, on the other hand, continued to exist as large, disconnected cell aggregates.

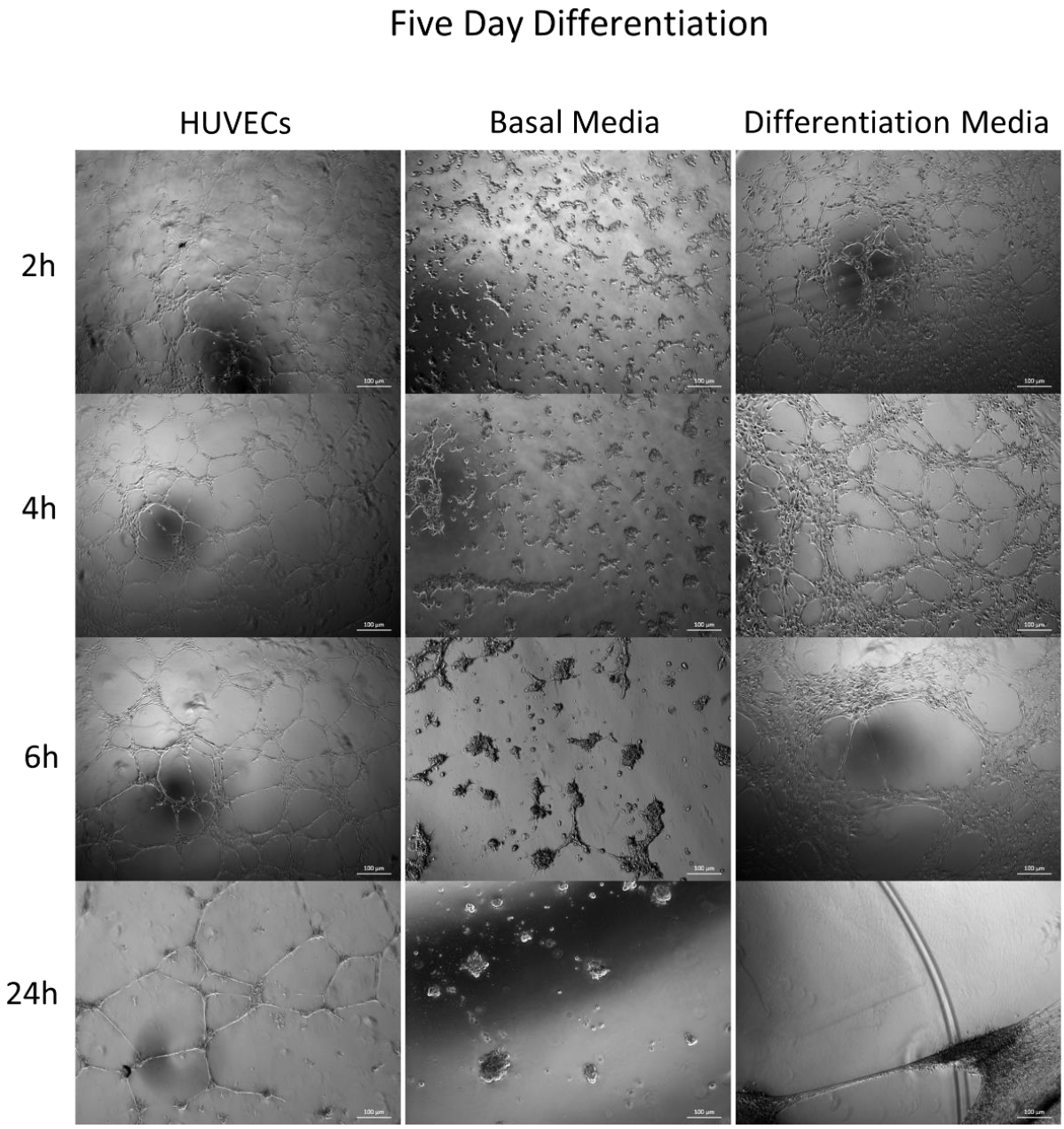

Figure 6 - Phase contrast images of Matrigel tube formation assays performed after 5 days of endothelial differentiation with HUVECs (left), Basal media (centre) and endothelial differentiation media (right) collected after 2, 4, 6 and 24 hours of culture. Each experiment was performed in triplicate using cells as described in Section 3.1.0.

Phase contrast images collected from DPSCs that were cultured for 10 days in basal media (centre) and endothelial media (right) with HUVECs (left) acting as a control can be seen in Figure 7. After 10 days of culture the morphology of the cells appeared similar to those seen after 5 days of differentiation, with DPSCs cultured in endothelial media forming a highly branched network closely resembling those that formed by HUVECs. Again, this was until the 24h time point where differentiated DPSCs formed dense clusters of cells that were interconnected whilst a network remained in the HUVECs.

The main difference in the 10-day culture tube formation experiment was that untreated DPSCs migrated much more slowly around the gel. The result of forming many disconnected cellular aggregates still occurred, however this appeared to progress at a slower rate after 2 and 4 hours of incubation. After 6 hours the results from each experiment more closely resemble each other though there are still more isolated cells in the 10 days basal media group than there are in the 5 days basal media group.

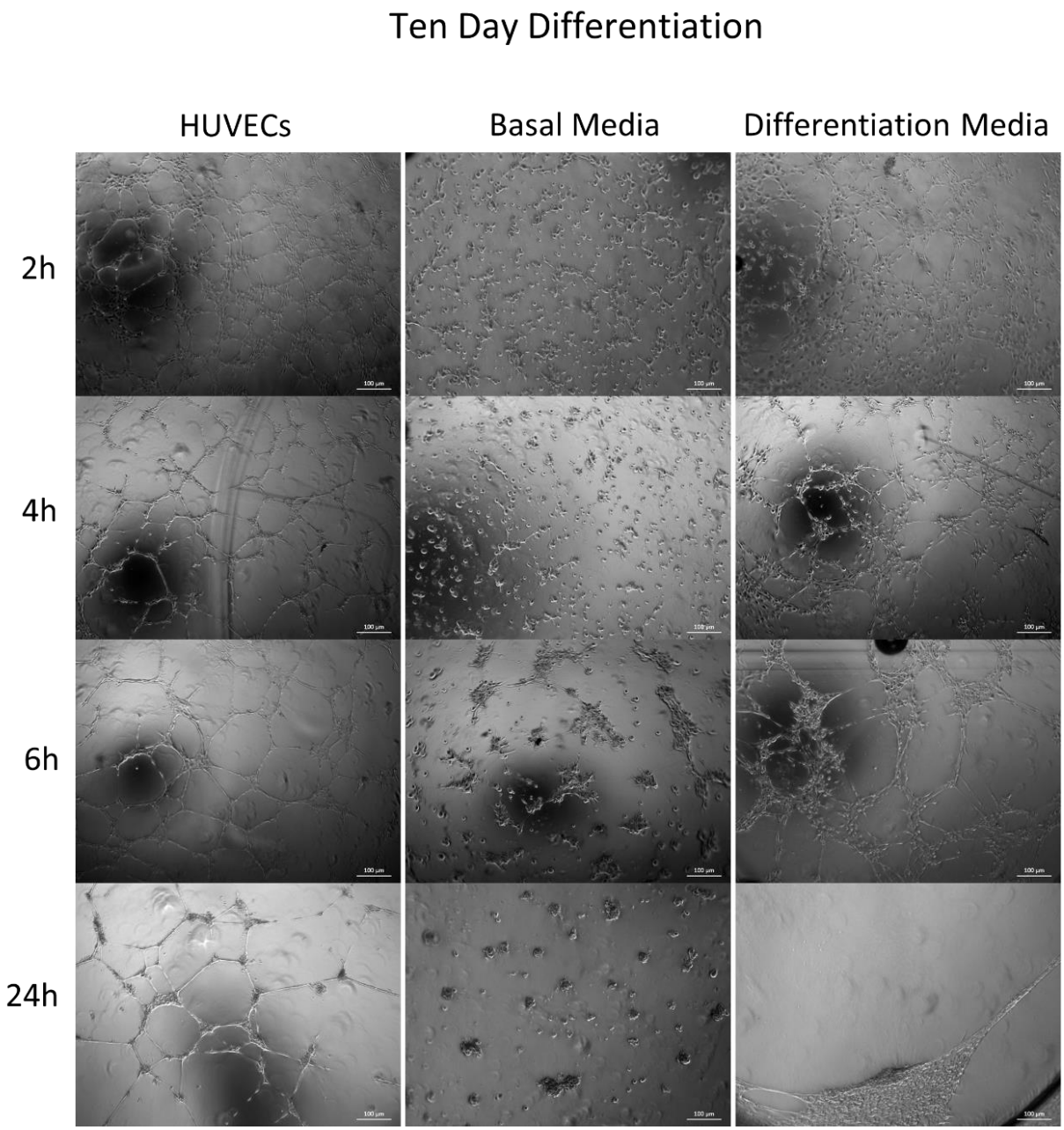

Figure 7 Phase contrast images of Matrigel tube formation assays performed after 10 days of endothelial differentiation with HUVECs (left), Basal media (centre) and endothelial differentiation media (right) collected after 2, 4, 6 and 24 hours of culture. Each experiment was performed in triplicate using cells as explained in Section 3.1.0.

4.3.4 Comparative analysis of the network forming ability of endothelial differentiated DPSCs

The network formed by DPSCs after 5 and 10 days of endothelial differentiation were quantified and compared to HUVECs, the graphs of this analysis can be found below in Figure 8.

As indicated, networks formed by DPSCs which had undergone 5 days of endothelial differentiation showed the least similarity to those formed by HUVECs. In all measures quantified except Mean Mesh Size, DPSCs differentiated for 5 days were found to have significantly higher measures ($P<0.001$) than those formed by both HUVECs and 10 days differentiated DPSCs. With regards to Mean Mesh Size, DPSCs which had undergone 5 days of endothelial differentiation had the lowest mean mesh size and were significantly lower than HUVECs and DPSCs differentiated for 10 days.

Unlike the networks formed by DPSCs after 5 days of differentiation, those formed by cells differentiated for 10 days were comparable to those formed by HUVECs in every measure apart from Mean Mesh Size. It was found that similarly to 5 days differentiated DPSCs, after 10 days of endothelial differentiation DPSCs still have a significantly lower average mesh size in comparison to those formed by HUVECs.

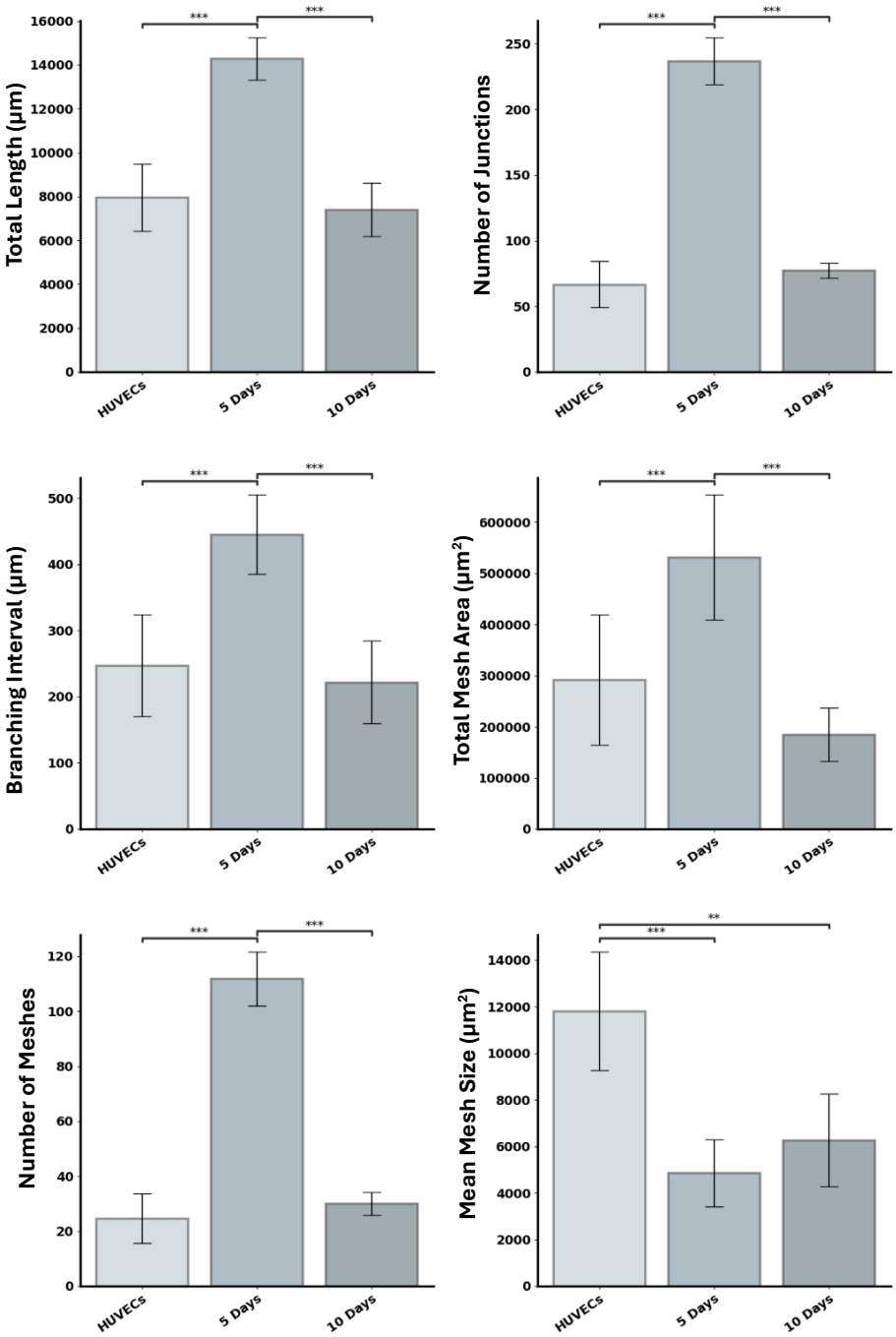

Figure 8 - Quantification of network formation in Matrigel tube formation assays comparing DPSCs differentiated for 5 or 10 days to HUVEC cells. Experiments were conducted in triplicate and were performed three times for each group as per Section 3.1.0. Statistical analysis was performed using GraphPad Prism as described in Section 3.5. Error bars represent mean ± standard deviation.

4.4 Discussion

The research presented in this chapter was conducted to ascertain whether it was possible to generate a population of endothelial-like cells from DPSCs using endothelial cell culture media as a differentiation medium. The results show that there was a significant upregulation in the mRNA expression levels of *VEGFR2* and *CD31* during differentiation and that the protein expression of each gene was also significantly increased. Tube formation assays confirmed that along with an increase in endothelial cell markers, differentiated DPSCs formed vascular-like networks comparable to HUVECs after 10 days of differentiation.

As both proteins measured in this study are key in the normal functioning of endothelial cells and the ability to form interconnected structures such as those seen in tube formation assays is required for the development of functional blood vessels, this research demonstrates that DPSCs possess the ability to differentiate into functional endothelial-like cells and may have the potential for creating vascularised tissue engineering constructs.

4.4.1 Endothelial gene and protein expression after treatment with endothelial differentiation media

The significant increase in VEGFR2 and CD31 gene and protein expression seen in this study support the hypothesis that DPSCs have a strong potential for endothelial differentiation. The expression of VEGFR2 is crucial for the ability of endothelial cells to be activated by VEGF signalling which regulates essential cell functions such as cell survival and proliferation (Wang et al., 2020b) and also the activation of endothelial cells in blood vessels so that angiogenesis can occur (Section 1.5). The expression of CD31 on the other hand is essential for forming cell-cell junctions which are key to the integrity of blood vessel walls. As such, the expression of these proteins demonstrates the differentiation of DPSCs into endothelial cells.

The gene and protein expression data reported in this study are consistent with other research into the endothelial differentiation of DPSCs which have also

demonstrated that after differentiation, the expression of endothelial genes such as VEGFR2 and CD31 are increased (Liu et al., 2014; Luzuriaga et al., 2019; Zhou and Sun, 2020). However, the results obtained in these studies are inconsistent in terms of levels of both mRNA and protein expression after treatment.

This study found that 10 days of differentiation led to the greatest increase in endothelial gene expression in treated DPSCs with the mRNA expression levels of CD31 being 142 ± 13-fold times greater than the control and the expression of VEGFR2 being 192 ± 16 greater. However, Luzuriaga and colleagues (2019) reported t after 7 days of differentiation CD31 mRNA in DPSCs increased by 249 ± 172-fold and VEGFR2 mRNA expression had increased by 17 ± 10-fold (Luzuriaga et al., 2019). Similarly, both Zhou (2020) and Liu (2014) investigated the endothelial differentiation of DPSCs and found that the expression of endothelial genes increased after differentiation but were lower than that presented here and by Luzuriaga (2019). In these studies, after 14 days of endothelial differentiation, Zhou (2020) found that VEGFR2 and CD31 expression had increased 3-fold and 16-respectively (Zhou and Sun, 2020) and Liu (2014) found that after 7 days of differentiation, CD31 mRNA expression was increased by only 2-fold (VEGFR2 was not measured) (Liu et al., 2014).

In addition to gene expression, the significant increase in VEGFR2 and CD31 protein expression reported here is also consistent with the findings of other research but the level of expression observed in the studies is again inconsistent.

In this study, the increase in protein expression of CD31 and VEGFR2 relative to controls was 422% and 165% respectively after 10 days of differentiation as measured by CTCF. However, in research conducted by Luzuriaga (2019) (which had the closest mRNA expression level to the data presented here), CD31 protein expression was found to increase by 62 ± 10% when using a similar method of analysis. They also found that VEGFR2 expression had increased from 22 ± 3 bright pixels per cell to 416 ± 79 bright pixels per cell which is an almost 2000% increase in expression.

Zhou (2020) also found an increase in protein expression as measured by Western blot with a 3.5-fold increase in VEGFR2 expression after 14 days and a 4-fold increase in CD31 protein expression. In the research conducted by Liu (2014), neither CD31 or VEGFR2 protein expression was not quantified.

While the results of these studies all support the endothelial potential of DPSCs, the degree of difference between the gene and protein expression levels between each paper is significant. The discrepancies between the results of the relevant literature suggest that methodological differences such as the use of different differentiation media and the length of treatment time used by each group have a substantial impact on the expression of key endothelial markers.

One of the most likely reasons for the difference between the results presented in this chapter and those published in the literature is the use of different differentiation media in each of the studies. Table 10 shows the growth factors contained in the media used in each of the mentioned papers investigating the endothelial differentiation of DPSCs. As shown, little consistency is found between the supplements used in each and given that they all have profound impacts on the pathways believed to be involved in endothelial differentiation, this is likely to have a significant effect on the downstream expression of endothelial markers.

Table 10 Components of differentiation media used by research investigating the endothelial differentiation of DPSCs

		Supplements					
Study	Basal Media	FCS (%)	$VEGF_{165}$ (ng/mL)	bFGF (ng/mL)	EGF (ng/mL)	Heparin (µg/mL)	Hydrocortisone (µg/mL)
This study	EGM	2	-	1	0.1	90	1
Luzuriaga (2019)	Neurocult	-	-	10	20	2	-
Zhou(2020)	DMEM	15	50	10	-	-	-
Liu (2014)	DMEM	2	50	10	-	-	-

As one of the key growth factors in endothelial cell function (Shibuya, 2011), VEGF has been used widely in differentiation media when trying to derive endothelial cells from adult stem cells. The use of VEGF in endothelial media was first found to induce the differentiation of BM-MSCs into endothelial cells at a concentration of 50 ng/mL (Oswald et al., 2004) and this figure has been carried forward in the endothelial differentiation of stem cells from other sources.

It is known that DPSCs secrete a larger amount of VEGF in culture than BM-MSCs as well as other pro-angiogenic factors (Matsumura-Kawashima et al., 2021b) and it has also been demonstrated that VEGF has a dose dependent response in endothelial cells (Unemori et al., 1992) which affects cell behaviour. In the study presented here, no VEGF was present in the culture media as was the case in the study performed by Luzuriaga (2019). However, in the studies conducted by Liu (2014) and Zhou (2020), the media was supplemented with 50 ng/mL VEGF. It is therefore possible that VEGF supplementation in addition to the VEGF secreted by cells in culture modifies the dose response to VEGF and has an inhibitory effect on their endothelial differentiation.

Another striking difference between the differentiation media used in the aforementioned research is the amount of heparin supplemented in each. Heparin has been shown to increase the binding of VEGF to VEGFR-1 and VEGFR-2 and increase the downstream signalling activity of both (Ashikari-Hada et al., 2005). The differentiation media used in this study was supplemented with 45 times as much heparin than the Luzuriaga (2019) research (90 ug/mL vs. 2 ug/mL) whilst the differentiation media used by Zhou (2020) and Liu (2014) was supplemented with none. The fact that heparin has a considerable impact on the signalling activity of VEGF and that it is present in high amounts in the differentiation media used in this study may account for at least some of the inconsistencies seen across each paper.

In addition to these growth factors, the studies use different concentrations of bFGF which has been shown to be highly important in the endothelial differentiation of stem cells (Section 2.5.2) and furthermore, the culture media used in each study varies in the concentration of FCS included which has been shown to alter signalling pathways involved in endothelial cell maintenance and survival (Karali et al., 2014; Liu et al., 2023).

Finally, aside from considerations of growth factors and supplements within the media, the experiments in each study also changed the differentiation media at different time intervals. In this study the differentiation media was changed every 24 hours, whereas Zhou (2020) changed media every three days and Liu (2014) changed media every two days. The frequency of media changes was not reported by Luzuriaga (2019).

Due to the short half-life of growth factors in cell culture media such as approximately 8 hours for bFGF (Kim et al., 2023), the frequency of how often media is changed has a significant impact on the intensity and consistency of the stimulus to differentiate that cells receive. As such, it is highly likely that in addition to the difference in composition of the different differentiation medias used, that differences in the frequency that cells received stimulation also impacted the consistency of gene and protein expression in each study.

Whilst the gene and protein expression data presented here confirm that DPSCs can be differentiated into endothelial-like cells using VEGF-free differentiation media and that these findings are in keeping with similar work, it also highlights the necessity for further research to define a precise endothelial differentiation protocol for DPSCs.

To do this, it would first be useful to define precisely what growth factors are secreted in culture by DPSCs as this would allow the tailoring of supplements to ensure that added growth factors don't have a negative dose response on differentiation. Secondly, developing a deeper understanding of which growth factors are necessary and which are redundant to endothelial cell culture as well as the optimal frequency of when they are applied could help establish a baseline to work from in developing a precise method of endothelial differentiation for stem cells. Thirdly, after establishing the necessary growth factors and frequency of stimulus by endothelial cells for optimal function, fine tuning the levels of these growth factors to induce differentiation would be necessary. Finally, the use of methods such as cell sorting have helped elucidate sub-populations of DPSCs which are more prone to endothelial differentiation (Bergamo et al., 2021) and as such, the pre-sorting of DPSCs may help in achieving an efficient method of endothelial differentiation and improve the purity of the end product.

4.4.2 Endothelial differentiation of DPSCs results in cells with comparable endothelial cell function to HUVECs as measured by *in vitro* tube formation assay

The results of the tube formation assay demonstrate that along with an increase in endothelial gene and protein expression, differentiated DPSCs also exhibit similar behaviour to true endothelial cells during tube formation assays. After both 5 and 10 days of differentiation, induced DPSCs formed pseudo-vascular networks similar to that of HUVECs which was not found in undifferentiated cells.

Interestingly, after 5 days of differentiation, the networks formed were quantified as being significantly greater in all measures of network formation aside from

mesh size in which it is significantly lower than HUVECs and non-significantly lower than cells differentiated for 10 days. This demonstrates that whilst having a larger total network area and more meshes, the networks formed by cells differentiated for 5 days form more highly branched networks which has been found to decrease the efficient flow of blood through vessels (Mirzapour-Shafiyi et al., 2021) and as such, cells differentiated for 10 days would likely be more suitable for use in tissue engineering.

Whilst many possible explanations could account for the increased branching seen after 5 days of differentiation, a likely contributor is the undifferentiated or not yet fully differentiated cells present in the population. Undifferentiated DPSCs form cellular aggregates when subject to the tube formation assay as shown in Figures 6 and 7. As discussed previously (Section 2.4.2), DPSCs secrete a range of pro-angiogenic factors and therefore it is possible that aggregates of undifferentiated cells secrete these factors which lead to the formation of more dense networks.

Gharaei (2018) found that by administering conditioned media from DPSCs to HUVECs, after 6-8 hours of incubation all measures of network formation were increased (Gharaei et al., 2018). Similar results were also found by Zhou (2020) who demonstrated that HUVECs treated with conditioned media from DPSCs produced networks during tube formation assays that were more than twice as branched as untreated cells (Zhou et al., 2020). It is therefore possible that the increase in network density seen after 5 days is caused by undifferentiated cells releasing proangiogenic factors.

Although the excessive branching measured after 5 days is no longer present after 10 days of differentiation (Figure 7), it is likely that undifferentiated or non-endothelial cells remain in the population. While studies have demonstrated that the inclusion of non-endothelial cells such as pericytes (Dibble et al., 2023) and vascular smooth muscle cells (Golas et al., 2013) support neovascularisation, and that DPSCs have also been found to do this (Janebodin et al., 2013), the presence of undifferentiated DPSCs in the population may pose a challenge for use in vascularised tissue engineered constructs due to their potential to cause

tumours (Cuiffo and Karnoub, 2012; Lee and Hong, 2017). Therefore, it will be necessary to ensure that only DPSCs fully differentiated into endothelial-like cells are used in the formation of vascularised tissue engineering constructs intended for clinical applications through the use of techniques such as fluorescence-activated cell sorting (FACS) to isolate a pure population of cells (Hu et al., 2016; Chowdhury et al., 2023).

4.5 Conclusion

In this study, it was demonstrated that DPSCs can be effectively differentiated into endothelial-like cells using VEGF-free endothelial culture media. The significant upregulation of key endothelial markers, VEGFR2 and CD31, at both the gene and protein levels confirm that DPSCs exhibit endothelial cell characteristics after 10 days of differentiation. Furthermore, DPSCs differentiated for 10 days formed vascular-like networks in Matrigel tube formations that were similar to those formed by HUVECs. The ability of DPSCs to express endothelial markers after differentiation and also be able to function similarly to HUVECs supports their potential as a viable stem cell source of endothelial cells for generating vascularised tissue constructs for tissue engineering applications.

The findings presented here are consistent with existing literature, however they also highlight the variability in endothelial differentiation outcomes due to differences in culture conditions, growth factors utilised and experimental protocols such as the frequency of differentiation media changes. This highlights the need to optimise differentiation protocols so that an efficient method of obtaining endothelial cells from DPSCs for clinical use can be achieved.

4.6 Future Research

While the results of this research are promising, several key issues remain such as the need for a deeper knowledge of the growth factors necessary for endothelial differentiation in DPSCs, the timing of when differentiating cells are exposed to growth factors and also the need to isolate pure populations of cells for potential future clinical applications.

Additionally, whilst endothelial differentiated DPSCs form vasculature-like structures similar to HUVECs *in vitro*, their ability to do the same *in vivo* will need to be tested to understand whether endothelial differentiated DPSCs produce functional vasculature. Furthermore, the use of dynamic culture systems such as bioreactors should be investigated to improve the differentiation of cells as mimicking physiological conditions such as blood flow has been demonstrated to improve the endothelial differentiation of other stem cell types (Ahsan and Nerem, 2010).

Chapter 5: Investigating the Vascularisation Potential of Self-Assembling Peptide P_{11}-4

5.1 Introduction

Various materials have been investigated for generating vascularised tissue engineering constructs with hydrogels being particularly appealing due to their tuneable properties as discussed in Section 1.3.2. The stiffness of biomaterials is the of the key mechanical properties critical in tissue engineering, especially regarding vascularisation(Yi et al., 2022).

Hydrogel stiffness is commonly measured in two ways: compression testing which measures material stiffness under compressive loads and provides Young's modulus (E) (Patel et al., 2019) and rheology, which measures stiffness under shear and provides the storage modulus (G') and loss modulus (G'') of the material. The storage modulus reflects the elastic portion of a materials behaviour and is how stiffness is defined in rheology whereas the loss modulus reflects the viscous behaviour of a material and is a measure of energy dissipation by the material (Ramli et al., 2022). By measuring these two parameters, rheology enables the study of the viscoelastic behaviour of materials and is commonly used in the measurement of stiffness in gels (Yan and Pochan, 2010).

Young's modulus and storage modulus are not directly comparable due to measuring a materials stiffness in different dimensions (compression vs. shear), however, Young's modulus can be related to the storage modulus using Equation 3.

$$E = 2G(1 + V)$$

Equation 3 – Formula to relate Young's modulus to storage modulus where E is Young's modulus, G is storage modulus and V is the materials Poisson's ratio

Due to the high water content of hydrogels, they are assumed to be incompressible and therefore researchers often assume a Poisson's ratio of 0.5 (Ahearne et al., 2005; Kaklamani et al., 2014; Derkus et al., 2020). While this assumption has been shown to cause inaccuracies in some hydrogels (Chippada et al., 2009), it allows the approximate comparison of material stiffness in hydrogel research that use different measurement methods.

Table 11 shows the stiffnesses of different materials that have been investigated for their potential to support vascularisation both *in vitro* and *in vivo*. Where compression testing was performed to obtain Young's modulus, it is also converted to storage modulus using Equation 3.

Table 11 Examples of hydrogel stiffnesses that have been shown to support vascularisation in vitro and in vivo

Hydrogel Material	Young's modulus (E)	Storage modulus (G')	Comments
Hyaluronic acid		3.2 kPa	HUVECs formed vasculature on 2D angiogenesis assay using gel (Derkus et al., 2020).
Poly(ethylene) glycol	0.7-1.3 kPa	0.2-0.4 kPa	HUVECs formed vascular sprouts in all stiffnesses tested *in vitro* with the lower stiffness demonstrating slightly better vascularisation (He et al., 2018).
Poly(ethylene) glycol	2.2 to 18.5 kPa	0.7 to 6.1 kPa	Hydrogels at both the highest and lowest stiffnesses supported vascularisation *in vivo* with the lower stiffness showing increased vascularisation (Schweller et al., 2017).
Hyaluronic acid		0.1 kPa	Hydrogels permitted vascularisation after 24 hours *in vitro* (Wei et al., 2023).
Fibrin		0.2 kPa	Hydrogels supported vascularisation *in vitro* (Juliar et al., 2018).
Dex-AE/PEGDa (polysaccharide based hydrogel)	4-15 kPa	1.3-5 kPa	Hydrogels with both stiffnesses were able to support vascularisation *in vitro* with increased vascularisation being demonstrated in the lower stiffness gel (Sun et al., 2011).
ECM-derived hydrogel	30-40 kPa	10-13 kPa	Hydrogels of both stiffnesses supported vascularisation *in vitro* (Pilipchuk et al., 2013).
RADA16 (SAP)		0.031 kPa	Hydrogel supported vascularisation after 5 days *in vitro* (Tran et al., 2020b).
Gelatin methacrylate	2-4.5 kPa	0.7-1.5 kPa	Gel was able to support vascularisation however, the lowest stiffness gel showed significantly better vascularisation (Chen et al., 2012).

As shown in Table 11, research has demonstrated that materials with a range of 0.031 kPa to 13 kPa are able to support vascularisation, however in all cases where multiple stiffnesses were tested, the lowest stiffness hydrogel demonstrated improved vascularisation.

P_{11}-4 is a self-assembling peptide (SAP) which forms hydrogels under physiological conditions and has been demonstrated to support the attachment of cells *in vitro* as discussed in Section 1.3.4.3. Furthermore, the stiffness of P_{11}-4 hydrogels can be tuned by altering the concentration of peptide used to generate the gel with stiffnesses ranging from 0.1 to >2kPa being reported in the literature (Koch, Müller, et al., 2018; El-Sayed et al., 2020).

To date, research has not been conducted into the ability of P_{11}-4 to support vascularisation, however, due to its biocompatibility, ability to support cellular attachment and tuneable stiffness within a range that has been shown to be conducive to vascularisation, it is a promising candidate for the creation of 3D vascularised tissue engineering constructs.

The research presented in this chapter aims to assess the biocompatibility of P_{11}-4 with both HUVECs and DPSCs, its ability to support cellular attachment of these cells and its ability to support vascularisation.

5.2 Results

5.2.1 Rheological Characterisation of P_{11}-4 hydrogels at different concentrations

Amplitude sweeps were performed in triplicate on four different concentration gels (2.5 mg/mL, 5 mg/mL, 10 mg/mL and 20 mg/mL) at both 1 Hz and 20Hz to establish the linear viscoelastic region (LVER) of the gel. The LVER was first determined so that a frequency sweep could be performed at a strain rate within this region to determine the stiffness of each concentration.

The LVER for each sample was determined from the amplitude sweep graphs displayed in Figure 9. It was found that a shear strain of 0.1% falls within the LVER and therefore would be suitable to perform a frequency sweep on P_{11}-4 at concentrations of 5, 10 and 20 mg/mL. It was not possible to determine the LVER of the 2.5 mg/mL gel due to wall slip of the sample.

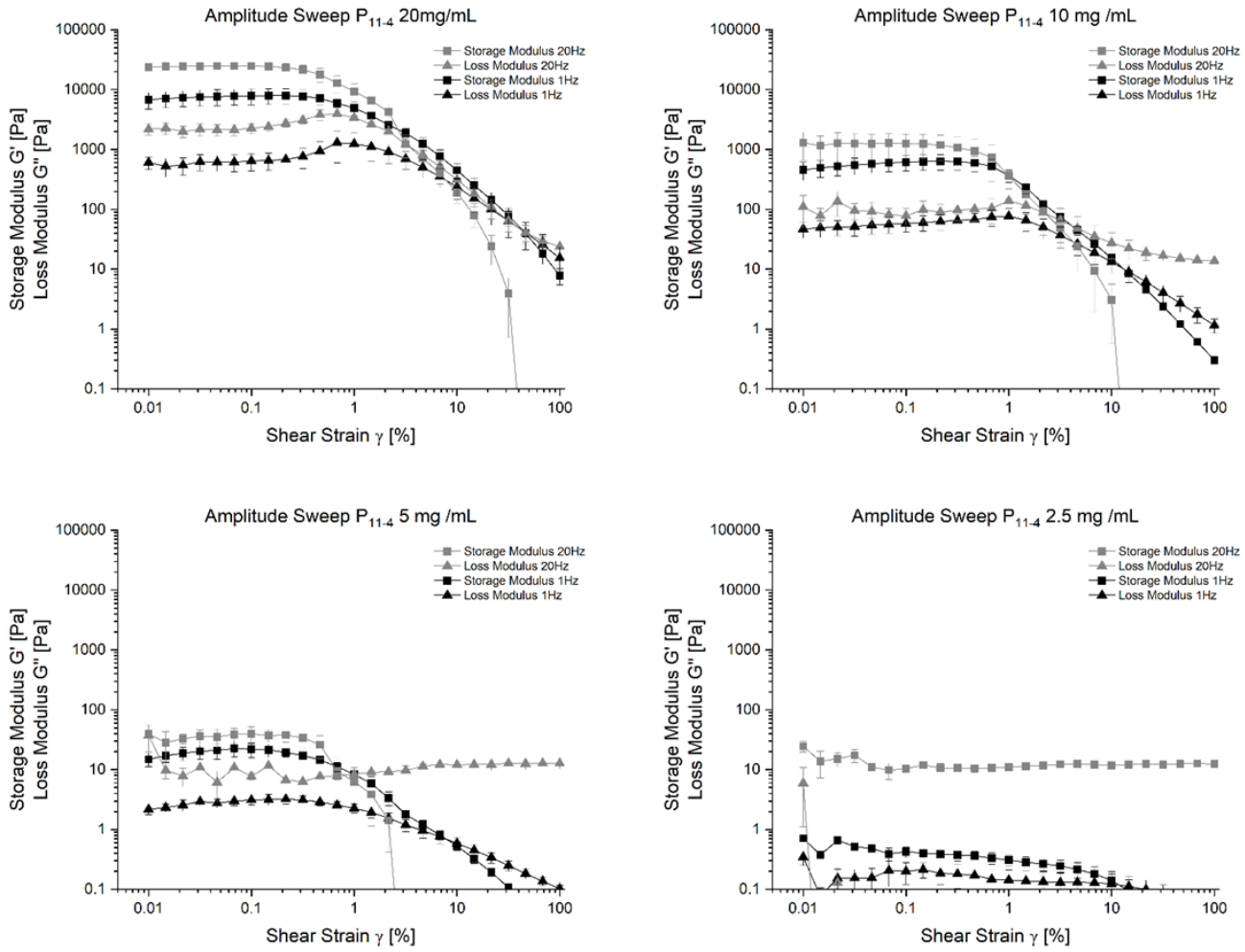

Figure 9 Amplitude sweep graphs obtained from 20, 10, 5 and 2.5 mg/mL $P_{11\text{-}4}$ gels at 1 and 20 Hz. A shear strain rate of 0.1% was determined to be in the linear viscoelastic region (LVER) for the gels with a concentration of 20, 10 and 5 mg/mL. It was not possible to determine a LVER for the 2.5 mg/mL concentration gel due to wall slip. The amplitude sweeps were performed in triplicate for each concentration to determine the LVER. Error bars represent standard error of the mean. Each experiment was performed in triplicate.

After establishing an appropriate strain, frequency sweeps were performed on each sample concentration three times to determine the stiffness of each material. The results, presented in Figure 10, demonstrated that the highest concentration gel, 20 mg/mL, had the greatest average storage modulus of 1726 ± 440 Pa. The storage modulus then decreased in a non-linear fashion to 710 ±196 Pa for the 10 mg/mL gel and 13 ± 7 Pa for the 5 mg/mL gel. Of note with the frequency sweep for the 5 mg/mL gel is the cross-over point of the storage modulus (G') and loss modulus (G'') at high frequencies. Although the explanation as to why this occurred is unclear, it demonstrates a change in the material property of the 5 mg/mL gel with the gel showing liquid behaviour above the cross over point and a shift to a solid like state below this when G' > G''. It is possible that this disruption to the sol-gel state impacted the data collected below this point by disrupting the network of bonds maintaining the internal structure of the P_{11}-4 gel. As such, the storage modulus data may underrepresent the actual stiffness of 5 mg/mL P_{11}-4 gels formed in tissue culture media. Nevertheless, the change in sol-gel state at such low strain highlights the fragility of low-concentration P_{11}-4 gels and the difficulty in handling them.

The data for the 2.5 mg/mL gel was obtained using the same strain rate as that used for other concentrations and confirms that wall slippage has occurred when measuring the sample meaning that the stiffness of the material cannot be determined.

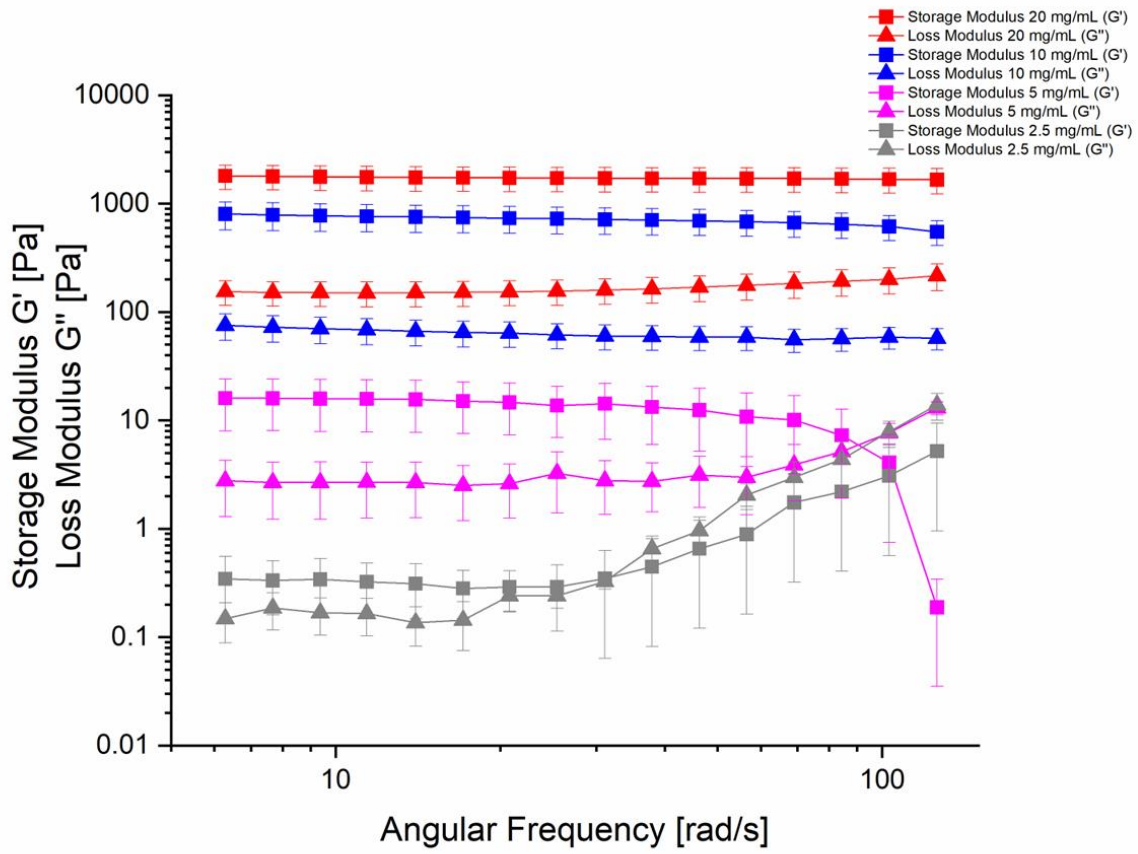

Figure 10 Frequency sweeps performed on 20, 10, 5 and 2.5 mg/mL $P_{11\text{-}4}$ gels at a strain rate of 0.1%. The storage modulus of the 20 mg/mL gel was found to be the highest. The storage modulus then reduced in a non-linear fashion as the gel concentration was reduced by 50%. Error bars represent the standard error of the mean. All experiments were performed in triplicate.

From the results of the rheology data, the 10 mg/mL gel offered a hydrogel system that had a stiffness in the range of other materials that have been demonstrated to facilitate vascularisation whilst at the same time being of a stiffness that allows handling of the gels during cell culture. Therefore, it was determined that the 10 mg/mL concentration gel would be taken forward into experimental work investigating whether P_{11}-4 can be used for supporting vascularisation.

5.2.2 2D cell culture on 10 mg/mL P_{11}-4 gels

To investigate whether 10 mg/mL P_{11}-4 gels could support cell growth, HUVECs and DPSCs were cultured on the surface of gels at a density of 1 x 10^5 cells/mL for 24 hours to observe if cells were able to attach to the surface of gels. After this time, HUVECs showed no attachment and displayed a non-adherent cell-type morphology (Figure 11). DPSCs on the other hand demonstrated cell attachment to the surface of the gel and had begun to spread (white arrows).

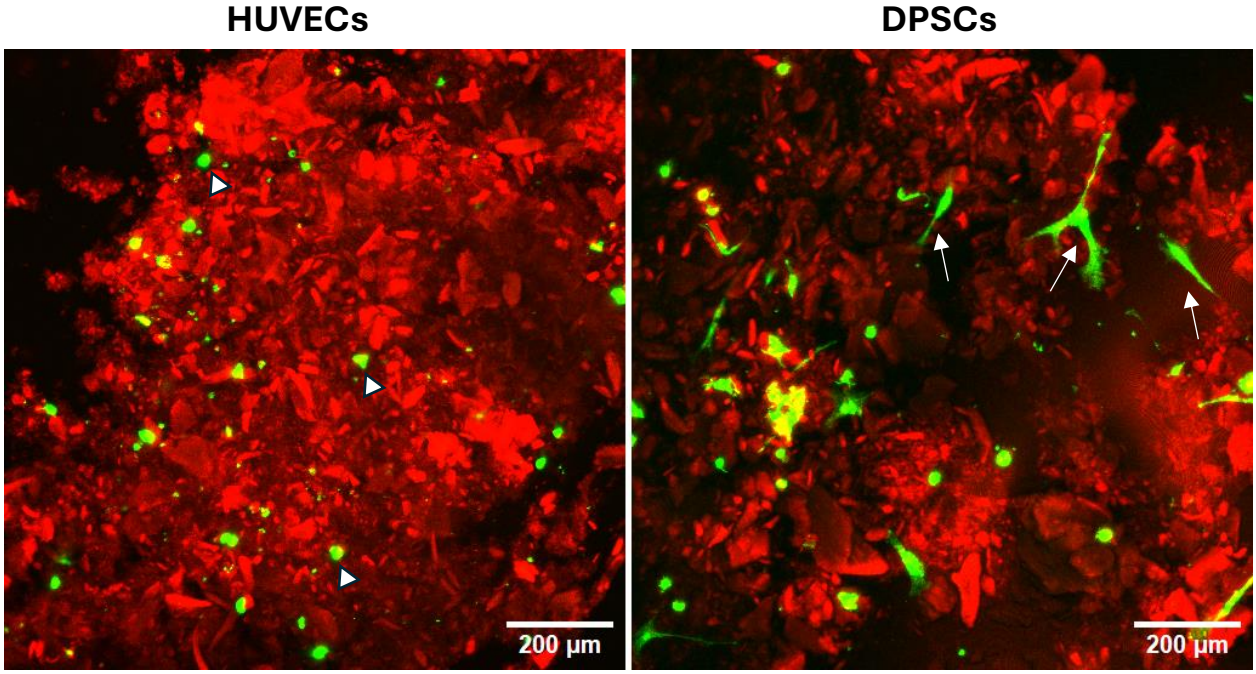

Figure 11 - Maximum intensity Z-stack projection of 2D cell culture of HUVECs (left) and DPSCs (right) on the surface of 10 mg/mL P11-4 gels after 24 hours of culture. Live cells are stained green using Calcein AM. Dead cells stained red with Ethidium Homodimer-1 are difficult to identify due to the intense red fluorescent signal produced by P11-4. HUVECs display a non-adherent circular cell morphology (left: white arrow heads) whereas several DPSCs have attached to the gel and spread out on the surface of the gel (right: white arrows). Experiments were performed in biological triplicates with technical replicates.

An analysis of cell area, perimeter and circularity was performed on HUVECs and DPSCs cultured on 10 mg/mL P_{11}-4 gels to compare parameters of cell spreading between both populations. As shown in Figure 12, HUVECs had a significantly smaller cell area and cell perimeter than DPSCs and a significantly greater measure of circularity with a measure of 1 being that of a perfect circle. These results demonstrate that HUVECs retained an unattached morphology being compact and almost perfectly circular whereas DPSCs had spread to cover a larger area and were significantly less circular.

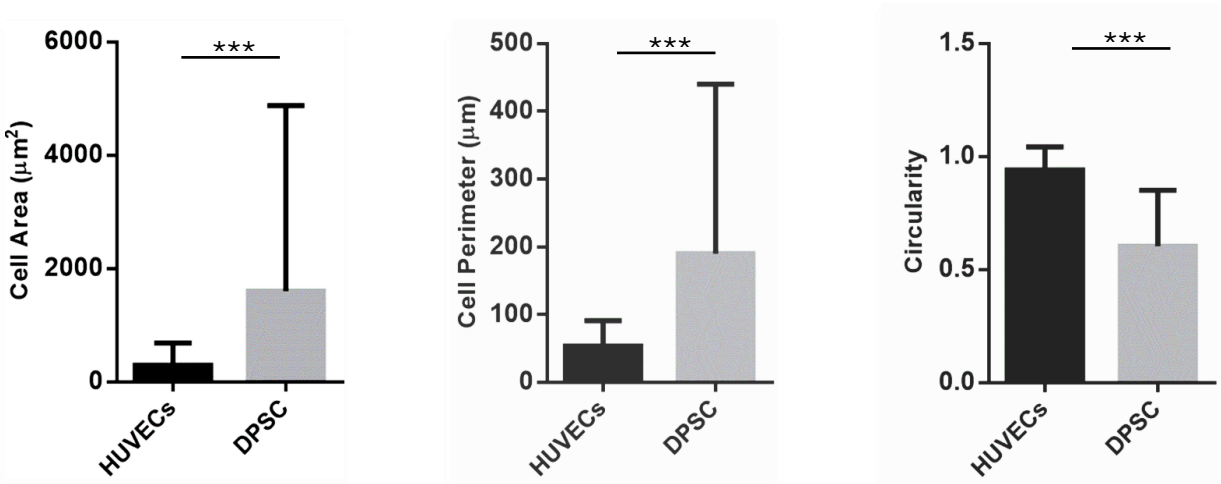

*Figure 12 – Graphs comparing the analysis of cell area, cell perimeter and circularity of HUVECs and DPSCs growing on 10 mg/mL P_{11}-4 gels. The graphs demonstrate the unattached cell phenotype of HUVECs having a cell area and perimeter which is significantly lower than DPSCs whilst having a circularity measure close to that of a perfect circle. Error bars represent standard deviation. Statistical analysis was performed using unpaired t-test. *** P-value <0.001.*

As HUVECs did not appear to have attached to the gel surface but remained viable after 24 hours, the experiment was repeated but cells were cultured for 48 hours to determine whether HUVECs would form an attachment after an extended period and stained with live/dead staining as described in Section 3.3.2. It was found that after a further 24 hours of culture, HUVECs did not appear to attach to the surface of the gels though processes extending from the cells were noted (Figure 13 – white arrows). After 48 hours of incubation, DPSCs were again found to have attached to the surface of the gel and had begun to migrate on its surface.

In both cell types, the number of cells seemed to have increased suggesting that cells were viable and healthy enough to multiply, however, it was not possible to quantify cell number or viability. Due to the fragile nature of P_{11}-4 hydrogels, during aspiration of cell culture media and pipetting, fragments of P_{11}-4 gels slough off the surface which interfere with measurements making testing using methods such as the Alamar Blue assay unreliable.

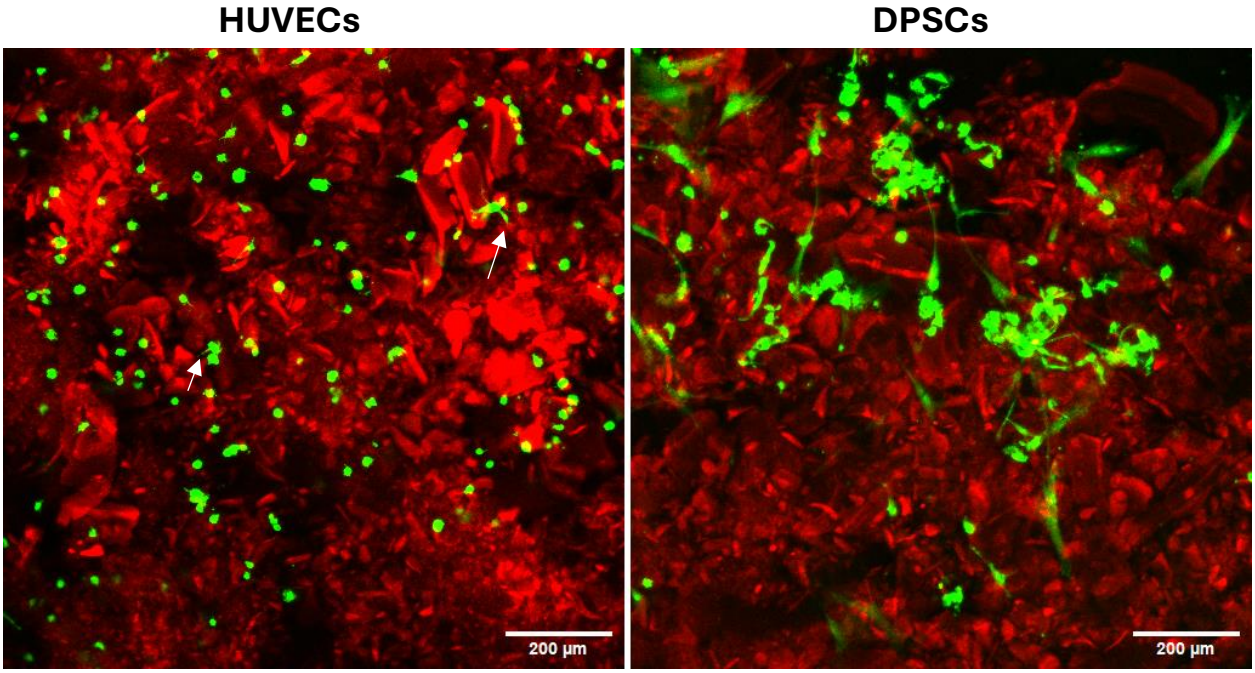

Figure 13 Maximum intensity Z-stack projection of HUVECs (left) and DPSCs (right) growing on the surface of 10 mg/mL P11-4 gels after 48 hours of cell culture. HUVECs largely express a non-adherent cell morphology though processes emanating from cells (white arrows) may indicate attempts to interact with the surface of the gel. DPSCs were found to have attached to the surface of the gel and spread. Experiments were performed in biological triplicates with technical replicates.

5.2.3 3D cell culture within 10 mg/mL P_{11}-4 gels

As HUVECs maintained a non-adherent cell morphology and did not spread on the surface of 2D P_{11}-4 gels, both HUVECs and DPSCs were cultured in 3D gels to explore whether this may improve their ability to attach to the gel. Cells were encapsulated and cultured at a seeding density of 1 x 10^6 cells/mL in 10 mg/mL P_{11}-4 gels and cultured for 24 hours and 48 hours. Cells were labelled after each time point as described in Section 3.3.2 for imaging.

After 24 hours, HUVECs remained viable within the gels as demonstrated by being positively labelled with Calcein green, however, no cellular attachment to the gel was found as shown by the round, non-adherent cell morphology of HUVECs in Figure 14. DPSCs on the other hand were found to attach to the surface of the gel and began spreading (white arrow – Figure 14)

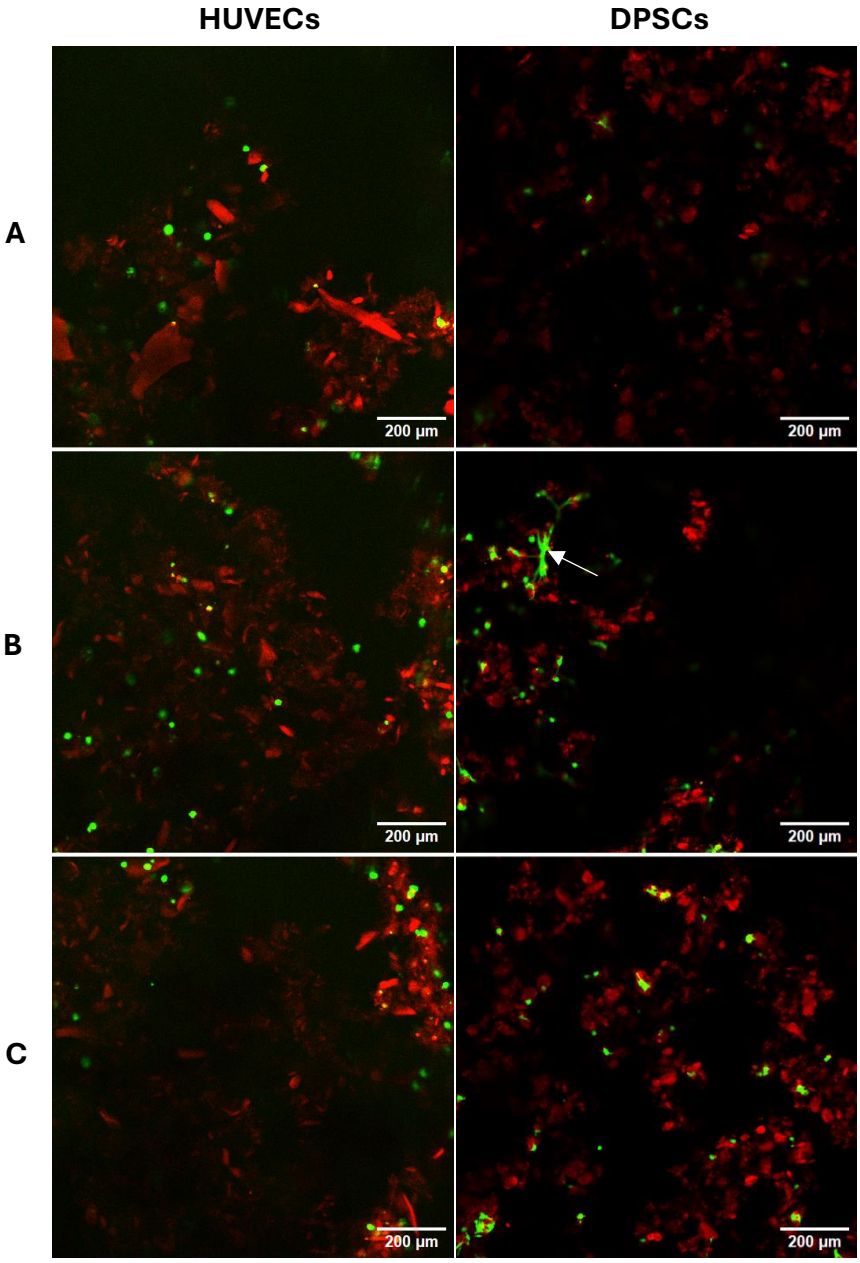

Figure 14 Z-stack montage of HUVECs (left) and DPSCs (right) cultured for 24 hours in 10 mg/mL P11-4 hydrogels. Samples were stained with Live/Dead staining prior to imaging which label viable cells as green and dead cells as red. Due to the fluorescent signal produced by P11-4 it is difficult to distinguish dead cells. Rows A, B and C correspond to the base of the gel, middle of the gel and top of the gel respectively. Images were captured at 10x magnification. Experiments were performed in biological triplicates with technical replicates.

After 48 hours of culture in 10 mg/mL P_{11}-4 gels, HUVECs showed no obvious signs of attachment and maintained a rounded, non-adherent cell morphology (Figure 15).

After 48 hours of culture, DPSCs showed a high degree of attachment and migration within the 3D P_{11}-4 gel as demonstrated by the number of elongated cells attached to the gel (Figure 15). This shows that whilst HUVECs remain unable to attach to the surface of 2D or 3D P_{11}-4 gels, the material is non-cytotoxic to DPSCs and is a suitable material to support their growth.

To quantify the spreading of DPSCs within P_{11}-4 and develop methods to assess HUVEC migration in future studies, analysis of the 3D cell images was attempted within ImageJ. To do this, thresholding of 3D image stacks was performed so that further processing such as skeletonisation could be utilised to map networks of cells and quantify parameters such as cell shape and connectivity. However, built in automatic thresholding algorithms were able to satisfactorily segment images and accurately identify cells throughout samples which prevented quantitation of cell migration and network formation within P_{11}-4 hydrogels.

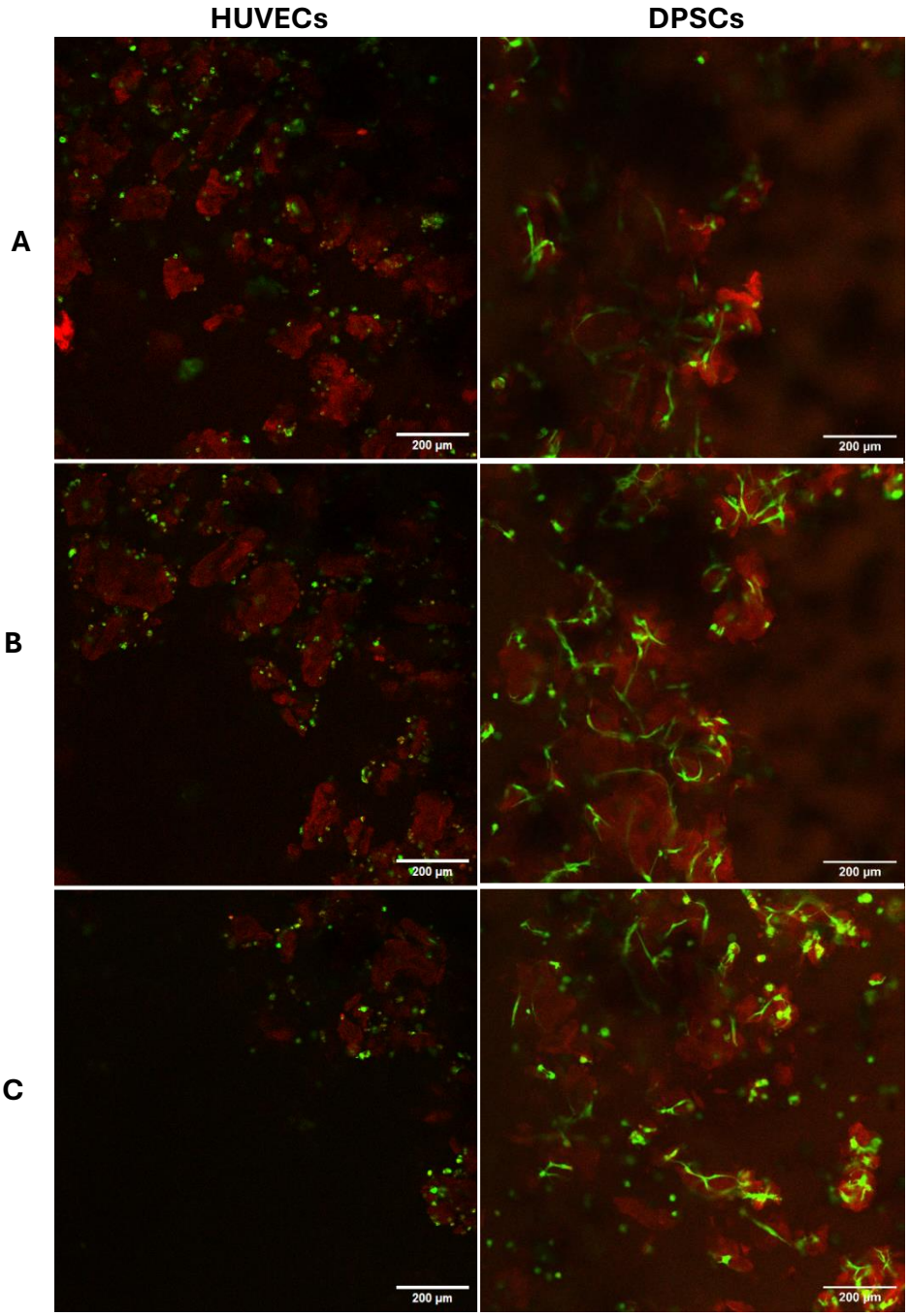

Figure 15 Z-stack montage of HUVECs (left) and DPSCs (right) cultured for 48 hours in 10 mg/mL P11-4 hydrogels. Samples were stained with Live/Dead staining prior to imaging which label viable cells as green and dead cells as red. Due to the fluorescent signal produced by P11-4 it is difficult to distinguish dead cells. Rows A, B and C correspond to the base of the gel, middle of the gel and top of the gel respectively. Images were captured at 10x magnification. Experiments were performed in biological triplicates with technical replicates.

5.2.4 Effect of Fibronectin Coating on HUVEC Adhesion to P_{11}-4 Hydrogels

As HUVECs had not attached and migrated on the surface of P_{11}-4 gels in previous experiments but had displayed some cellular processes that may have been an attempt to attach (Figure 13), P_{11}-4 gels were surface coated with a layer of fibronectin as described in Section 3.4.5 to determine whether the presence of an extracellular matrix protein could aid in their attachment.

After 24 hours of culture on the surface of a 10 mg/mL P_{11}-4 gel without fibronectin, HUVECs remained unattached to the gel as in all previous experiments (Figure 16 – A). However, after being cultured on the surface of a 10mg/mL P_{11}-4 gel coated with fibronectin, HUVECs displayed a high degree of attachment and spreading (Figure 16 - B) showing that it is possible that HUVECs require a greater amount of ECM proteins to bind to the surface of the gel in comparison to DPSCs.

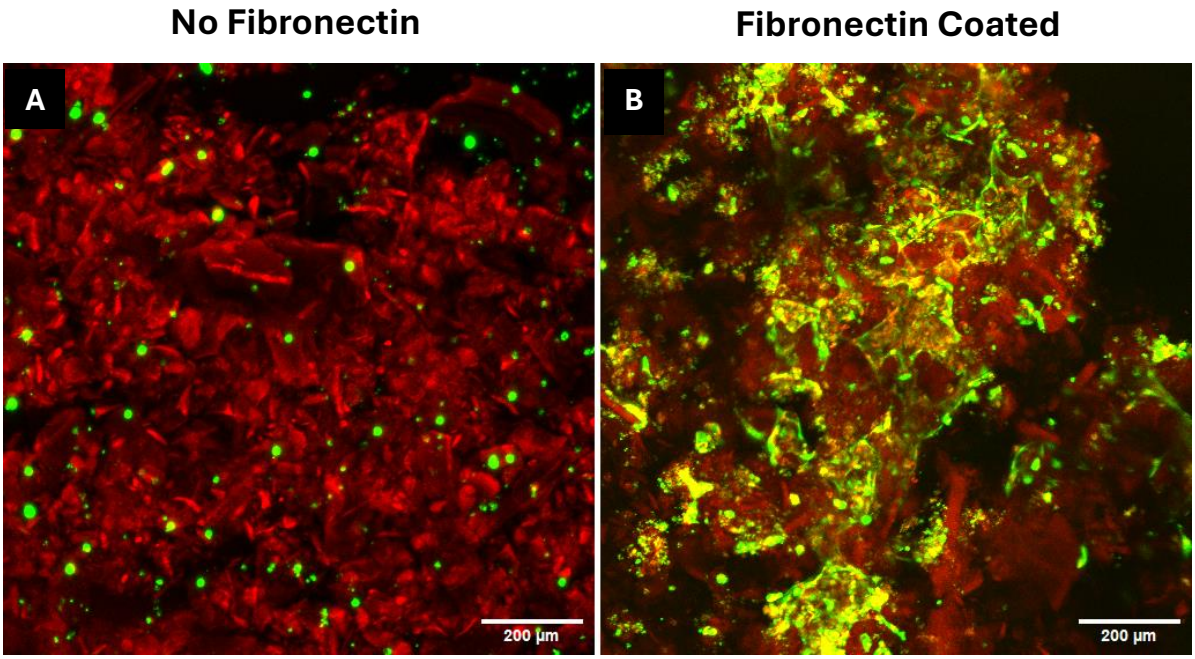

Figure 16 Maximum intensity Z-stack projections of HUVECs growing on P11-4 gels either uncoated (A) or coated with fibronectin (B). The cells cultured on the P11-4 gel without fibronectin maintained a non-adherent cell morphology whereas the HUVECs cultured on the fibronectin coated gel display a high degree of attachment and spreading. Experiments were performed in biological triplicates with technical replicates.

5.2.5 3D culture of HUVECs and DPSCs within agarose encapsulated P_{11}-4 hydrogels

As HUVECs were able to attach and spread on P_{11}-4 gels coated with fibronectin, it was hypothesised that extending the amount of time in culture would allow HUVECs to secrete a sufficient amount of ECM to attach to P_{11}-4 without the need for supplemental fibronectin. However, as previously discussed, 10 mg/mL P_{11}-4 gels are fragile and erode with repeated exposure to shear forces such as those created by aspirating media and replacing it during cell culture. To overcome this, agarose moulds were created as described in Section 3.4.7 so that P_{11}-4 gels could be protected during the number of media changes required to culture cells for long time periods. The envelope of agarose that contained the P_{11}-4 gels was prepared using a final concentration of 0.5% which was sufficiently strong to protect the sample whilst also allowing mass transport to the cells contained within it.

After 24 hours of culture within the agarose encapsulated P_{11}-4 gels, HUVECs displayed no obvious signs of attachment and maintained a non-adherent cell morphology as expected (Figure 17 - Left). DPSCs on the other hand demonstrated a high degree of attachment and spreading on the gel (Figure 17 – Right).

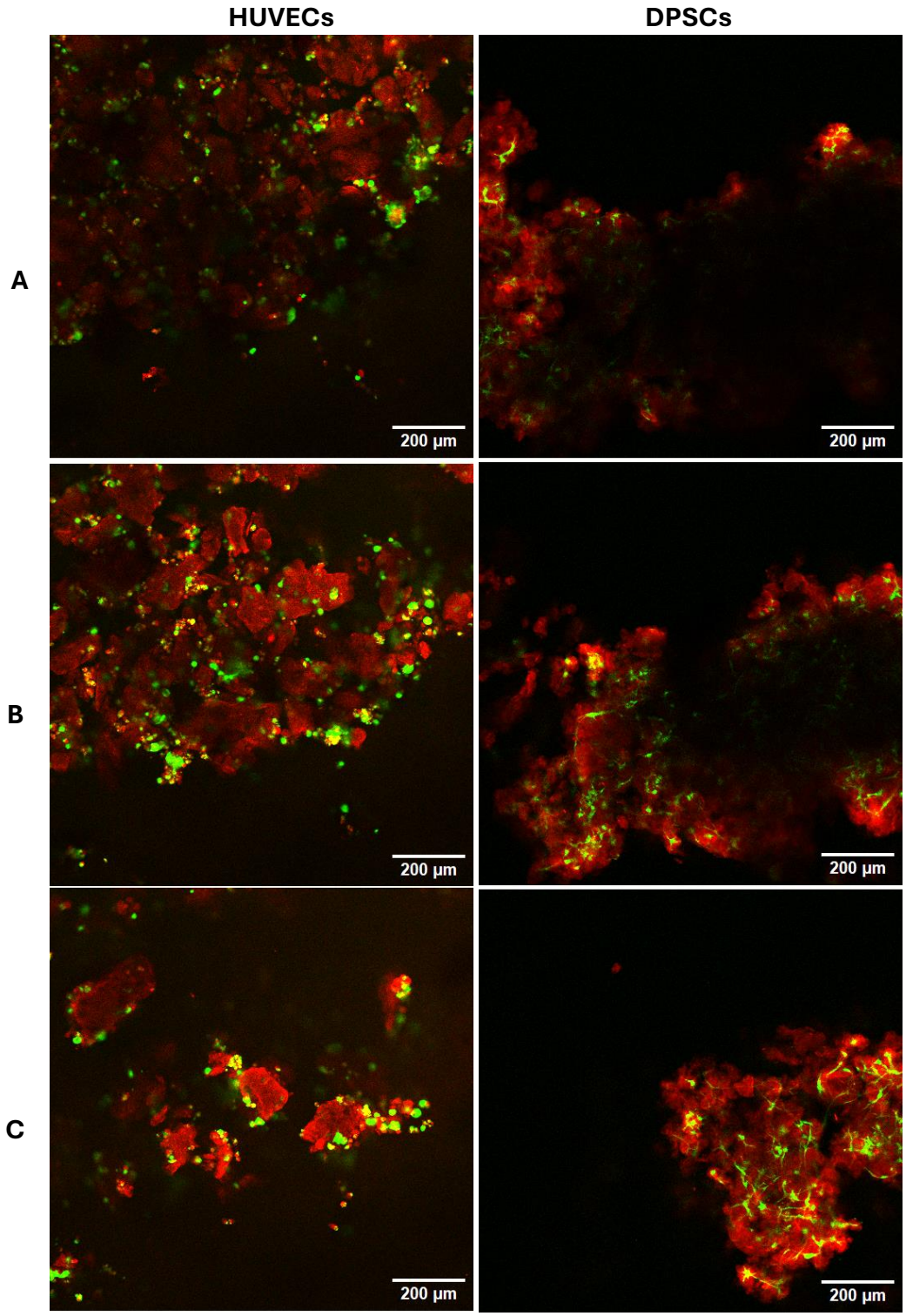

Figure 17 Z-stack montage of HUVECs (left) and DPSCs (right) growing within 10 mg/mL P11-4 gels encapsulated within 0.5% agarose gels for 24 hours. HUVECs show no obvious sign of attachment to the gel maintaining a rounded cell morphology whereas DPSCs display a high degree of attachment and spreading. Samples were stained with Live/Dead staining prior to imaging which label viable cells as green and dead cells as red. Due to the fluorescent signal produced by P11-4 it is difficult to distinguish dead cells. Rows A, B and C correspond to the base of the gel, middle of the gel and top of the gel respectively. Images were captured at 10x magnification. Experiments were performed in biological triplicates with technical replicates.

After 7 days of culture within an agarose encapsulated P_{11}-4 gel, HUVECs remained unassociated with the P_{11}-4 gel as displayed below in Figure 18 - Left. Surprisingly, the cells remained viable after this time without attachment to the surface and had in fact appeared to have increased in number. However, after remaining unattached from the gel for a full week it was concluded that a lower rate of ECM production by HUVECs in comparison to DPSCs was unlikely to be the reason for an inability to attach to P_{11}-4.

Unlike HUVECs, the culture of DPSCs in agarose encapsulated P_{11}-4 gels yielded a densely cellularised gel after 7 days of culture with a high degree of cell proliferation throughout its entirety as displayed in Figure 18 - Right. This demonstrates that whilst encapsulation did not improve the adhesion of HUVECs to the gel, the encapsulation of P_{11}-4 may be useful for the creation of tissue engineering constructs using other cell types.

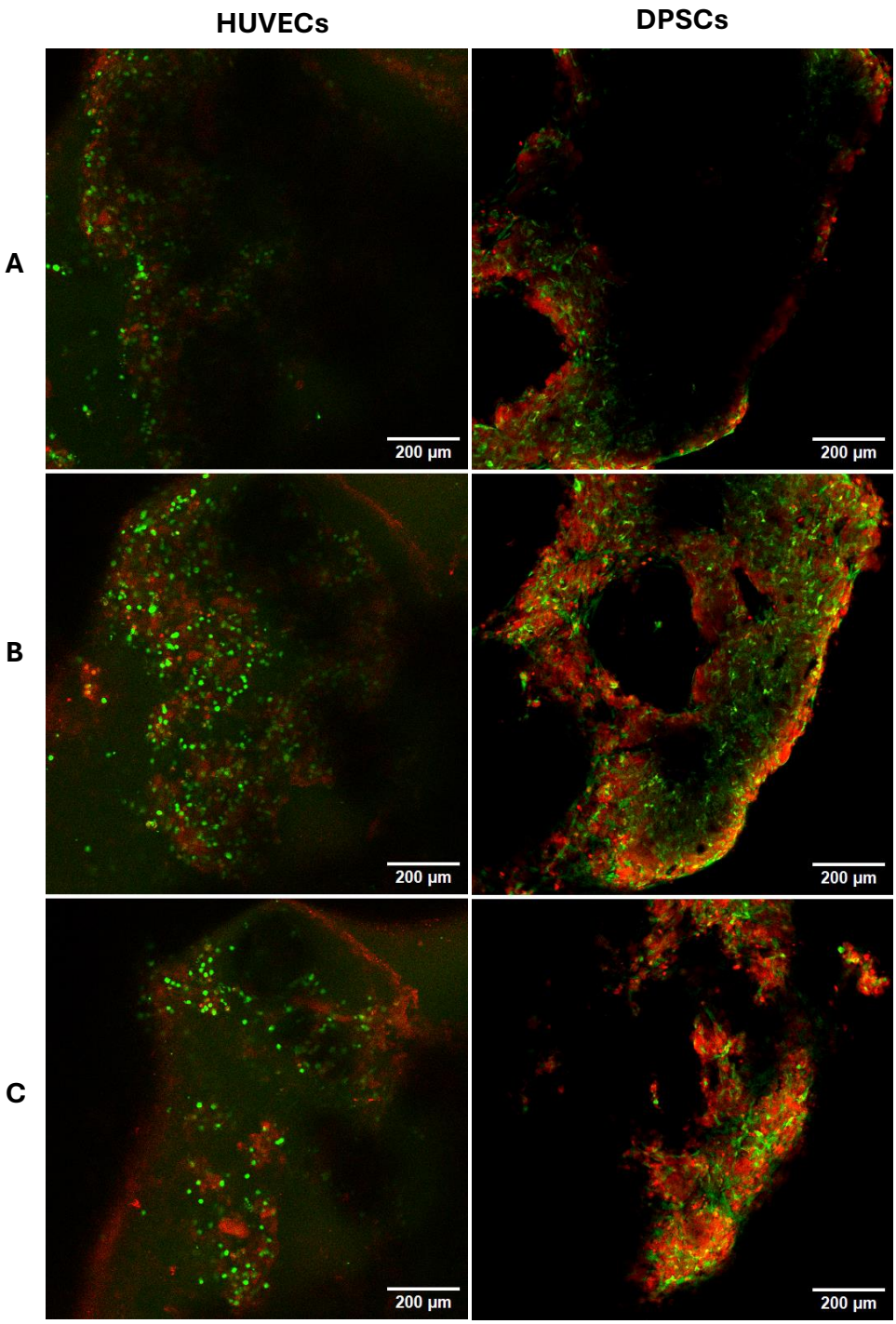

Figure 18 Z-stack montage of HUVECs (left) and DPSCs (right) growing within 10 mg/mL P11-4 gels encapsulated within 0.5% agarose gels for 7 days. HUVECs show no obvious sign of attachment to the gel maintaining a rounded cell morphology whereas DPSCs have proliferated within the gel to form a densely cellularised construct. Samples were stained with Live/Dead staining prior to imaging which label viable cells as green and dead cells as red. Due to the fluorescent signal produced by P11-4 it is difficult to distinguish dead cells. Rows A, B and C correspond to the base of the gel, middle of the gel and top of the gel respectively. Images were captured at 10x magnification. Experiments were performed in biological triplicates with technical replicates.

5.2.6 Assessment of HUVEC Surface Adhesion After Exposure to P_{11}-4

As HUVECs had been unable to attach to P_{11}-4 gels and spread as demonstrated by maintaining a rounded morphology in all previous experiments, it was decided to investigate whether P_{11}-4 disrupted the ability of HUVECs to form cellular attachments to surfaces through an unknown mechanism. To do this, HUVECs were grown in monolayer on 96 well plates until reaching approximately 80% confluency as described in Section 3.4.8. Following this, cells were exposed to different concentrations of P_{11}-4 gel (10 mg/mL, 5 mg/mL and 2.5 mg/mL) to determine if exposure to the gel would cause the cells to detach from tissue culture plastic.

As can be seen in Figure 19, exposure to 10 mg/mL and 5 mg/mL P_{11}-4 gels for 24 hours had no noticeable impact on the morphology of cells or their ability to adhere to the surface of tissue culture plastic in comparison to untreated control HUVECs. Due to P_{11}-4 gels being fragile, gels fracture whilst pipetting which leaves some areas with no gel (dark regions). In both the 10 mg/mL and 5 mg/mL exposure groups, being in a region with or without gel appeared to have no impact on cell morphology or the general arrangement of the cells. However, after exposure to 2.5 mg/mL P_{11}-4 gel, the overall organization of cells appeared to have altered in response to the location of gel particulates with some cells appearing to interact directly with the gel (white arrows Figure 19-D).

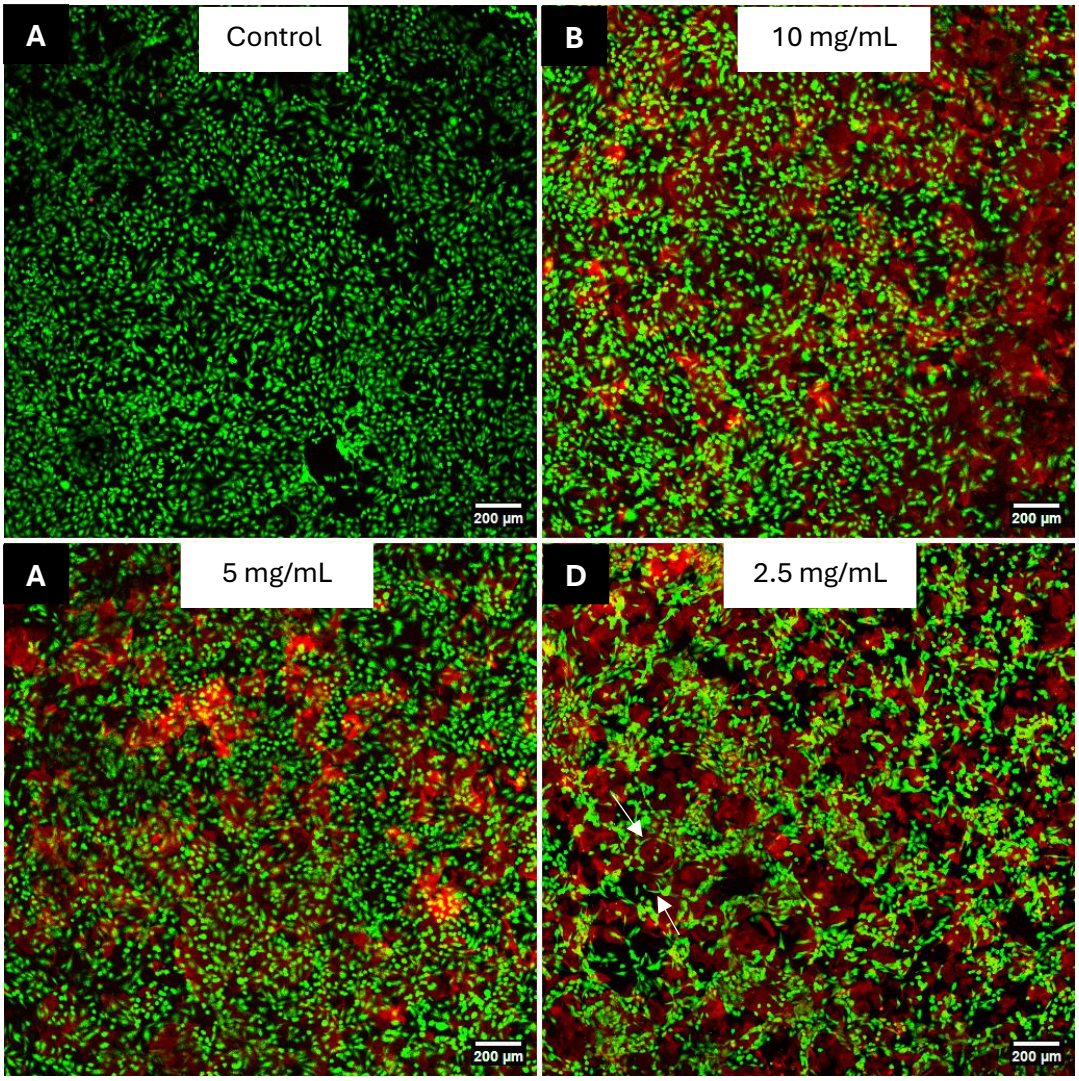

Figure 19 Max intensity projections displaying confluent HUVEC monolayers treated with different concentrations of P11-4 gel. Treatment with 10 and 5 mg/mL concentration gels did not appear to impact the ability of HUVECs to adhere to the surface of tissue culture plastic. Treatment with 2.5 mg/mL however appears to alter the general arrangement of cells and some cells can be seen to be interacting directly with the gel (white arrows, D). Experiments were performed in biological triplicates with technical replicates.

5.2.7 2D culture of HUVECs on low concentration P_{11}-4 hydrogels

As exposure to 2.5 mg/mL P_{11}-4 gels appeared to result in cell migration and attachment, it was decided to explore whether HUVECs were able to interact with P_{11}-4 at this lower concentration when cultured directly on its surface. HUVECs were cultured on the surface of 10 mg/mL, 5 mg/mL and 2.5 mg/mL gels for 24 hours to assess whether they would attach to the gel. Although no change in cell morphology or gel attachment was seen in the 5 mg/mL concentration exposure treatment in the previous experiment (Figure 19), this concentration was also tested to ensure that it was unable to support cellular attachment.

After 24 hours of culture on 10 mg/mL gels, HUVECs remained unattached as in previous experiments (Figure 20 – Top) as was the case for HUVECs cultured on 5 mg/mL gels (Figure 20 – Centre). However, HUVECs cultured on the surface of 2.5 mg/mL gels displayed a high degree of attachment and spreading after 24 hours (Figure 20 – Bottom). This demonstrates that HUVECs are in fact able to attach to P_{11}-4 though the concentration of peptide used must be lower than 5 mg/mL.

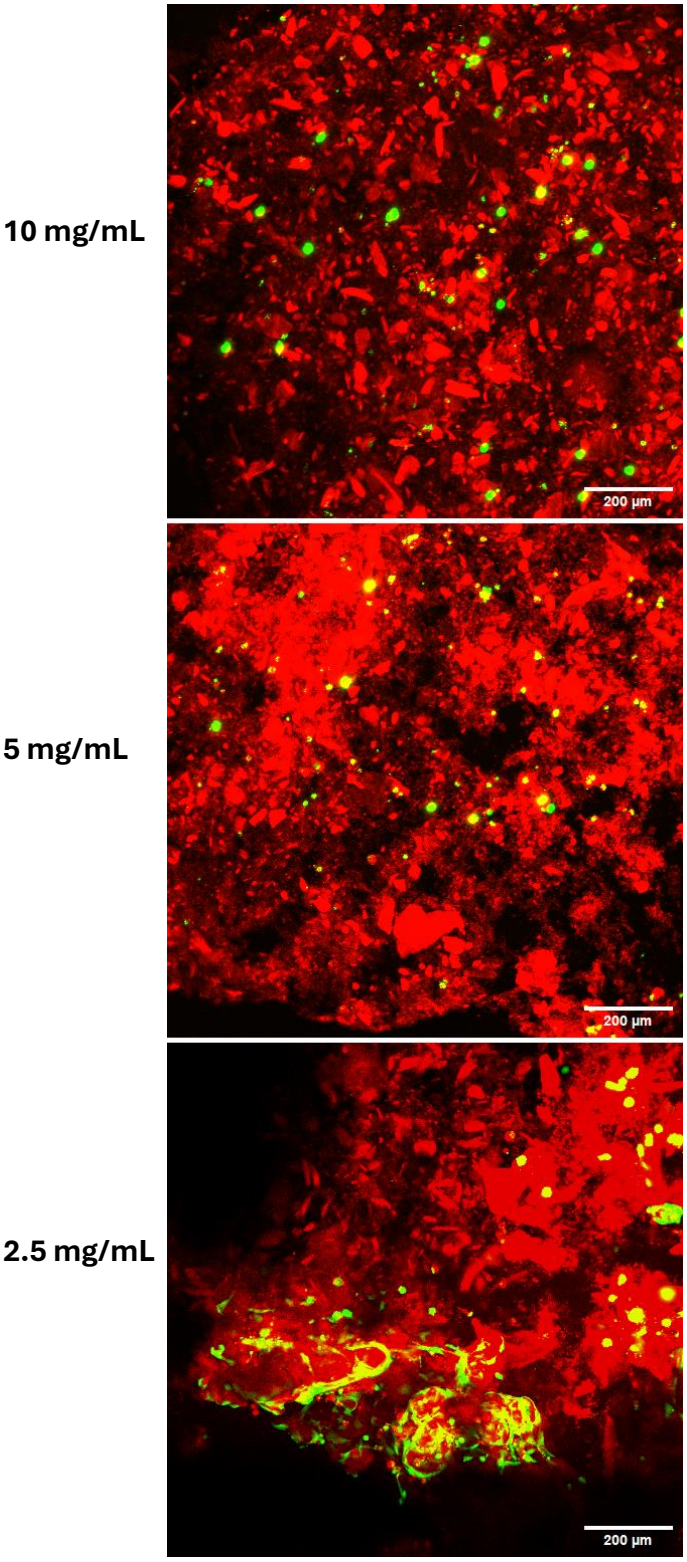

Figure 20 Maximum intensity Z-stack projections of HUVECs (green) growing on 10 mg/mL (top), 5 mg/mL (centre) and 2.5 mg/mL (bottom) P11-4 gels after 24 hours of cell culture. HUVECs cultured on the surface of the 10 mg/mL and 5 mg/mL gels exhibit a non-adherent cell morphology whereas HUVECs growing on 2.5 mg/mL gels display a high degree of attachment and spreading on its surface. Experiments were performed in biological triplicates with technical replicates.

5.2.8 3D culture of HUVECs in 2.5 mg/mL P_{11}-4 hydrogels

After establishing that HUVECs were capable of attaching to 2D 2.5 mg/mL P_{11}-4 gels, their ability to grow within 3D gels of the same concentration was investigated. To do this, HUVECs were encapsulated within a 3D 2.5 mg/mL P_{11}-4 gel for 24 hours, the results of which can be found in Figure 21 - A. As shown, HUVECs attached to the surface of the 3D 2.5 mg/mL P_{11}-4 gel and rapidly formed continuous networks of cells throughout the full thickness of the gel.

It was not possible to determine whether the structures formed were lumenised vascular-like structures due to being unable to perform immunofluorescent staining on the gels. This was not possible due to the number of times fluid is aspirated and replaced during staining protocols which eroded the gel and also due to the level of background signal during labelling caused by non-specific binding of antibodies to the gel surface.

HUVECs were also cultured in 3D 2.5 mg/mL P_{11}-4 gels for 48 hours to determine if the networks formed after 24 hours were stable. As shown in Figure 21 - B, the structures formed by HUVECs within the low concentration gels collapse between 24-48 hours of culture, similar to that seen in networks formed by HUVECs during Matrigel tube formation assays.

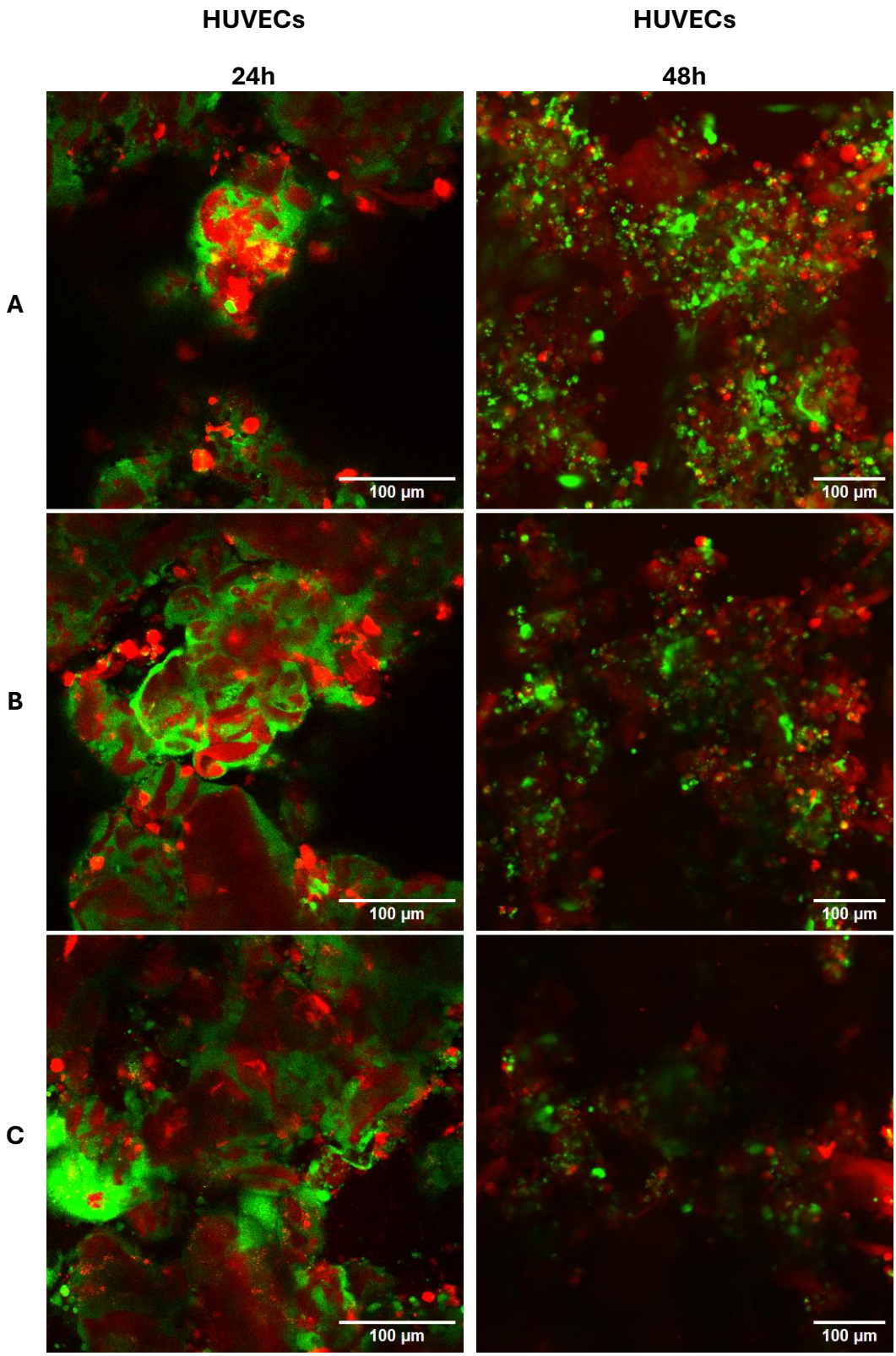

Figure 21 Z-stack montages of HUVECs cultured for 24h (left) and 48h (right) growing within 3D 2.5 mg/mL P11-4 gels. After 24h, HUVECs formed continuous cellular networks throughout the P11-4 gels. After 48h of culture, these structures had collapsed, similar to the process seen network collapse during Matrigel tube formation assays after 24 hours. Samples were stained with Live/Dead staining prior to imaging which label viable cells as green and dead cells as red. Due to the fluorescent signal produced by P11-4 it is difficult to distinguish dead cells. Rows A, B and C correspond to the base of the gel, middle of the gel and top of the gel respectively. Images were captured at 10x magnification. Experiments were performed in biological triplicates with technical replicates.

5.2.9 3D culture of differentiated DPSCs in 2.5 mg/mL P_{11}-4 hydrogels

Once it was established that HUVECs were able to form structures within P_{11}-4 hydrogels, DPSCs differentiated into endothelial cells for 10 days (as described in Chapter 4) were investigated using the same concentration of gel to determine whether they formed similar structures to HUVECs. To do this, cells were encapsulated within 3D 2.5 mg/mL P_{11}-4 gels at a density of 1 x 10^6 cells/mL and cultured for 24 hours. The results for HUVECs, untreated DPSCs and endothelial-differentiated DPSCs are displayed below in Figure 22.

As shown, HUVECs cultured in 2.5 mg/mL gels formed a continuous network of cells throughout the full thickness of the gel. However, neither untreated nor differentiated DPSCs behaved in a similar fashion. In the untreated DPSCs, cells can be seen interacting with the P_{11}-4 gel, however many cells appear to have a less flattened morphology than in previous experiments such as those seen in Figure 15 previously. This pattern of attachment and spreading is also true for differentiated DPSCs which are almost indistinguishable from their undifferentiated counterpart.

These results therefore indicate that whilst differentiated DPSCs were shown to be similar in function to HUVECs on Matrigel tube formation assays in Chapter 4, they are not comparable to true endothelial cells within this type of gel.

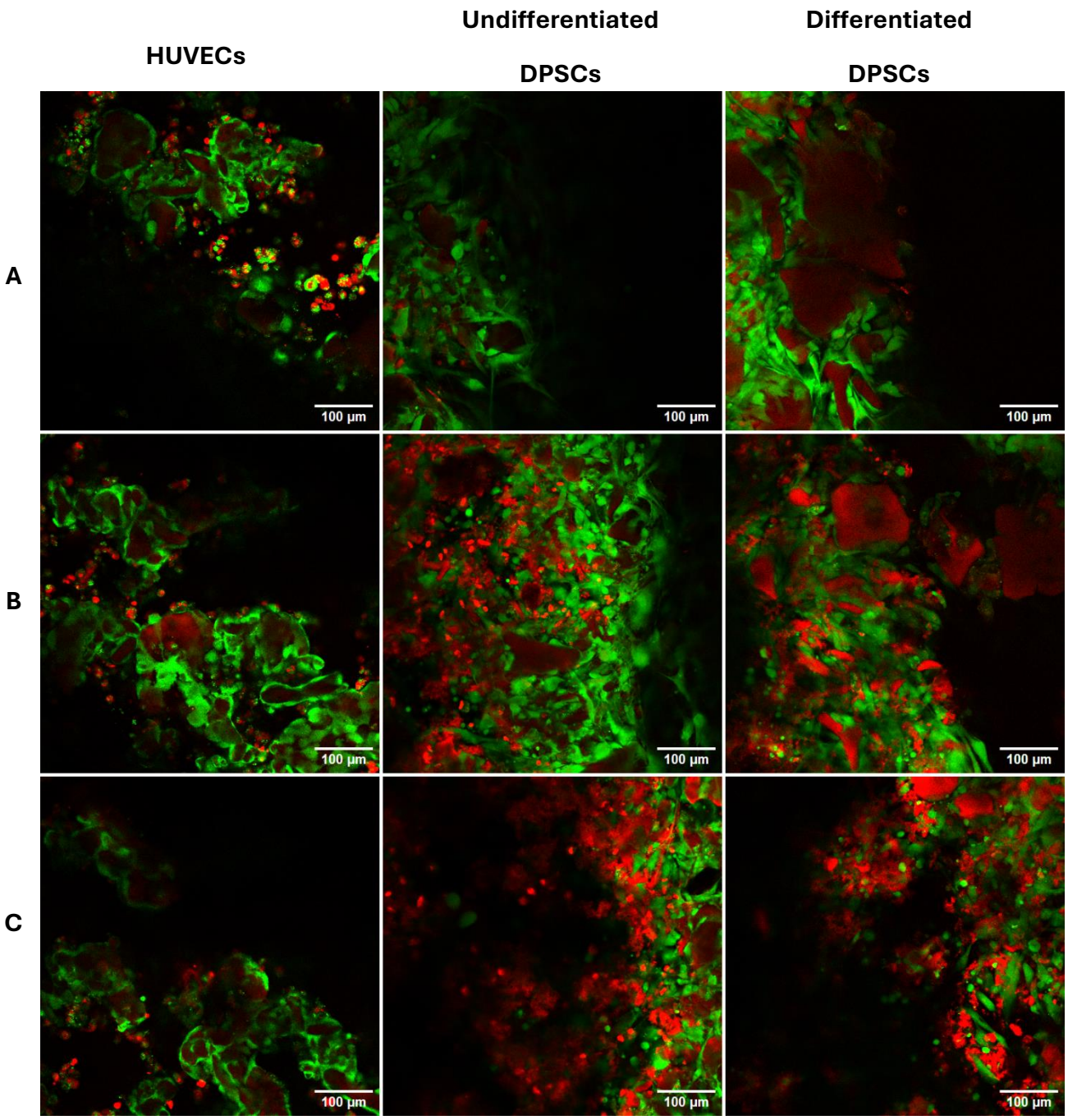

Figure 22 Z-stack montages of HUVECs (left), undifferentiated DPSCs (center) and DPSCs which had undergone 10 days of endothelial differentiation (right) growing in 3D 2.5 mg/mL P11-4 hydrogels for 24 hours. HUVECs formed attached to the gel and formed continuous cellular networks after this time period. Undifferentiated DPSCs interacted with the gel and were able to attach and spread on its surface and were arranged in a random fashion on the gel surface. Differentiated DPSCs demonstrated the same morphology and did not form networks. Samples were stained with Live/Dead staining prior to imaging which label viable cells as green and dead cells as red. Due to the fluorescent signal produced by P11-4 it is difficult to distinguish dead cells. Rows A, B and C correspond to the base of the gel, middle of the gel and top of the gel respectively. Experiments were performed in biological triplicates with technical replicates.

5.3 Discussion

The research presented in this chapter was conducted to assess the suitability of the self-assembling peptide P_{11}-4 to be used as a scaffold material for the generation of vascularised 3D tissue engineering constructs. This was investigated by first selecting a P_{11}-4 peptide concentration that would generate a hydrogel with a material stiffness in the same range as soft tissues. The selected P_{11}-4 gel concentration (10 mg/mL) was then assessed for its biocompatibility and suitability as a material to support vascularisation.

It was found that P_{11}-4 was biocompatible with both HUVECs and DPSCs, however, the 10 mg/mL gel concentration was only able to support the growth and proliferation of DPSCs with HUVECs being unable to either attach or spread on its surface. Nevertheless, it was also found that a low concentration of P_{11}-4 (2.5 mg/mL) was able to facilitate HUVEC attachment in both 2D and 3D cell culture and that when cultured in 3D hydrogels at this concentration, HUVECs were able to form continuous cell networks. Additionally, the ability of DPSCs which had underwent 10 days of endothelial differentiation to form networks on the 2.5 mg/mL P_{11}-4 gel was also investigated. It was found that differentiated DPSCs were unable to form networks on the gel and that their behaviour was indistinguishable from undifferentiated cells.

This research demonstrates for the first time that P_{11}-4 hydrogels are able to facilitate the growth and development of cellular networks by endothelial cells (HUVECs), albeit at a concentration with limited applications in tissue engineering. Furthermore, by encapsulating P_{11}-4 gels within a protective barrier it was also demonstrated that it is possible to culture cells within the scaffold for at least 7 days *in vitro*. This method made it possible to overcome one of the greatest problems of using P_{11}-4 as a scaffold material *in vitro* which may enable it to be explored for different tissue engineering applications in the future.

5.3.2 Peptide concentration selection based on hydrogel stiffness

As no prior work existed regarding the use of P_{11}-4 as a scaffold material for the development of vasculature; the most appropriate way to select a concentration of peptide to be used in experiments was based on material stiffness. As discussed in the introduction of this chapter, material stiffness has been demonstrated to greatly impact the behaviour of endothelial cells and their ability to form vasculature.

Hydrogels have been successfully vascularised with stiffnesses ranging from 0.031- 13 kPa (Table 11) with stiffnesses in the range of 200-600 Pa being demonstrated to be optimal for vascularisation in several studies that compared different stiffness materials.

Previous work examining what effect peptide concentration has on the stiffness of P_{11}-4 hydrogels has yielded varying results. For example, El-Sayed (2020) found that P_{11}-4 gels with a concentration of 30 mg/mL had a storage modulus (G') of < 1 kPa (El-Sayed et al., 2020) whereas research conducted by Koch (2018) found that P_{11}-4 gels with a concentration of 15 mg/mL have a storage modulus of 2 kPa (Koch, Müller, et al., 2018). The most likely cause of the discrepancy between the publications is the constituents of the buffer that the gels were prepared in as differences in properties such as ionic strength (Feng et al., 2012) have been demonstrated to alter the stiffness of SAP hydrogels.

A range of concentrations (20, 10, 5 and 2.5 mg/mL) of P_{11}-4 were selected to establish the stiffness of different hydrogel concentrations in endothelial cell culture media as this appeared as a likely range to yield gels with stiffnesses similar to those that have supported vascularisation in previous research.

The results of the rheology experiments found that the storage modulus of 20, 10 and 5 mg/mL P_{11}-4 gels was 1726 ± 440 Pa, 710 ±196 Pa and 13 ± 7 Pa respectively. It was decided that a concentration of 10 mg/mL offered an appropriate concentration to begin cell culture experiments with for two primary reasons.

Firstly, prior research has demonstrated that whilst hydrogels with a wide range of stiffnesses are able to support vascularisation, materials with a stiffness <1 kPa often improve vascularisation when compared to the same material with a stiffness >1 kPa. Therefore, a concentration of 10 mg/mL was preferred over the 20 mg/mL concentration.

Secondly, whilst a peptide concentration of 5 mg/mL also produced a hydrogel with a stiffness <1 kPa, it had a stiffness considerably lower than what has been reported as supporting vascularisation previously (13 Pa vs 31 Pa). Furthermore, the low storage modulus of the 5 mg/mL concentration P_{11}-4 gel was also deemed unsuitable as an initial gel concentration to work with due to the nature of P_{11}-4 gels. The assembly of self-supporting P_{11}-4 gels is accomplished through hydrogen bonding between peptide fibrils as discussed in Section 1.3.4. P_{11}-4 hydrogels are thixotropic and agitation by direct movement or shear forces produced by aspirating and pipetting media during cell culture can overcome these intermolecular forces returning the gel to a liquid state. This is further exacerbated by increased temperature which weakens bonding and makes reassembly after returning to rest kinetically unviable. As the number of hydrogen bonds decreases with decreasing peptide concentration, low concentration P_{11}-4 gels are impractical to use due to being unstable.

To the author's knowledge, only one piece of published literature exists in which P_{11}-4 has been used at a concentration of <10 mg/mL and this study investigated whether the peptide was able to influence cell differentiation at concentrations of 1 mg/mL or less rather than utilising the peptide for its gel-forming properties (Camassari et al., 2023).

A concentration of 10 mg/mL was therefore selected for use in cell culture experiments as it was found to be of a stiffness within the range of other vascularisation research and that if vascularisation was possible on the material, the concentration of the P_{11}-4 gel could be optimized further.

5.3.3 Biocompatibility of P_{11}-4 and Cell Attachment

Throughout all experiments conducted in this research, P_{11}-4 has been found to have excellent biocompatibility as measured using live/dead staining on cells in direct contact with hydrogels. Live/dead staining was chosen as a measure of cytotoxicity as it provides an indication of viability whilst at the same time allowing visualisation of cells growing within the material.

The ability to visualise the cells in contact with the gel whilst assessing cell viability provided interesting insight into the behaviour of the cells as even though HUVECs did not appear to be attached to the gels, they remained viable for seven days in culture when the P_{11}-4 gel was protected by agarose (Figure - 11). This was an unexpected finding as HUVECs are an anchor dependent cell type which undergo anoikis, apoptosis resulting from prolonged detachment from the extracellular matrix (Fujio and Walsh, 1999). The rate of apoptosis in HUVECs has been found to be over 90% after being detached from a surface for 48 hours (Schulz et al., 2021) which raises the question of why the HUVECs which appeared to be non-adherent in this study were still viable much past this point.

To prevent anoikis, ligand binding alone is not sufficient (Re et al., 1994) and therefore the prolonged cell viability cannot be explained by the release of low concentrations of P_{11}-4 from the gel binding to receptors on HUVECs providing them with cues that they are attached to a substrate. Therefore, sufficient cellular attachment to the 10 mg/mL P_{11}-4 gel must have been present to prevent apoptosis but not allow normal flattening behaviour of the cells.

Several ECM proteins have been used to improve the attachment of HUVECs to surfaces *in vitro* such as fibronectin (Cornelissen et al., 2013) and laminin (Yu et al., 2021) and have been demonstrated to increase both attachment of cells to the surface of materials and to enhance their ability to spread. Previous research has demonstrated that fibronectin is able to be adsorbed onto the surface of P_{11}-4 gels (Koch, Wolff, et al., 2018b) and as such, 10 mg/mL P_{11}-4 gels were coated with fibronectin as described in Section 3.4.5 to determine if this improved the attachment and spreading of HUVECs on its surface.

The addition of fibronectin significantly improved the attachment and spreading of HUVECs on P_{11}-4 in this research (Figure 16) which led to the hypothesis that if provided with more time, HUVECs would secrete a sufficient amount of their own ECM to allow cell attachment and spreading on P_{11}-4 gels without the need for supplemental fibronectin. However, after 7 days in 3D culture on 10 mg/mL P_{11}-4 gels encapsulated in agarose, it was found that increasing the amount of time for ECM production did not improve HUVEC attachment or spreading.

Given that it has long been established that endothelial cells are capable of secreting a number of ECM proteins including fibronectin and that the secretion is directed towards the site of surface attachment (Unemoris et al., 1990; Kowalczyk et al., 1990; Davis and Senger, 2005; Wei et al., 2019), that P_{11}-4 has been shown to adsorb fibronectin and that this supported the growth of HUVECs in this study, plus the evidence that at least a weak attachment to the gel surface must have been present between the cells and gel to prevent apoptosis, why after a week in culture HUVECs were still not able to attach and spread on the surface of 10 mg/mL P_{11}-4 hydrogels remains an issue which is unresolved.

What is of interest is the fact that although HUVECs were unable to attach and spread on 10 mg/mL P_{11}-4 gels, they were able to on 2.5 mg/mL concentration gels without the addition of fibronectin.

5.3.4 Low P_{11}-4 peptide concentration facilitates HUVEC attachment and spreading

Several possible factors may explain why HUVECs are able to bind to P_{11}-4 at low peptide concentrations with one of them being hydrogel stiffness. Although the stiffness of 2.5 mg/mL hydrogel was unable to be measured in this research, the reduction of peptide concentration showed a non-linear decrease in storage modulus between the 20 mg/mL and 10 mg/mL P_{11}-4 gel (2.4-fold reduction) and between the 10 mg/mL and 5 mg/mL P_{11}-4 gel (54-fold reduction). Therefore, it is presumed that the stiffness of a 2.5 mg/mL gel would be lower than that of 13 Pa which was measured for the 5 mg/mL P_{11}-4 gel.

It is unclear why such a low material stiffness would facilitate HUVEC attachment in P_{11}-4 given that the ~700 Pa 10 mg/mL gel is much closer to the stiffnesses reported for vascularisation in other hydrogel materials than this (Table 11). Furthermore, there was also no observable change in the morphology of the cell monolayer after treatment with 5 mg/mL P_{11}-4 (Figure 19) and HUVECs were also unable to attach to the 5 mg/mL gel when cultured on its surface (Figure 20). If the sole driving force of attachment to 2.5 mg/mL P_{11}-4 gels was lower gel stiffness, some degree of attachment would likely have been expected on the 5 mg/mL P_{11}-4 gel (stiffness of 13 Pa)

While it is possible that the stiffness reduction alone in the 2.5 mg/mL gel was responsible for the ability of HUVECs to attach to the gel, the reduction in peptide concentration also alters other properties of P_{11}-4 gel assembly that may contribute to the improved attachment.

Self-assembling peptides have a critical aggregation concentration (C*), the concentration at which peptide monomers begin assembling into higher order structures rather than remaining in a non-aggregated state (Warren et al., 2023). It has been found that in P_{11}-4 (dissolved in an NMR buffer solution containing D_2O, 130 mM NaCl, DCl and NaOD), the C* is reached at a concentration of approximately 100 μM (1.6 x 10^{-4} mg/mL) and follows a sigmoidal curve until approximately 10,000 μM (1.6 mg/mL) where almost complete aggregation occurs.

Similar studies have also been carried out with positively charged members of the P_{11}-X library. It was reported by Maude (2011) that positively charged members of the P_{11}-X library such as P_{11}-8 are able to form self-supporting hydrogels in cell culture media and also measured the C* of gelation for this peptide (Maude et al., 2011). The C* at which point P_{11}-8 formed aggregates was ~400 μM and the C* where gelation occurred was ~1000 μM. However, although gels had been prepared in tissue culture media for cell culture experiments, the data obtained for experiments regarding peptide aggregation was performed in NMR buffer solution which was the same as that used by Warren (2023) above but contained 140 mM NaCl instead of 130 mM NaCl.

Peptide solutions are often prepared in deuterated water for techniques such as FTIR as the absorption of IR radiation by water overlaps the amide I and amide II regions of IR spectra that are used to analyse protein structures (Kristoffersen et al., 2020). This is especially important when working with low peptide concentrations such as those used to calculate C* as the signal to noise ratio is weak (Chon et al., 2021). Therefore, whilst these experiments provide valuable information of how SAPs assemble and the concentrations that this occurs at, the results are not necessarily directly comparable between solutions.

The exact composition of the tissue culture media used to study gels in this research is unknown as it is not declared by the manufacturer, however, most tissue culture media contain a range of ions such as Na^+, K^+, Ca^{2+}, Cl^-, Mg^{2+} and SO_4^{2-} and it is expected that endothelial culture media contains at least some of these. Furthermore, endothelial culture media is known to contain a concentration of 5% FCS as well as a number of other supplements outlined in Table 10. These components may interfere with the spectra obtained from FTIR and is the reason why when FTIR is performed directly on cells, the cells are stored in or are washed with PBS prior to taking readings (Mourant et al., 2003; Hu et al., 2020).

However, the interaction between ions and SAPs as well as between proteins in solution and SAPs can alter the assembly dynamics of hydrogels. Koch (2018) investigated the material properties of P_{11}-4 prepared using different buffers (Tris-NaCl, artificial saliva and DMEM) and when exposed to different salts (NaCl and $MgSO_4$) (Koch, Müller, et al., 2018). It was shown that assembly in buffers containing different salts had a significant impact on the stiffness of P_{11}-4 gels and that assembly in artificial saliva or DMEM also significantly affected the gelation speed, yield point and material stiffness. This demonstrates that solutions used to form P_{11}-4 gels significantly impact the bulk properties of gels and therefore it is reasonable to assume that changes are likely to occur in the assembly dynamics at a molecular level.

If the self-assembly of P_{11}-4 is comparable to data obtained from FTIR in tissue culture media, then it would be fair to assume that HUVECs were able to attach

to 2.5 mg/mL P_{11}-4 gels due to the gel being of a much lower stiffness. However, if assembly dynamics are affected by the components of tissue culture media, especially at 37°C with low concentration peptides, a number of properties of the gel may have been altered in addition to stiffness such as whether full assembly of the gel occurs, the secondary structure of the assembled peptide, arrangement of P_{11}-4 fibrils and the surface topology of the gel which could potentially influence cellular attachment.

As such, whilst it was possible for HUVECs to form cellular networks on 3D 2.5 mg/mL P_{11}-4 gels but not to attach to 10 mg/mL P_{11}-4 gels, the exact mechanism that led to this remains unknown.

5.4 Conclusions and future work

The research presented in this chapter was performed to assess whether the self-assembling peptide P_{11}-4 could be utilised as a scaffold material for the development of vascularised 3D tissue engineering constructs.

To the authors knowledge, the results demonstrate for the first time that P_{11}-4 is able to support the 3D culture of HUVECs and that HUVECs are able to form what appear to be interconnected cellular networks on its surface. Furthermore, the results presented in this chapter are the first to demonstrate the use of P_{11}-4 as a scaffold material at a concentration of less than 10 mg/mL and that this is necessary for the attachment and spreading of some cell types on its surface.

Additionally, the research presented demonstrates that whilst one of the limitations of using P_{11}-4 as a scaffold material is that it is thixotropic and that the gel is easily destroyed during routine tissue culture, that by encapsulating P_{11}-4 within a protective envelope of agarose it is possible to perform 3D cell culture within P_{11}-4 gels that result in highly cellularised scaffold material using DPSCs. This technique could be explored further in tissue engineering and the agarose be replaced by a more bioactive material that could be used for the generation of tissue constructs for tissue repair

However, whilst this research helped explore P_{11}-4 in a novel application, the creation of a 3D vascularised tissue engineering construct was sadly not achieved. One of the key issues that prevented this is that HUVECs were only able to associate with P_{11}-4 gels at a concentration that makes handling difficult. Due to the ability of P_{11}-4 gels to withstand mechanical agitation decreasing in line with decreasing concentration, 2.5 mg/mL P_{11}-4 gels could only be formed in 96 well plates as the volume of liquid in larger wells disrupted the gels when moved due to having more inertia. As such, the volume of gel solution that could be prepared for each sample was limited to approximately 300 µL which yielded a gel thickness of approximately only 100 µm. Furthermore, due to the fragile nature of P_{11}-4 this was easily disrupted even in small wells which produced disconnected gels and due to the instability of low concentration P_{11}-4 gels, excess media could not be removed and replaced with additional gel solution to increase gel depth due to destruction of the gel.

As such, the use of 2.5 mg/mL P_{11}-4 gels as a stand-alone scaffold is unlikely to have any application in tissue engineering to form vascularised tissue engineering constructs. However, it is possible that it could be combined with a porous scaffold material in the future to enhance vascularisation. This could improve cell attachment and HUVEC spreading in materials that do not support this whilst the porous scaffold material would shield the 2.5 mg/mL P_{11}-4 gel from external forces.

Chapter 6: General Discussion

Despite significant efforts, the ability to form functional vasculature within engineered tissues remains a key challenge in the field of tissue engineering. This is problematic as the generation of most tissues suitable for clinical applications requires vasculature for two primary reasons; firstly, vasculature is essential for mass transport which supplies cells within tissues with oxygen and nutrients and for the removal of waste products (Vajda et al., 2021). Secondly, vasculature is required so that the transplanted tissues are able to be integrated with the host's vasculature to prevent necrosis of the engineered tissue after transplantation (Lim et al., 2022).

Several approaches for creating vasculature within engineered tissues have been explored with most involving the use of an endothelial cell source for the formation of vasculature and a biomaterial to act as a scaffold to support vascularisation. However, an ideal cell source and biomaterial are yet to be found. The research presented in this thesis aimed to investigate potential candidates for both components, a cell source capable of differentiating into endothelial cells and a SAP hydrogel to act as a scaffold material to support vascularisation.

6.1 Dental Pulp Stem Cells for Vascular Engineering

One of the primary challenges in vascular engineering is the selection of a suitable cell source for the formation of vasculature (Deng et al., 2024). As discussed in Section 1.2, autologous cells are generally preferred for use in the clinical application of tissue engineering strategies due to their lower risk of immune rejection after transplantation. However, autologous endothelial cells are not suitable in most instances due to difficulties in harvesting a sufficient number of cells and their limited capacity for proliferation (Section 1.2.2).

To address the limitations of autologous endothelial cells, adult stem cell populations have been explored for their capacity to differentiate into functional endothelial cells. BM-MSCs for instance have been demonstrated to be able to differentiate into endothelial-like cells capable of forming networks in Matrigel

tube formation assays and in the formation of vasculature in *in vivo* models (Yao et al., 2020). As such, these two stem cell populations have largely dominated research in this field.

DPSCs are another adult stem cell population which offer a promising alternative to BM-MSCs and AD-MSCs. DPSCs originate from a neurovascular niche (Luzuriaga et al., 2021), are convenient to harvest and have been demonstrated to produce higher amounts of pro-angiogenic growth factors than other adult stem cell sources (Matsumura-Kawashima et al., 2021a). Furthermore, whilst only a limited amount of research has been conducted into the endothelial differentiation of DPSCs, they have been shown to have the potential for endothelial differentiation (Liu et al., 2014; Luzuriaga et al., 2019; Zhou and Sun, 2020). For these reasons, DPSCs were selected for use as an endothelial cell source in this research.

In this study, it was shown that expression of the key endothelial genes *VEGFR2* and *CD31* was significantly increased in human DPSCs after both 5 and 10 days of treatment with endothelial cell culture media compared with the control group. Matrigel tube formation assays confirmed that after 5 days, differentiated DPSCs were able to form networks similar to HUVECs and that this functionality was increased after 10 days of differentiation. When quantified, the structures formed by DPSCs that had undergone 10 days of endothelial induction were comparable to those formed by HUVECs in almost all measures of network formation. Therefore, by these measures, it was concluded that DPSCs had been differentiated into endothelial-like cells in agreement with prior research into the cells (Liu et al., 2014; Zhou and Sun, 2020; Luzuriaga et al., 2020).

However, despite the promising results observed in the experiments performed in Chapter 4, endothelial induced DPSCs did not mimic HUVECs when cultured on 2.5 mg/mL P_{11}-4. As presented in Chapter 5, DPSCs that had undergone 10 days of endothelial differentiation did not form cellular networks on 2.5 mg/mL P_{11}-4 hydrogels in the same way as HUVECs and were in fact indistinguishable from control cells. As DPSCs and HUVECs behaved very differently in contact with different concentrations of P_{11}-4 throughout the study, this suggests that

differentiated DPSCs had not transitioned into a true endothelial cell phenotype and that earlier measures of differentiation were potentially misleading.

This result highlights one of the critical limitations of this study regarding endothelial differentiation, the fact that only two endothelial markers (VEGFR2 and CD31) were investigated. Whilst both markers are commonly used as indicators of endothelial differentiation (Liu et al., 2014; Luzuriaga et al., 2019; Zhou and Sun, 2020), the differences between DPSCs and HUVECs in contact with P_{11}-4 suggest they may not be adequate to confirm full differentiation of stem cells into endothelial cells. Therefore, given that there are many proteins required for normal endothelial cell function, measuring changes in expression of several of these markers such as endoglin and thrombomodulin may improve accuracy in confirming the endothelial differentiation of stem cells (Kopczyńska and Makarewicz, 2012; Chambers et al., 2021).

In addition, Matrigel is also commonly used to measure cell function after the endothelial differentiation of stem cells (Harding et al., 2017; Wang et al., 2018; Luzuriaga et al., 2020). However, it has been reported previously that non-endothelial cells such as corneal fibroblasts are also capable of forming networks similar to those formed by HUVECs (Berthaut et al., 2009). As such, while the Matrigel tube formation assay is undoubtedly a useful tool in endothelial cell research and the development of anti-angiogenic therapies for cancers, it perhaps lacks specificity when used to determine whether stem cells have fully differentiated into endothelial cells. This research highlights the limitation of relying solely on the Matrigel tube formation assay for measuring endothelial cell function after differentiation and that other materials more specific for endothelial cell attachment should also be used or developed.

Due to the significant differences between how HUVECs and DPSCs interacted with different concentration P_{11}-4 hydrogels in this research, P_{11}-4 could be explored further for the development of such an assay. It may be beneficial to test different cell types with low concentration P_{11}-4 gels to ensure endothelial specificity. However, if this was found to be the case, it could be possible to

develop an assay P_{11}-4 for the determination of true endothelial differentiation from stem cells with a greater specificity than Matrigel.

6.2 Mechanical Sensitivity of P11-4 hydrogels

One of the greatest challenges encountered during this research was the fragility of P_{11}-4 hydrogels at the concentrations used. Due to being thixotropic, P_{11}-4 hydrogels were highly sensitive to shear forces created during routine cell culture. As outlined in Chapter 5, this prevented the culture of cells in 10 mg/mL P_{11}-4 hydrogels for periods longer than three days as the requirement for media changes after this time significantly impacted the integrity of gels. To overcome this challenge, P_{11}-4 gels were encapsulated in a protective layer of agarose which shielded gels from shear forces during cell culture enabling cells to be cultured for 7 days.

While this did not improve the attachment or spreading of HUVECs on the surface of P_{11}-4, it did allow the creation of highly cellularised constructs using DPSCs. It has been previously demonstrated *in vivo* that when P_{11}-4 hydrogels are used in an environment that experiences little mechanical agitation, that the gel is able to support the regrowth of bone after injury (Saha et al., 2019). Nevertheless, P_{11}-4 is relatively poorly studied *in vitro* as a tissue engineering scaffold due to the instability of gels. The encapsulation of P_{11}-4 in a protective environment therefore may be used as a method to perform *in vitro* experimental work to investigate the potential of P_{11}-4 to be used in clinical applications.

However, despite the improvement in mechanical stability of P_{11}-4 gels within agarose, HUVECs were still unable to vascularise P_{11}-4 gels at a concentration that could feasibly be used in clinical applications. As such, the development of clinically relevant constructs is unlikely to be achieved using this method though it has the potential to be used in the creation of *in vitro* tissue models.

6.3 P_{11}-4 and the Creation of Vascularised Tissue Engineering Constructs

The research presented in Chapter 5 demonstrated that 2.5 mg/mL P_{11}-4 hydrogels supported the attachment and spreading of HUVECs and that they appear to form networks on its surface in 3D. However, due to the fact that that gels of this concentration are incredibly fragile and that networks formed by HUVECs collapse between 24 to 48 hours, it was not possible to establish whether the structures formed were lumenised or merely networks of flattened cells.

It is likely that for a true understanding of whether 2.5 mg/mL P_{11}-4 hydrogels can support vascularisation, the gel would need to be implanted into an *in vivo* model of vascularisation such as the chick chorioallantoic membrane (CAM) assay. The use of the CAM assay would be ideal as gels would not be exposed to mechanical agitation which they would be in a hind limb ischaemia model. However, regardless of the ability of 2.5 mg/mL P_{11}-4 hydrogels to facilitate vascularisation, due to the fragility of such low concentration gels it is unlikely that they would be able to be applied to many areas of tissue engineering.

One possible application for using P_{11}-4 to facilitate vascularisation could be in bone or dental pulp regenerative therapies where gels would be protected from external forces by surrounding tissue. However, the volume of 2.5 mg/mL P_{11}-4 gel solution required to create gels may be prohibitive in most use cases. In the creation of the 2.5 mg/mL P_{11}-4 hydrogels used in this research, 300 µL of gel mixture was added to each well of 96 well plates resulting in the formation of a gel a final gel thickness of around 100 µm. This means that approximately 1 mL of gel solution is required to coat an area of 1 cm^2 with a gel of 0.1mm thickness, making it impractical for larger tissue defects. Additionally, as the gels disassemble under shear forces it is not possible to layer gels in circumstances where a larger volume of material would be required.

A further problem with the generation of vascularised 3D tissue engineering constructs using P_{11}-4 gels is the way in which different cells behave on its

surface depending on peptide concentration. In this research it was demonstrated that on 10 mg/mL P_{11}-4 gels, DPSCs are able to attach to its surface and spread rapidly whereas HUVECs do not display the same behaviour. The opposite was true when HUVECs and DPSCs were cultured on 2.5 mg/mL P_{11}-4 gels in that HUVECs rapidly formed cellular networks on its surface and DPSCs showed limited interaction. As such, for the creation of vascularised tissues with P_{11}-4 it would be necessary to create graduated P_{11}-4 gels with areas of low stiffness to support vascularisation and regions of higher stiffness to enable the correct functioning of other cells such as DPSCs. Whilst it is possible that such a scaffold could be created with the use of techniques such as 3D printing, it would be extremely difficult to create and perhaps even more difficult to use therapeutically.

As such, if P_{11}-4 gels were to be used for vascularisation in tissue engineering, it would likely need to be used in conjunction with another biomaterial. As an example, silk fibroin sponges have been shown to facilitate the attachment of some cell types such as osteoblasts (Varkey et al., 2015) but often needs to be modified to support efficient vascularisation (Shao and Sun, 2024). Therefore, it may be possible to soak materials such as these in 2.5 mg/mL P_{11}-4 solution to form hydrogels within the pores of the material to facilitate vascularisation whilst the bulk of the material would support the growth of other cells. However, ensuring that the 2.5 mg/mL P_{11}-4 gel remained within the pores and didn't wash out would present another challenged that would need to be addressed.

6.4 Lessons from P_{11}-4 Hydrogels

Despite the limitations encountered with P_{11}-4 hydrogels in this study, the research offers insights that could guide the development of future P_{11}-X peptides for use in the creation of 3D vascularised tissue engineering constructs. The fact that HUVECs were able to attach to P_{11}-4 hydrogels, albeit at a low concentration, suggests that P_{11}-4 has properties that are conducive to endothelial cell function and vascularisation and therefore could potentially serve as the basis of a novel peptide designed specifically for use in vascularisation research.

One of the key limitations in the study of P_{11}-4 presented here was the inability to measure the stiffness of 2.5 mg/mL P_{11}-4 hydrogels. This could have provided insight into why HUVECs were able to attach to the gel at this concentration and provided a basis for designing a P_{11}-X peptide for vascularisation. However, as discussed in Chapter 5, the stiffness of the 2.5 mg/mL P_{11}-4 gel is expected to be lower than that of the 5 mg/mL gel and therefore stiffness may not fully explain HUVEC attachment in low concentration gels.

If it could be elucidated why HUVECs were able to attach to low concentration gels, it may be possible to design SAPs with these functions in mind. For instance, if HUVECs were able to attach and spread on 2.5 mg/mL P_{11}-4 gels due to changes in the secondary structures formed at low peptide concentrations, a new SAP could be designed to form these structures at higher concentrations. This would make it possible to create stiffer gels within a range that still facilitates endothelial cell attachment and function whilst at the same time increasing its application to tissue engineering by being more stable.

Chapter 7: Future Work

While the research presented in this thesis did not achieve the goal of creating vascularised 3D tissue engineering constructs, it has raised unanswered questions in how best to achieve endothelial differentiation in stem cells, how differentiation is commonly quantified and improvements that can be made to this process. By answering these questions through further research, the differentiation of functional endothelial cells from DPSCs may be achieved providing a suitable cell source for vascularisation in tissue engineering.

Furthermore, this research demonstrated that in particular conditions endothelial cells are able to attach and spread on P_{11}-4 and assemble into cellular networks. Although this finding has limited application in tissue engineering due to the stability of P_{11}-4 hydrogels, it provides an opportunity for the development of new members of the P_{11}-X library specifically directed at the formation of vasculature. Additionally, while pursuing vascularisation of P_{11}-4, a method was developed for the long-term culture of cells on the material which could be used to enhance the investigation of P_{11}-4 as a scaffold material for tissue engineering *in vitro*.

7.1 Improving Endothelial Differentiation of DPSCs and Analysis of Differentiation

Two key issues surrounding the endothelial differentiation of DPSCs were highlighted by the research presented in this thesis.

Firstly, while the increase in endothelial gene and protein expression agreed with other research that DPSCs have the capacity to differentiate into endothelial-like cells (Liu et al., 2014; Luzuriaga et al., 2019; Zhou and Sun, 2020; Luzuriaga et al., 2020), the difference in both gene and protein expression between each piece of research was significant (Chapter 4). As discussed in Chapter 4, the most likely explanation for this was that in each study the components in differentiation media were significantly different. As such, research should be focussed on determining what growth factors and culture conditions are essential for endothelial differentiation taking into account the natural production of growth

factors from stem cells in culture. By doing this, it may be possible to develop protocols that can precisely control the endothelial differentiation of stem cells and provide a suitable source of endothelial cells for clinical applications and tissue engineering.

Secondly, the way in which many studies including this one define endothelial differentiation appears to be inadequate. It was shown that while it is standard practice to measure a small number of endothelial cell markers and endothelial cell function using Matrigel, this may not be precise enough to confirm a true endothelial cell phenotype after differentiation. As such, more research is needed to understand critical proteins in the function of endothelial cells so that these can be used as markers for differentiation. Furthermore, the development of an assay more specific to endothelial cells than the Matrigel tube formation is necessary for investigating endothelial cell function after differentiation. This could be achieved using P_{11}-4 if research confirmed that other cell types are unable to form cellular networks when cultured on 2.5 mg/mL P_{11}-4 hydrogels.

7.2 Investigating Endothelial Cell Function on P_{11}-4 Hydrogels and P_{11}-X Design

While this research demonstrated that P_{11}-4 gels have properties that support the attachment and spreading of endothelial cells at low concentrations, it remains to be answered why this is. To begin investigating this, it would be necessary to accurately measure the stiffness of 2.5 mg/mL P_{11}-4 hydrogels through the use of different rheological techniques such as by employing cross-hatched geometries that are designed to reduce slippage during measurement (Carotenuto et al., 2015). Following this, developing techniques to investigate the assembly of P_{11}-4 under tissue culture conditions in complete tissue culture media would be necessary to understand what changes occur to peptide structure when used in low concentrations. The results of these experiments could then be used to develop P_{11}-X SAPs with properties that facilitate vascularisation in more stable hydrogels that could be used in tissue engineering.

7.3 Advancing P_{11}-4 Hydrogels as Tissue Engineering Scaffolds *in vitro*

As encapsulating P_{11}-4 hydrogels in a protective environment supported cell culture for at least 7 days, this method could be used to further investigate P_{11}-4 as a scaffold material for tissue engineering *in vitro*. Due to the mechanical properties of P_{11}-4, it is most likely that it will only have applications as a scaffold material in hard tissue engineering or in soft tissues with a protective environment such as dental pulp. As such, the utilisation of a protective environment helps more closely mimic the *in vivo* environment that scaffolds will be used in. This could help in understanding how P_{11}-4 will behave when applied as a scaffold in these environments and also in developing cell-based therapies for use in these applications.

Chapter 8: Conclusion

In conclusion, the research presented in this thesis supported the view that DPSCs are capable of differentiating into endothelial-like cells and also found for the first time that P_{11}-4 possesses properties that may support vascularisation. However, through comparing the functionality of differentiated DPSCs to HUVECs on 2.5 mg/mL P_{11}-4 hydrogels, questions were raised about whether differentiated DPSCs had a true endothelial cell phenotype. Furthermore, as HUVECs were only able to attach and migrate on the surface of 2.5 mg/mL P_{11}-4 hydrogels which are unstable, it was not possible to generate vascularised 3D tissue engineering constructs using it in its current state.

Nevertheless, this research has highlighted key research areas that require further investigation to develop protocols for the complete endothelial differentiation of DPSCs and the development of novel P_{11}-X SAPs that could be used to generate 3D vascularised tissue engineering constructs.

Chapter 9: References

Aggeli, A., Bell, M., Carrick, L.M., Fishwick, C.W.G., Harding, R., Mawer, P.J., Radford, S.E., Strong, A.E. and Boden, N. 2003. pH as a trigger of peptide β-sheet self-assembly and reversible switching between nematic and isotropic phases. *Journal of the American Chemical Society*. 125(32), pp.9619–9628.

Aggeli, A., Nyrkova, I.A., Bell, M., Harding, R., Carrick, L., McLeish, T.C.B., Semenov, A.N. and Boden, N. 2001. Hierarchical self-assembly of chiral rod-like molecules as a model for peptide β-sheet tapes, ribbons, fibrils, and fibers. *Proceedings of the National Academy of Sciences of the United States of America*. 98(21), pp.11857–11862.

Ahearne, M., Yang, Y., El Haj, A.J., Then, K.Y. and Liu, K.K. 2005. Characterizing the viscoelastic properties of thin hydrogel-based constructs for tissue engineering applications. *Journal of the Royal Society Interface*. 2(5), p.455.

Ahsan, T. and Nerem, R.M. 2010. Fluid Shear Stress Promotes an Endothelial-Like Phenotype During the Early Differentiation of Embryonic Stem Cells. *Tissue Engineering. Part A*. 16(11), p.3547.

Alberts, B., Johnson, A., Lewis, J., Raff, M., Roberts, K. and Walter, P. 2002. Blood Vessels and Endothelial Cells.

Alge, D.L., Zhou, D., Adams, L.L., Wyss, B.K., Shadday, M.D., Woods, E.J., Chu, T.M.G. and Goebel, W.S. 2010. Donor-matched comparison of dental pulp stem cells and bone marrow-derived mesenchymal stem cells in a rat model. *Journal of tissue engineering and regenerative medicine*. 4(1), p.73.

Alijotas-Reig, J., Fernández-Figueras, M.T. and Puig, L. 2013. Inflammatory, immune-mediated adverse reactions related to soft tissue dermal fillers. *Seminars in arthritis and rheumatism*. 43(2), pp.241–258.

Apte, R.S., Chen, D.S. and Ferrara, N. 2019. VEGF in Signaling and Disease: Beyond Discovery and Development. *Cell*. 176(6), p.1248.

Arderiu, G., Peña, E., Aledo, R., Juan-Babot, O., Crespo, J., Vilahur, G., Oñate, B., Moscatiello, F. and Badimon, L. 2019. MicroRNA-145 regulates the differentiation of adipose stem cells toward microvascular endothelial cells and promotes angiogenesis. *Circulation Research*. 125(1), pp.74–89.

Asahara, T., Murohara, T., Sullivan, A., Silver, M., Van Der Zee, R., Li, T., Witzenbichler, B., Schatteman, G. and Isner, J.M. 1997. Isolation of putative progenitor endothelial cells for angiogenesis. *Science (New York, N.Y.)*. 275(5302), pp.964–967.

Ashikari-Hada, S., Habuchi, H., Kariya, Y. and Kimata, K. 2005. Heparin Regulates Vascular Endothelial Growth Factor165-dependent Mitogenic Activity, Tube Formation, and Its Receptor Phosphorylation of Human Endothelial Cells: COMPARISON OF THE EFFECTS OF HEPARIN AND MODIFIED HEPARINS. *Journal of Biological Chemistry*. 280(36), pp.31508–31515.

Assmann, J.C., Müller, K., Wenzel, J., Walther, T., Brands, J., Thornton, P., Allan, S.M. and Schwaninger, M. 2017. Isolation and Cultivation of Primary Brain Endothelial Cells from Adult Mice. *Bio-protocol*. 7(10).

Auerbach, R., Lewis, R., Shinners, B., Kubai, L. and Akhtar, N. 2003. Angiogenesis Assays: A Critical Overview. *Clinical Chemistry*. 49(1), pp.32–40.

Baldwin, M.E., Huan Liang, Xiao., Ruchatz, A., Busch, J., Gu, Z., Roose-Girma, M., Olsson, C., Erickson, S., Ferrara, N. and Gerber, H.-P. 2004. Generation of mice carrying floxed VEGFR-1 and VEGFR-2 alleles to study the effects of postnatal gene ablation on angiogenesis and hematopoiesis | Cancer Research | American Association for Cancer Research. *Cancer Research*. [Online], pp.64–596. [Accessed 10 July 2024]. Available from: https://aacrjournals.org/cancerres/article/64/7_Supplement/596/513904/Generation-of-mice-carrying-floxed-VEGFR-1-and.

Barco, A., Ingham, E., Fisher, J., Fermor, H. and Davies, R.P.W. 2018. On the design and efficacy assessment of self-assembling peptide-based hydrogel-glycosaminoglycan mixtures for potential repair of early stage cartilage degeneration. *Journal of Peptide Science*. 24(8–9), p.e3114.

Beenken, A. and Mohammadi, M. 2009. The FGF family: biology, pathophysiology and therapy. *Nature Reviews Drug Discovery 2009 8:3*. 8(3), pp.235–253.

Bergamo, M.T., Zhang, Z., Oliveira, T.M. and Nör, J.E. 2021. VEGFR1 primes a unique cohort of dental pulp stem cells for vasculogenic differentiation. *European cells & materials*. 41, p.332.

Berthaut, A., Mirshahi, P., Benabbou, N., Azzazene, D., Bordu, C., Therwath, A., Legeais, J.M. and Mirshahi, M. 2009. Vascular endothelial growth factor

receptor-1 (VEGFR-1) expression in human corneal fibroblast decreased with age. *Molecular Vision*. 15, p.1997.

Bittner-Frank, M., Reisinger, A.G., Andriotis, O.G., Pahr, D.H. and Thurner, P.J. 2024. Cortical and trabecular mechanical properties in the femoral neck vary differently with changes in bone mineral density. *JBMR Plus*. 8(6).

Blanco, R. and Gerhardt, H. 2013. VEGF and Notch in Tip and Stalk Cell Selection. *Cold Spring Harbor Perspectives in Medicine*. 3(1).

Böttcher, R.T. and Niehrs, C. 2005. Fibroblast growth factor signaling during early vertebrate development. *Endocrine reviews*. 26(1), pp.63–77.

Bray, S.J. 2006. Notch signalling: a simple pathway becomes complex. *Nature Reviews Molecular Cell Biology 2006 7:9*. 7(9), pp.678–689.

Bröseler, F., Tietmann, C., Bommer, C., Drechsel, T., Heinzel-Gutenbrunner, M. and Jepsen, S. 2020. Randomised clinical trial investigating self-assembling peptide P11-4 in the treatment of early caries. *Clinical oral investigations*. 24(1), pp.123–132.

Brown, A.C. and Barker, T.H. 2014. Fibrin-based biomaterials: Modulation of macroscopic properties through rational design at the molecular level. *Acta Biomaterialia*. 10(4), pp.1502–1514.

Budd, S., Byfield, G., Martiniuk, D., Geisen, P. and Hartnett, M.E. 2009. Reduction in endothelial tip cell filopodia corresponds to reduced intravitreous but not intraretinal vascularization in a model of ROP. *Experimental eye research*. 89(5), p.718.

Burdick, D., Soreghan, B., Kwon, M., Kosmoski, J., Knauer, M., Henschen, A., Yatest, J., Cotmans, C. and Glabell, C. 1992. *THE JOURNAL OF BIOLOGICAL CHEMISTRY Assembly and Aggregation Properties of Synthetic Alzheimer's A4/@ Amyloid Peptide Analogs**.

Camassari, J.R., de Sousa, I.T.C., Cogo-Müller, K. and Puppin-Rontani, R.M. 2023. The Self-assembling peptide P11-4 influences viability and osteogenic differentiation of stem cells of the apical papilla (SCAP). *Journal of Dentistry*. 134, p.104551.

Canovic, E.P., Qing, B., Mijailovic, A.S., Jagielska, A., Whitfield, M.J., Kelly, E., Turner, D., Sahin, M. and Van Vliet, K.J. 2016. Characterizing Multiscale Mechanical Properties of Brain Tissue Using Atomic Force Microscopy, Impact Indentation, and Rheometry. *Journal of Visualized Experiments : JoVE*. 2016(115), p.54201.

Cao, N. and Yao, Z.X. 2011. The Hemangioblast: From Concept to Authentication. *The Anatomical Record: Advances in Integrative Anatomy and Evolutionary Biology*. 294(4), pp.580–588.

Cao, Y., Sun, Z., Liao, L., Meng, Y., Han, Q. and Zhao, R.C. 2005. Human adipose tissue-derived stem cells differentiate into endothelial cells in vitro and improve postnatal neovascularization in vivo. *Biochemical and biophysical research communications*. 332(2), pp.370–379.

Carmeliet, P. 2003. Angiogenesis in health and disease. *Nature Medicine 2003 9:6*. 9(6), pp.653–660.

Carotenuto, C., Vananroye, A., Vermant, J. and Minale, M. 2015. Predicting the apparent wall slip when using roughened geometries: A porous medium approach. *Journal of Rheology*. 59(5), pp.1131–1149.

Carpentier, G., Berndt, S., Ferratge, S., Rasband, W., Cuendet, M., Uzan, G. and Albanese, P. 2020. Angiogenesis Analyzer for ImageJ — A comparative morphometric analysis of "Endothelial Tube Formation Assay" and "Fibrin Bead Assay". *Scientific Reports 2020 10:1*. 10(1), pp.1–13.

Carrick, L.M., Aggeli, A., Boden, N., Fisher, J., Ingham, E. and Waigh, T.A. 2007. Effect of ionic strength on the self-assembly, morphology and gelation of pH responsive β-sheet tape-forming peptides. *Tetrahedron*. 63(31), pp.7457–7467.

Cavallo, C., Boffa, A., de Girolamo, L., Merli, G., Kon, E., Cattini, L., Santo, E., Grigolo, B. and Filardo, G. 2023. Bone marrow aspirate concentrate quality is affected by age and harvest site. *Knee Surgery, Sports Traumatology, Arthroscopy*. 31(6), p.2140.

Chambers, S.E.J., Pathak, V., Pedrini, E., Soret, L., Gendron, N., Guerin, C.L., Stitt, A.W., Smadja, D.M. and Medina, R.J. 2021. Current concepts on endothelial stem cells definition, location, and markers. *Stem Cells Translational Medicine*. 10(Suppl 2), p.S54.

Chavda, H. and Patel, C. 2011. Effect of crosslinker concentration on characteristics of superporous hydrogel. *International Journal of Pharmaceutical Investigation*. 1(1), p.17.

Chen, J. and Zou, X. 2019. Self-assemble peptide biomaterials and their biomedical applications. *Bioactive Materials*. 4, pp.120–131.

Chen, Y.C., Lin, R.Z., Qi, H., Yang, Y., Bae, H., Melero-Martin, J.M. and Khademhosseini, A. 2012. Functional human vascular network generated

in photocrosslinkable gelatin methacrylate hydrogels. *Advanced Functional Materials*. 22(10), pp.2027–2039.

Cheng, F., Zhang, Y., Wang, Y., Jiang, Q., Zhao, C.J., Deng, J., Chen, X., Yao, Y., Xia, Z., Cheng, L., Dai, L., Shi, G., Yang, Y., Zhang, S., Yu, D., Wei, Y. and Deng, H. 2018. Conversion of human adipose-derived stem cells into functional and expandable endothelial-like cells for cell-based therapies. *Stem Cell Research and Therapy*. 9(1), pp.1–15.

Chippada, U., Langrana, N. and Yurke, B. 2009. Complete mechanical characterization of soft media using nonspherical rods. *Journal of Applied Physics*. 106(6).

Chon, B., Xu, S. and Lee, Y.J. 2021. Compensation of Strong Water Absorption in Infrared Spectroscopy Reveals the Secondary Structure of Proteins in Dilute Solutions. *Analytical chemistry*. 93(4), p.2215.

Chopra, H., Hung, M.K., Kwong, D.L., Zhang, C.F. and Pow, E.H.N. 2018. Insights into Endothelial Progenitor Cells: Origin, Classification, Potentials, and Prospects. *Stem Cells International*. 2018(1), p.9847015.

Chowdhury, S., Fried, K.D., Iwakiri, Y., Brancale, J. and Vilarinho, S. 2023. Protocol for enrichment, purification, and cytocentrifugation of mouse liver endothelial cells. *STAR protocols*. 4(3).

Christman, K.L., Fok, H.H., Sievers, R.E., Fang, Q. and Lee, R.J. 2004. Fibrin Glue Alone and Skeletal Myoblasts in a Fibrin Scaffold Preserve Cardiac Function after Myocardial Infarction. *https://home.liebertpub.com/ten*. 10(3–4), pp.403–409.

Cockman, M.E., Masson, N., Mole, D.R., Jaakkola, P., Chang, G.W., Clifford, S.C., Maher, E.R., Pugh, C.W., Ratcliffe, P.J. and Maxwell, P.H. 2000. Hypoxia Inducible Factor-α Binding and Ubiquitylation by the von Hippel-Lindau Tumor Suppressor Protein. *Journal of Biological Chemistry*. 275(33), pp.25733–25741.

Cohen, R., Baruch, E.S., Cabilly, I., Shapira, A. and Dvir, T. 2023. Modified ECM-Based Bioink for 3D Printing of Multi-Scale Vascular Networks. *Gels 2023, Vol. 9, Page 792*. 9(10), p.792.

Cornelissen, C.G., Dietrich, M., Gromann, K., Frese, J., Krueger, S., Sachweh, J.S. and Jockenhoevel, S. 2013. Fibronectin coating of oxygenator membranes enhances endothelial cell attachment. *BioMedical Engineering Online*. 12(1), pp.1–8.

Cudmore, M.J., Hewett, P.W., Ahmad, S., Wang, K.Q., Cai, M., Al-Ani, B., Fujisawa, T., Ma, B., Sissaoui, S., Ramma, W., Miller, M.R., Newby, D.E., Gu, Y., Barleon, B., Weich, H. and Ahmed, A. 2012. The role of heterodimerization between VEGFR-1 and VEGFR-2 in the regulation of endothelial cell homeostasis. *Nature Communications 2012 3:1*. 3(1), pp.1–12.

Cuiffo, B.G. and Karnoub, A.E. 2012. Mesenchymal stem cells in tumor development: Emerging roles and concepts. *Cell Adhesion & Migration*. 6(3), p.220.

d'Aquino, R., Graziano, A., Sampaolesi, M., Laino, G., Pirozzi, G., De Rosa, A. and Papaccio, G. 2007. Human postnatal dental pulp cells co-differentiate into osteoblasts and endotheliocytes: a pivotal synergy leading to adult bone tissue formation. *Cell death and differentiation*. 14(6), pp.1162–1171.

Davidenko, N., Schuster, C.F., Bax, D. V., Farndale, R.W., Hamaia, S., Best, S.M. and Cameron, R.E. 2016. Evaluation of cell binding to collagen and gelatin: a study of the effect of 2D and 3D architecture and surface chemistry. *Journal of Materials Science: Materials in Medicine*. 27(10), pp.1–14.

Davies, R.P.W., Aggeli, A., Beevers, A.J., Boden, N., Carrick, L.M., Fishwick, C.W.G., McLeish, T.C.B., Nyrkova, I. and Semenov, A.N. 2006. Self-assembling β-Sheet Tape Forming Peptides. *Supramolecular Chemistry*. 18(5), pp.435–443.

Davis, G.E. and Senger, D.R. 2005. Endothelial extracellular matrix: Biosynthesis, remodeling, and functions during vascular morphogenesis and neovessel stabilization. *Circulation Research*. 97(11), pp.1093–1107.

Deng, C.X., Wynshaw-Boris, A., Shen, M.M., Daugherty, C., Ornitz, D.M. and Leder, P. 1994. Murine FGFR-1 is required for early postimplantation growth and axial organization. *Genes & development*. 8(24), pp.3045–3057.

Deng, D., Zhang, Y., Tang, B. and Zhang, Z. 2024. Sources and applications of endothelial seed cells: a review. *Stem Cell Research & Therapy 2024 15:1*. 15(1), pp.1–14.

Derkus, B., Okesola, B.O., Barrett, D.W., D'Este, M., Chowdhury, T.T., Eglin, D. and Mata, A. 2020. Multicomponent hydrogels for the formation of vascularized bone-like constructs in vitro. *Acta Biomaterialia*. 109, pp.82–94.

Desai, M., Seifalian, A.M. and Hamilton, G. 2011. Role of prosthetic conduits in coronary artery bypass grafting. *European Journal of Cardio-Thoracic Surgery*. 40(2), pp.394–398.

Desai, N., Rambhia, P. and Gishto, A. 2015. Human embryonic stem cell cultivation: Historical perspective and evolution of xeno-free culture systems. *Reproductive Biology and Endocrinology*. 13(1), pp.1–15.

Deshmukh, S.N., Dive, A.M., Moharil, R. and Munde, P. 2016. Enigmatic insight into collagen. *Journal of Oral and Maxillofacial Pathology : JOMFP*. 20(2), p.276.

Diamantides, N., Slyker, L., Martin, S., Rodriguez, M.R. and Bonassar, L.J. 2022. Pre-glycation Impairs Gelation of High Concentration Collagen Solutions. *Journal of biomedical materials research. Part A*. 110(12), p.1953.

Dibble, M., Di Cio', S., Luo, P., Balkwill, F. and Gautrot, J.E. 2023. The impact of pericytes on the stability of microvascular networks in response to nanoparticles. *Scientific Reports 2023 13:1*. 13(1), pp.1–13.

Dong, C. and Lv, Y. 2016. Application of Collagen Scaffold in Tissue Engineering: Recent Advances and New Perspectives. *Polymers*. 8(2).

Doppelt-Flikshtain, O., Younis, A., Tamari, T., Ginesin, O., Shentzer-Kutiel, T., Nikomarov, D., Bar-Sela, G., Coyac, B.R., Assaraf, Y.G. and Zigdon-Giladi, H. 2023. Endothelial Progenitor Cells Promote Osteosarcoma Progression and Invasiveness via AKT/PI3K Signaling. *Cancers*. 15(6).

Duong, H., Wu, B. and Tawil, B. 2009. Modulation of 3D fibrin matrix stiffness by intrinsic fibrinogen-thrombin compositions and by extrinsic cellular activity. *Tissue Engineering - Part A*. 15(7), pp.1865–1876.

Dzierżyńska, M., Sawicka, J., Deptuła, M., Sosnowski, P., Sass, P., Peplińska, B., Pietralik-Molińska, Z., Fularczyk, M., Kasprzykowski, F., Zieliński, J., Kozak, M., Sachadyn, P., Pikuła, M. and Rodziewicz-Motowidło, S. 2023. Release systems based on self-assembling RADA16-I hydrogels with a signal sequence which improves wound healing processes. *Scientific Reports*. 13(1).

Edman, N.I., Phal, A., Redler, R.L., Schlichthaerle, T., Srivatsan, S.R., Ehnes, D.D., Etemadi, A., An, S.J., Favor, A., Li, Z., Praetorius, F., Gordon, M., Vincent, T., Marchiano, S., Blakely, L., Lin, C., Yang, W., Coventry, B., Hicks, D.R., Cao, L., Bethel, N., Heine, P., Murray, A., Gerben, S., Carter, L., Miranda, M., Negahdari, B., Lee, S., Trapnell, C., Zheng, Y., Murry, C.E., Schweppe, D.K., Freedman, B.S., Stewart, L., Ekiert, D.C., Schlessinger, J., Shendure, J., Bhabha, G., Ruohola-Baker, H. and Baker, D. 2024. Modulation of FGF pathway signaling and vascular differentiation using designed oligomeric assemblies. *Cell*. 187(14), pp.3726-3740.e43.

Elomaa, L., Lindner, M., Leben, R., Niesner, R. and Weinhart, M. 2022. In vitro vascularization of hydrogel-based tissue constructs via a combined approach of cell sheet engineering and dynamic perfusion cell culture. *Biofabrication*. 15(1), p.015004.

El-Sayed, B., Davies, R.P.W., El-Zehery, R.R., Ibrahim, F.M., Grawish, M.E., Kirkham, J. and El-Gendy, R. 2020. An in-vivo Intraoral Defect Model for Assessing the Use of P11-4 Self-Assembling Peptide in Periodontal Regeneration. *Frontiers in Bioengineering and Biotechnology*. 8, p.559494.

Fazary, A.E., Mohamed, A.F. and Lebedeva, N.S. 2006. Protonation equilibria studies of the standard α-amino acids in NaNO3 solutions in water and in mixtures of water and dioxane. *The Journal of Chemical Thermodynamics*. 38(11), pp.1467–1473.

Feng, Y., Taraban, M. and Yu, Y.B. 2012. The Effect of Ionic Strength on the Mechanical, Structural and Transport Properties of Peptide Hydrogels. *Soft matter*. 8(46), p.11723.

Feng, Y.X., Li, W., Wen, X.D., Zhang, N., Liu, W.H. and Yang, Z.Y. 2020. Sinusoidal Endothelial Cell Progenitor Cells Promote Tumour Progression in Patients with Hepatocellular Carcinoma. *Stem cells international*. 2020.

Ferrara, N., Carver-Moore, K., Chen, H., Dowd, M., Lu, L., O'Shea, K.S., Powell-Braxton, L., Hillan, K.J. and Moore, M.W. 1996. Heterozygous embryonic lethality induced by targeted inactivation of the VEGF gene. *Nature*. 380(6573), pp.439–442.

Ferretti, E. and Hadjantonakis, A.K. 2019. Mesoderm specification and diversification: from single cells to emergent tissues. *Current opinion in cell biology*. 61, p.110.

Forristal, C.E., Wright, K.L., Hanley, N.A., Oreffo, R.O.C. and Houghton, F.D. 2010. Hypoxia inducible factors regulate pluripotency and proliferation in human embryonic stem cells cultured at reduced oxygen tensions. *Reproduction (Cambridge, England)*. 139(1), p.85.

Friend, N.E., Beamish, J.A., Margolis, E.A., Schott, N.G., Stegemann, J.P. and Putnam, A.J. 2024. Pre-cultured, cell-encapsulating fibrin microbeads for the vascularization of ischemic tissues. *Journal of Biomedical Materials Research Part A*. 112(4), pp.549–561.

Fujio, Y. and Walsh, K. 1999. Akt Mediates Cytoprotection of Endothelial Cells by Vascular Endothelial Growth Factor in an Anchorage-dependent Manner. *Journal of Biological Chemistry*. 274(23), pp.16349–16354.

Gale, N.W., Dominguez, M.G., Noguera, I., Pan, L., Hughes, V., Valenzuela, D.M., Murphy, A.J., Adams, N.C., Lin, H.C., Holash, J., Thurston, G. and Yancopoulos, G.D. 2004. Haploinsufficiency of delta-like 4 ligand results in embryonic lethality due to major defects in arterial and vascular development. *Proceedings of the National Academy of Sciences of the United States of America*. 101(45), pp.15949–15954.

Gao, Y., Tian, Z., Liu, Q., Wang, T., Ban, L.K., Lee, H.H.C., Umezawa, A., Almansour, A.I., Arumugam, N., Kumar, R.S., Ye, Q., Higuchi, A., Chen, H. and Sung, T.C. 2022. Neuronal Cell Differentiation of Human Dental Pulp Stem Cells on Synthetic Polymeric Surfaces Coated With ECM Proteins. *Frontiers in Cell and Developmental Biology*. 10, p.893241.

Gaona, C.G.C., Alonso, M.C.I., Céspedes, R.I.N., Rosas, M.M.T., Martínez, R.R. and Escareño, M.P.L. 2023. Novel Studies in the Designs of Natural, Synthetic, and Compound Hydrogels with Biomedical Applications. *Revista Mexicana de Ingenieria Biomedica*. 44(2), pp.74–96.

Garcia-Urkia, N., Luzuriaga, J., Uribe-Etxebarria, V., Irastorza, I., Fernandez-San-Argimiro, F.J., Olalde, B., Briz, N., Unda, F., Ibarretxe, G., Madarieta, I. and Pineda, J.R. 2022. Enhanced Adipogenic Differentiation of Human Dental Pulp Stem Cells in Enzymatically Decellularized Adipose Tissue Solid Foams. *Biology*. 11(8).

Geary, L. and Labonne, C. 2018. FGF mediated MAPK and PI3K/Akt Signals make distinct contributions to pluripotency and the establishment of Neural Crest. *eLife*. 7.

Gehling, U.M., Ergün, S., Schumacher, U., Wagener, C., Pantel, K., Otte, M., Schuch, G., Schafhausen, P., Mende, T., Kilic, N., Kluge, K., Schäfer, B., Hossfeld, D.K. and Fiedler, W. 2000. In vitro differentiation of endothelial cells from AC133-positive progenitor cells. *Blood*. 95(10), pp.3106–3112.

Gelain, F., Luo, Z., Rioult, M. and Zhang, S. 2021. Self-assembling peptide scaffolds in the clinic. *npj Regenerative Medicine 2021 6:1*. 6(1), pp.1–8.

Gensler, M., Malkmus, C., Ockermann, P., Möllmann, M., Hahn, L., Salehi, S., Luxenhofer, R., Boccaccini, A.R. and Hansmann, J. 2024. Perfusable Tissue Bioprinted into a 3D-Printed Tailored Bioreactor System. *Bioengineering 2024, Vol. 11, Page 68*. 11(1), p.68.

Gerhardt, H., Golding, M., Fruttiger, M., Ruhrberg, C., Lundkvist, A., Abramsson, A., Jeltsch, M., Mitchell, C., Alitalo, K., Shima, D. and Betsholtz, C. 2003. VEGF guides angiogenic sprouting utilizing endothelial tip cell filopodia. *The Journal of Cell Biology*. 161(6), p.1163.

Gharaei, M.A., Xue, Y., Mustafa, K., Lie, S.A. and Fristad, I. 2018. Human dental pulp stromal cell conditioned medium alters endothelial cell behavior. *Stem Cell Research and Therapy*. 9(1), pp.1–12.

Golas, A.R., Perez, J.L., Fullerton, N., Lekic, N., Hooper, R.C. and Spector, J.A. 2013. Vascular Smooth Muscle Cell Optimization of Vasculogenesis within Naturally Derived, Biodegradable Hybrid Hydrogel Scaffolds. *Plastic and reconstructive surgery*. 132(6).

Goldie, L.C., Nix, M.K. and Hirschi, K.K. 2008. Embryonic vasculogenesis and hematopoietic specification. *Organogenesis*. 4(4), p.257.

Goodell, M.A., Nguyen, H. and Shroyer, N. 2015. Somatic stem cell heterogeneity: diversity in the blood, skin and intestinal stem cell compartments. *Nature reviews. Molecular cell biology*. 16(5), p.299.

Gorres, K.L. and Raines, R.T. 2010. Prolyl 4-hydroxylase. *Critical reviews in biochemistry and molecular biology*. 45(2), p.106.

Gronthos, S., Mankani, M., Brahim, J., Robey, P.G. and Shi, S. 2000. Postnatal human dental pulp stem cells (DPSCs) in vitro and in vivo. *Proceedings of the National Academy of Sciences of the United States of America*. 97(25), p.13625.

Guilliatt, R.S. 2013. *Self-assembling functionalised peptides into decellularised materials for application in small diameter vascular grafts*.

Habibi, N., Kamaly, N., Memic, A. and Shafiee, H. 2016. Self-assembled peptide-based nanostructures: Smart nanomaterials toward targeted drug delivery. *Nano Today*. 11(1), pp.41–60.

Hadjipanayi, E., Kuhn, P.H., Moog, P., Bauer, A.T., Kuekrek, H., Mirzoyan, L., Hummel, A., Kirchhoff, K., Salgin, B., Isenburg, S., Dornseifer, U., Ninkovic, M., Machens, H.G. and Schilling, A.F. 2015. The fibrin matrix regulates angiogenic responses within the hemostatic microenvironment through biochemical control. *PLoS ONE*. 10(8).

Harding, A., Cortez-Toledo, E., Magner, N.L., Beegle, J.R., Coleal-Bergum, D.P., Hao, D., Wang, A., Nolta, J.A. and Zhou, P. 2017. Highly Efficient Differentiation of Endothelial Cells from Pluripotent Stem Cells Requires the MAPK and the PI3K Pathways. *Stem Cells*. 35(4), pp.909–919.

Hayashi, T., Tokihiro, T., Kurihara, H. and Yasuda, K. 2017. Community effect of cardiomyocytes in beating rhythms is determined by stable cells. *Scientific Reports 2017 7:1*. 7(1), pp.1–9.

He, Y.J., Young, D.A., Mededovic, M., Li, K., Li, C., Tichauer, K., Venerus, D. and Papavasiliou, G. 2018. Protease-Sensitive Hydrogel Biomaterials with Tunable Modulus and Adhesion Ligand Gradients for 3D Vascular Sprouting. *Biomacromolecules*. 19(11), pp.4168–4181.

Hellström, M., Phng, L.K., Hofmann, J.J., Wallgard, E., Coultas, L., Lindblom, P., Alva, J., Nilsson, A.K., Karlsson, L., Gaiano, N., Yoon, K., Rossant, J., Iruela-Arispe, M.L., Kalén, M., Gerhardt, H. and Betsholtz, C. 2007. Dll4 signalling through Notch1 regulates formation of tip cells during angiogenesis. *Nature*. 445(7129), pp.776–780.

Herrmann, M., Hildebrand, M., Menzel, U., Fahy, N., Alini, M., Lang, S., Benneker, L., Verrier, S., Stoddart, M.J. and Bara, J.J. 2019. Phenotypic Characterization of Bone Marrow Mononuclear Cells and Derived Stromal Cell Populations from Human Iliac Crest, Vertebral Body and Femoral Head. *International Journal of Molecular Sciences*. 20(14), p.3454.

Hilkens, P., Fanton, Y., Martens, W., Gervois, P., Struys, T., Politis, C., Lambrichts, I. and Bronckaers, A. 2014. Pro-angiogenic impact of dental stem cells in vitro and in vivo. *Stem Cell Research*. 12(3), pp.778–790.

Hu, P., Zhang, W., Xin, H. and Deng, G. 2016. Single cell isolation and analysis. *Frontiers in Cell and Developmental Biology*. 4(OCT), p.212316.

Hu, R., Zong, C., Lin, L. xiang, Wei, T., Cheng, Q., Jiang, Y. xia, Lin, C. jian, Ren, B. and Tian, Z. qun 2020. Facile Chemical Analysis of Live Cell Activities by Fourier Transform Infrared (FTIR) Spectroscopy in the Transmission Mode. *Vibrational Spectroscopy*. 109, p.103068.

Huang, R., Wang, Y., Qi, W., Su, R. and He, Z. 2014. Temperature-induced reversible self-assembly of diphenylalanine peptide and the structural transition from organogel to crystalline nanowires. *Nanoscale Research Letters*. 9(1), p.653.

Huppert, S.S., Le, A., Schroeter, E.H., Mumm, J.S., Saxena, M.T., Milner, L.A. and Kopan, R. 2000. Embryonic lethality in mice homozygous for a processing-deficient allele of Notch1. *Nature*. 405(6789), pp.966–970.

Iqbal, M.Z., Riaz, M., Biedermann, T. and Klar, A.S. 2024. Breathing new life into tissue engineering: exploring cutting-edge vascularization strategies for skin substitutes. *Angiogenesis 2024*., pp.1–35.

Jaffe, E.A., Nachman, R.L., Becker, C.G. and Minick, C.R. 1973. Culture of Human Endothelial Cells Derived from Umbilical Veins. IDENTIFICATION BY MORPHOLOGIC AND IMMUNOLOGIC CRITERIA. *Journal of Clinical Investigation*. 52(11), p.2745.

Jakobsson, L., Franco, C.A., Bentley, K., Collins, R.T., Ponsioen, B., Aspalter, I.M., Rosewell, I., Busse, M., Thurston, G., Medvinsky, A., Schulte-Merker, S. and Gerhardt, H. 2010. Endothelial cells dynamically compete for the tip cell position during angiogenic sprouting. *Nature cell biology*. 12(10), pp.943–953.

Jammalamadaka, U. and Tappa, K. 2018. Recent Advances in Biomaterials for 3D Printing and Tissue Engineering. *Journal of Functional Biomaterials 2018, Vol. 9, Page 22*. 9(1), p.22.

Janebodin, K., Chavanachat, R., Hays, A. and Reyes Gil, M. 2021. Silencing VEGFR-2 Hampers Odontoblastic Differentiation of Dental Pulp Stem Cells. *Frontiers in Cell and Developmental Biology*. 9, p.665886.

Janebodin, K., Zeng, Y., Buranaphatthana, W., Ieronimakis, N. and Reyes, M. 2013. VEGFR2-dependent angiogenic capacity of pericyte-like dental pulp stem cells. *Journal of Dental Research*. 92(6), pp.524–531.

Janeczek Portalska, K., Leferink, A., Groen, N., Fernandes, H., Moroni, L., van Blitterswijk, C. and de Boer, J. 2012. Endothelial Differentiation of Mesenchymal Stromal Cells. *PLOS ONE*. 7(10), p.e46842.

Jang, J.W., Min, K.E., Kim, C., Shin, J., Lee, J. and Yi, S. 2023. Review: Scaffold Characteristics, Fabrication Methods, and Biomaterials for the Bone Tissue Engineering. *International Journal of Precision Engineering and Manufacturing 2023 24:3*. 24(3), pp.511–529.

Janmey, P.A., Winer, J.P. and Weisel, J.W. 2009. Fibrin gels and their clinical and bioengineering applications. *Journal of the Royal Society Interface*. 6(30), pp.1–10.

Joensuu, K., Uusitalo, L., Alm, J.J., Aro, H.T., Hentunen, T.A. and Heino, T.J. 2015. Enhanced osteoblastic differentiation and bone formation in co-culture of human bone marrow mesenchymal stromal cells and peripheral blood mononuclear cells with exogenous VEGF. *Orthopaedics & Traumatology: Surgery & Research*. 101(3), pp.381–386.

Ju, H.J., Ji, Y.B., Kim, S., Yun, H.W., Kim, J.H., Min, B.H. and Kim, M.S. 2023. Development and In Vivo Assessment of an Injectable Cross-Linked Cartilage Acellular Matrix-PEG Hydrogel Scaffold Derived from Porcine Cartilage for Tissue Engineering. *Macromolecular bioscience*. 23(6).

Juliar, B.A., Keating, M.T., Kong, Y.P., Botvinick, E.L. and Putnam, A.J. 2018. Sprouting angiogenesis induces significant mechanical heterogeneities and ECM stiffening across length scales in fibrin hydrogels. *Biomaterials*. 162, pp.99–108.

Kaklamani, G., Cheneler, D., Grover, L.M., Adams, M.J. and Bowen, J. 2014. Mechanical properties of alginate hydrogels manufactured using external gelation. *Journal of the mechanical behavior of biomedical materials*. 36, pp.135–142.

Kane, K.I.W., Lucumi Moreno, E., Lehr, C.M., Hachi, S., Dannert, R., Sanctuary, R., Wagner, C., Fleming, R.M.T. and Baller, J. 2018. Determination of the rheological properties of Matrigel for optimum seeding conditions in microfluidic cell cultures. *AIP Advances*. 8(12), p.125332.

Kang, S. Do, Carlon, T.A., Jantzen, A.E., Lin, F.H., Ley, M.M., Allen, J.D., Stabler, T. V., Haley, N.R., Truskey, G.A. and Achneck, H.E. 2013. Isolation of Functional Human Endothelial Cells from Small Volumes of Umbilical Cord Blood. *Annals of biomedical engineering*. 41(10), pp.2181–2192.

Karali, E., Bellou, S., Stellas, D., Klinakis, A., Murphy, C. and Fotsis, T. 2014. VEGF Signals through ATF6 and PERK to Promote Endothelial Cell Survival and Angiogenesis in the Absence of ER Stress. *Molecular Cell*. 54(4), pp.559–572.

Kaully, T., Kaufman-Francis, K., Lesman, A. and Levenberg, S. 2009. Vascularization—The Conduit to Viable Engineered Tissues. *https://home.liebertpub.com/teb*. 15(2), pp.159–169.

Keeper, J.H., Kibbe, L.J., Thakkar-Samtani, M., Heaton, L.J., Desrosiers, C., Vela, K., Amaechi, B.T., Jablonski-Momeni, A., Young, D.A., MacLean, J., Weyant, R.J., Zandona, A.F., Sohn, W., Pitts, N. and Frantsve-Hawley, J. 2023. Systematic review and meta-analysis on the effect of self-assembling peptide P11-4 on arrest, cavitation, and progression of initial caries lesions. *The Journal of the American Dental Association*. 154(7), pp.580-591.e11.

Kim, S., Kang, G.H., Lim, K.M., Shin, Y., Song, K., Park, S., An, J., Kim, D.Y., Shin, H.C. and Cho, S.G. 2023. Thermostable Human Basic Fibroblast Growth Factor (TS-bFGF) Engineered with a Disulfide Bond Demonstrates Superior Culture Outcomes in Human Pluripotent Stem Cell. *Biology*. 12(6).

Kinnaird, T., Stabile, E., Burnett, M.S., Lee, C.W., Barr, S., Fuchs, S. and Epstein, S.E. 2004. Marrow-derived stromal cells express genes encoding a broad spectrum of arteriogenic cytokines and promote in vitro and in vivo arteriogenesis through paracrine mechanisms. *Circulation research*. 94(5), pp.678–685.

Koch, F., Müller, M., König, F., Meyer, N., Gattlen, J., Pieles, U., Peters, K., Kreikemeyer, B., Mathes, S. and Saxer, S. 2018. Mechanical characteristics

of beta sheet-forming peptide hydrogels are dependent on peptide sequence, concentration and buffer composition. *Royal Society Open Science*. 5(3).

Koch, F., Wolff, A., Mathes, S., Pieles, U., Saxer, S.S., Kreikemeyer, B. and Peters, K. 2018a. Amino acid composition of nanofibrillar self-assembling peptide hydrogels affects responses of periodontal tissue cells in vitro. *International Journal of Nanomedicine*. 13, p.6717.

Koch, F., Wolff, A., Mathes, S., Pieles, U., Saxer, S.S., Kreikemeyer, B. and Peters, K. 2018b. Amino acid composition of nanofibrillar self-assembling peptide hydrogels affects responses of periodontal tissue cells in vitro. *International Journal of Nanomedicine*. 13, p.6717.

Kopczyńska, E. and Makarewicz, R. 2012. Endoglin – a marker of vascular endothelial cell proliferation in cancer. *Contemporary Oncology*. 16(1), p.68.

Kowalczyk, A., Tulloh, R. and McKeown-Longo, P. 1990. Polarized Fibronectin Secretion and Localized Matrix Assembly Sites Correlate With Subendothelial Matrix Formation. *Blood*. 75(12), pp.2335–2342.

Kristoffersen, K.A., van Amerongen, A., Böcker, U., Lindberg, D., Wubshet, S.G., de Vogel-van den Bosch, H., Horn, S.J. and Afseth, N.K. 2020. Fourier-transform infrared spectroscopy for monitoring proteolytic reactions using dry-films treated with trifluoroacetic acid. *Scientific Reports*. 10(1).

Kumar, S., Sarma, P., Kaur, Hardeep, Prajapat, M., Bhattacharyya, A., Avti, P., Sehkhar, N., Kaur, Harpinder, Bansal, S., Mahendiratta, S., Mahalmani, V.M., Singh, H., Prakash, A., Kuhad, A. and Medhi, B. 2021. Clinically relevant cell culture models and their significance in isolation, pathogenesis, vaccine development, repurposing and screening of new drugs for SARS-CoV-2: a systematic review. *Tissue & cell*. 70.

Kuo, K.C., Lin, R.Z., Tien, H.W., Wu, P.Y., Li, Y.C., Melero-Martin, J.M. and Chen, Y.C. 2015. Bioengineering vascularized tissue constructs using an injectable cell-laden enzymatically crosslinked collagen hydrogel derived from dermal extracellular matrix. *Acta biomaterialia*. 27, pp.151–166.

Leconte, I., Fox, J.C., Scott Baldwin, H., Buck, C.A. and Swain, J.L. 1998. Adenoviral-Mediated Expression of Antisense RNA to Fibroblast Growth Factors Disrupts Murine Vascular Development. . 213, pp.421–430.

Lee, H.Y. and Hong, I.S. 2017. Double-edged sword of mesenchymal stem cells: Cancer-promoting versus therapeutic potential. *Cancer Science*. 108(10), p.1939.

Lee, J.H. and Kim, H.W. 2018. Emerging properties of hydrogels in tissue engineering. *Journal of Tissue Engineering*. 9.

Li, H., Shang, Y., Zeng, J. and Matsusaki, M. 2024. Technology for the formation of engineered microvascular network models and their biomedical applications. *Nano Convergence 2024 11:1*. 11(1), pp.1–20.

Lim, D.S., Jackson, J.D., Atala, A. and Yoo, J.J. 2022. Leading Approaches to Vascularize Kidney Constructs in Tissue Engineering. *Engineering*. 19, pp.117–127.

Liu, C., Tsai, A.L., Li, P.C., Huang, C.W. and Wu, C.C. 2017. Endothelial differentiation of bone marrow mesenchyme stem cells applicable to hypoxia and increased migration through Akt and NFκB signals. *Stem Cell Research and Therapy*. 8(1), pp.1–11.

Liu, R. and Hudalla, G.A. 2019. Using self-assembling peptides to integrate biomolecules into functional supramolecular biomaterials. *Molecules*. 24(8).

Liu, S., Yang, W., Li, Y. and Sun, C. 2023. Fetal bovine serum, an important factor affecting the reproducibility of cell experiments. *Scientific Reports 2023 13:1*. 13(1), pp.1–8.

Liu, W., Gong, Q., Ling, J., Zhang, W., Liu, Z. and Quan, J. 2014. Role of miR-424 on angiogenic potential in human dental pulp cells. *Journal of endodontics*. 40(1), pp.76–82.

Liu, X., Xia, F., Wu, X., Tang, Y., Wang, L., Sun, Q., Xue, M., Chang, W., Liu, L., Guo, F., Yang, Y. and Qiu, H. 2021. Isolation of Primary Mouse Pulmonary Microvascular Endothelial Cells and Generation of an Immortalized Cell Line to Obtain Sufficient Extracellular Vesicles. *Frontiers in Immunology*. 12, p.759176.

Lobov, I.B., Renard, R.A., Papadopoulos, N., Gale, N.W., Thurston, G., Yancopoulos, G.D. and Wiegand, S.J. 2007. Delta-like ligand 4 (Dll4) is induced by VEGF as a negative regulator of angiogenic sprouting. *Proceedings of the National Academy of Sciences of the United States of America*. 104(9), p.3219.

Lu, J. and Wang, X. 2018. Biomimetic self-assembling peptide hydrogels for tissue engineering applications *In*: *Advances in Experimental Medicine and Biology* [Online]. Springer New York LLC, pp.297–312. [Accessed 29 June 2020]. Available from: https://pubmed.ncbi.nlm.nih.gov/30471040/.

Luo, X., Feng, W., Huang, S., Miao, S., Jiang, T., Lei, Q., Yin, J., Zhang, S., Bai, X., Hao, C., Li, W. and Ma, D. 2023. Odontoblasts release exosomes to regulate the odontoblastic differentiation of dental pulp stem cells. *Stem Cell Research and Therapy*. 14(1), pp.1–16.

Luzuriaga, J., Irurzun, J., Irastorza, I., Unda, F., Ibarretxe, G. and Pineda, J.R. 2020. Vasculogenesis from Human Dental Pulp Stem Cells Grown in Matrigel with Fully Defined Serum-Free Culture Media. *Biomedicines*. 8(11), pp.1–19.

Luzuriaga, J., Pastor-Alonso, O., Encinas, J.M., Unda, F., Ibarretxe, G. and Pineda, J.R. 2019. Human dental pulp stem cells grown in neurogenic media differentiate into endothelial cells and promote neovasculogenesis in the mouse brain. *Frontiers in Physiology*. 10.

Luzuriaga, J., Polo, Y., Pastor-alonso, O., Pardo-rodríguez, B., Larrañaga, A., Unda, F., Sarasua, J.R., Pineda, J.R. and Ibarretxe, G. 2021. Advances and Perspectives in Dental Pulp Stem Cell Based Neuroregeneration Therapies. *International Journal of Molecular Sciences*. 22(7).

Maity, J., Barthels, D., Sarkar, J., Prateeksha, P., Deb, M., Rolph, D. and Das, H. 2022. Ferutinin induces osteoblast differentiation of DPSCs via induction of KLF2 and autophagy/mitophagy. *Cell Death & Disease 2022 13:5*. 13(5), pp.1–12.

Marchionni, C., Bonsi, L., Alviano, F., Lanzoni, G., Di Tullio, A., Costa, R., Montanari, M., Tazzari, P.L., Ricci, F., Pasquinelli, G., Orrico, C., Grossi, A., Prati, C. and Bagnara, G.P. 2009. Angiogenic Potential of Human Dental Pulp Stromal (STEM) Cells. *http://dx.doi.org/10.1177/039463200902200315*. 22(3), pp.699–706.

Marion, N.W. and Mao, J.J. 2006. Mesenchymal Stem Cells and Tissue Engineering. *Methods in enzymology*. 420, p.339.

Matsumura-Kawashima, M., Ogata, K., Moriyama, M., Murakami, Y., Kawado, T. and Nakamura, S. 2021a. Secreted factors from dental pulp stem cells improve Sjögren's syndrome via regulatory T cell-mediated immunosuppression. *Stem Cell Research and Therapy*. 12(1), pp.1–16.

Matsumura-Kawashima, M., Ogata, K., Moriyama, M., Murakami, Y., Kawado, T. and Nakamura, S. 2021b. Secreted factors from dental pulp stem cells improve Sjögren's syndrome via regulatory T cell-mediated immunosuppression. *Stem Cell Research & Therapy*. 12(1).

Maude, S., Miles, D.E., Felton, S.H., Ingram, J., Carrick, L.M., Wilcox, R.K., Ingham, E. and Aggeli, A. 2011. De novo designed positively charged tape-

forming peptides: self-assembly and gelation in physiological solutions and their evaluation as 3D matrices for cell growth. *Soft Matter*. 7(18), pp.8085–8099.

Medina, R.J., O'neill, C.L., O'doherty, T.M., Chambers, S.E.J., Guduric-Fuchs, J., Neisen, J., Waugh, D.J., Simpson, D.A. and Stitt, A.W. 2013. Ex vivo expansion of human outgrowth endothelial cells leads to IL-8-mediated replicative senescence and impaired vasoreparative function. *Stem cells (Dayton, Ohio)*. 31(8), pp.1657–1668.

Mentzer, S.J. and Konerding, M.A. 2014. Intussusceptive Angiogenesis: Expansion and Remodeling of Microvascular Networks. *Angiogenesis*. 17(3), p.499.

Miller, E.J. and Lappin, S.L. 2022. Physiology, Cellular Receptor. *StatPearls*.

Mirzapour-Shafiyi, F., Kametani, Y., Hikita, T., Hasegawa, Y. and Nakayama, M. 2021. Numerical evaluation reveals the effect of branching morphology on vessel transport properties during angiogenesis. *PLOS Computational Biology*. 17(6), p.e1008398.

Mourant, J.R., Yamada, Y.R., Carpenter, S., Dominique, L.R. and Freyer, J.P. 2003. FTIR Spectroscopy Demonstrates Biochemical Differences in Mammalian Cell Cultures at Different Growth Stages. *Biophysical Journal*. 85(3), p.1938.

Mühleder, S., Pill, K., Schaupper, M., Labuda, K., Priglinger, E., Hofbauer, P., Charwat, V., Marx, U., Redl, H. and Holnthoner, W. 2018. The role of fibrinolysis inhibition in engineered vascular networks derived from endothelial cells and adipose-derived stem cells. *Stem Cell Research and Therapy*. 9(1).

Naito, H., Iba, T. and Takakura, N. 2020. Mechanisms of new blood-vessel formation and proliferative heterogeneity of endothelial cells. *International Immunology*. 32(5), pp.295–305.

Naomi, R., Ridzuan, P.M. and Bahari, H. 2021. Current Insights into Collagen Type I. *Polymers*. 13(16).

Ng, H.L., Quail, E., Cruickshank, M.N. and Ulgiati, D. 2021. To Be, or Notch to Be: Mediating Cell Fate from Embryogenesis to Lymphopoiesis. *Biomolecules*. 11(6).

Nicodemus, G.D. and Bryant, S.J. 2008. Cell Encapsulation in Biodegradable Hydrogels for Tissue Engineering Applications. *https://home.liebertpub.com/teb*. 14(2), pp.149–165.

Ning, H., Liu, G., Lin, G., Yang, R., Lue, T.F. and Lin, C.S. 2009. Fibroblast Growth Factor 2 Promotes Endothelial Differentiation of Adipose Tissue-Derived Stem Cells. *The journal of sexual medicine*. 6(4), p.967.

Oswald, J., Boxberger, S., Joergensen, B., Bornhaeuser, M., Ehninger, G. and Werner, C. 2004. Mesenchymal stem cells can be differentiated into endothelial cells in vitro. *Stem cells (Dayton, Ohio)*. 22(3), p.506.

Patel, J.M., Wise, B.C., Bonnevie, E.D. and Mauck, R.L. 2019. A Systematic Review and Guide to Mechanical Testing for Articular Cartilage Tissue Engineering. *Tissue Engineering. Part C, Methods*. 25(10), p.593.

Pien, N., Pezzoli, D., Van Hoorick, J., Copes, F., Vansteenland, M., Albu, M., De Meulenaer, B., Mantovani, D., Van Vlierberghe, S. and Dubruel, P. 2021. Development of photo-crosslinkable collagen hydrogel building blocks for vascular tissue engineering applications: A superior alternative to methacrylated gelatin? *Materials Science and Engineering: C*. 130, p.112460.

Pilipchuk, S.P., Vaicik, M.K., Larson, J.C., Gazyakan, E., Cheng, M.H. and Brey, E.M. 2013. Influence of crosslinking on the stiffness and degradation of dermis-derived hydrogels. *Journal of Biomedical Materials Research Part A*. 101(10), pp.2883–2895.

Pita-López, M.L., Fletes-Vargas, G., Espinosa-Andrews, H. and Rodríguez-Rodríguez, R. 2021. Physically cross-linked chitosan-based hydrogels for tissue engineering applications: A state-of-the-art review. *European Polymer Journal*. 145, p.110176.

Pyšná, A., Bém, R., Němcová, A., Fejfarová, V., Jirkovská, A., Hazdrová, J., Jude, E.B. and Dubský, M. 2019. Endothelial Progenitor Cells Biology in Diabetes Mellitus and Peripheral Arterial Disease and their Therapeutic Potential. *Stem cell reviews and reports*. 15(2), pp.157–165.

Qian, C., Xin, T., Xiao, W., Zhu, H., Zhang, Q., Liu, L., Cheng, R., Wang, Z., Cui, W. and Ge, Z. 2020. Vascularized silk electrospun fiber for promoting oral mucosa regeneration. *NPG Asia Materials 2020 12:1*. 12(1), pp.1–16.

Qin, M., Guan, X., Wang, H., Zhang, Y., Shen, B., Zhang, Q., Dai, W., Ma, Y. and Jiang, Y. 2017. An effective ex-vivo approach for inducing endothelial progenitor cells from umbilical cord blood CD34+ cells. *Stem Cell Research and Therapy*. 8(1), pp.1–10.

Quirici, N., Soligo, D., Caneva, L., Servida, F., Bossolasco, P. and Deliliers, G.L. 2001. Differentiation and expansion of endothelial cells from human bone marrow CD133(+) cells. *British journal of haematology*. 115(1), pp.186–194.

Rademakers, T., Horvath, J.M., van Blitterswijk, C.A. and LaPointe, V.L.S. 2019. Oxygen and nutrient delivery in tissue engineering: Approaches to graft vascularization. *Journal of Tissue Engineering and Regenerative Medicine*. 13(10), p.1815.

Ramirez-Labrada, A., Santiago, L., Pesini, C., Arrieta, M., Arias, M., Calvo Pérez, A., Ciulla, M.G., Forouharshad, M., Pardo, J., Gálvez, E.M. and Gelain, F. 2024. Multiparametric in vitro and in vivo analysis of the safety profile of self-assembling peptides. *Scientific Reports 2024 14:1*. 14(1), pp.1–19.

Ramli, H., Zainal, N.F.A., Hess, M. and Chan, C.H. 2022. Basic principle and good practices of rheology for polymers for teachers and beginners. *Chemistry Teacher International*. 4(4), pp.307–326.

Re, F., Zanetti, A., Sironi, M., Polentarutti, N., Lanfrancone, L., Dejana, E. and Colotta, F. 1994. Inhibition of anchorage-dependent cell spreading triggers apoptosis in cultured human endothelial cells. *The Journal of Cell Biology*. 127(2), p.537.

Ream, M.W., Randolph, L.N., Jiang, Y., Chang, Y., Bao, X. and Lian, X.L. 2024. Direct programming of human pluripotent stem cells into endothelial progenitors with SOX17 and FGF2. *Stem Cell Reports*. 19(4), pp.579–595.

Ribatti, D. and Crivellato, E. 2012. “Sprouting angiogenesis”, a reappraisal. *Developmental Biology*. 372(2), pp.157–165.

Ricard-Blum, S. 2011. The Collagen Family. *Cold Spring Harbor Perspectives in Biology*. 3(1), pp.1–19.

Rodrigues, M., Griffith, L.G. and Wells, A. 2010. Growth factor regulation of proliferation and survival of multipotential stromal cells. *Stem Cell Research and Therapy*. 1(4), pp.1–12.

Rouwkema, J. and Khademhosseini, A. 2016. Vascularization and Angiogenesis in Tissue Engineering: Beyond Creating Static Networks. *Trends in Biotechnology*. 34(9), pp.733–745.

Ruijtenberg, S. and van den Heuvel, S. 2016. Coordinating cell proliferation and differentiation: Antagonism between cell cycle regulators and cell type-specific gene expression. *Cell Cycle*. 15(2), p.196.

Rýglová, Š., Braun, M., Suchý, T., Hříbal, M., Žaloudková, M. and Vištějnová, L. 2023. The investigation of batch-to-batch variabilities in the composition of isolates from fish and mammalian species using different protocols. *Food Research International*. 169, p.112798.

Sacchi, V., Mittermayr, R., Hartinger, J., Martino, M.M., Lorentz, K.M., Wolbank, S., Hofmann, A., Largo, R.A., Marschall, J.S., Groppa, E., Gianni-Barrera, R., Ehrbar, M., Hubbell, J.A., Redl, H. and Banfi, A. 2014. Long-lasting fibrin matrices ensure stable and functional angiogenesis by highly tunable, sustained delivery of recombinant VEGF164. *Proceedings of the National Academy of Sciences of the United States of America*. 111(19), pp.6952–6957.

Saha, S., Yang, X.B., Wijayathunga, N., Harris, S., Feichtinger, G.A., Davies, R.P.W. and Kirkham, J. 2019. A biomimetic self-assembling peptide promotes bone regeneration in vivo: A rat cranial defect study. *Bone*. 127, pp.602–611.

Sakai, V.T., Zhang, Z., Dong, Z., Neiva, K.G., MacHado, M.A.A.M., Shi, S., Santos, C.F. and Nör, J.E. 2010. SHED differentiate into functional odontoblasts and endothelium. *Journal of dental research*. 89(8), pp.791–796.

Salerno, A., Ronca, A., Abbadessa, A., Eom, Y.-S., Park, J.-H. and Kim, T.-H. 2023. Recent Advances in Stem Cell Differentiation Control Using Drug Delivery Systems Based on Porous Functional Materials. *Journal of Functional Biomaterials 2023, Vol. 14, Page 483*. 14(9), p.483.

Salvador-Clavell, R., Martín De Llano, J.J., Milián, L., Oliver, M., Mata, M., Carda, C. and Sancho-Tello, M. 2021. Chondrogenic Potential of Human Dental Pulp Stem Cells Cultured as Microtissues. *Stem Cells International*. 2021.

Samanta, D., Prabhakar, N.R. and Semenza, G.L. 2017. Systems Biology of Oxygen Homeostasis. *Wiley interdisciplinary reviews. Systems biology and medicine*. 9(4).

Sanderson, J.B. and Hospital, J.R. 2002. Phase Contrast Microscopy.

Santhini, E., Parthasarathy, R., Shalini, M., Dhivya, S., Mary, L.A. and Padma, V.V. 2022. Bio inspired growth factor loaded self assembling peptide nano hydrogel for chronic wound healing. *International Journal of Biological Macromolecules*. 197, pp.77–87.

Sanz-Horta, R., Matesanz, A., Gallardo, A., Reinecke, H., Jorcano, J.L., Acedo, P., Velasco, D. and Elvira, C. 2023. Technological advances in fibrin for tissue engineering. *Journal of Tissue Engineering*. 14.

Schmittgen, T.D. and Livak, K.J. 2008. Analyzing real-time PCR data by the comparative CT method. *Nature Protocols 2008 3:6*. 3(6), pp.1101–1108.

Schofield, C.J. and Ratcliffe, P.J. 2005. Signalling hypoxia by HIF hydroxylases. *Biochemical and Biophysical Research Communications*. 338(1), pp.617–626.

Schulz, C., Krüger-Genge, A., Lendlein, A., Küpper, J.H. and Jung, F. 2021. Potential Effects of Nonadherent on Adherent Human Umbilical Venous Endothelial Cells in Cell Culture. *International Journal of Molecular Sciences*. 22(3), pp.1–17.

Schweller, R.M., Wu, Z.J., Klitzman, B. and West, J.L. 2017. Stiffness of Protease Sensitive and Cell Adhesive PEG Hydrogels Promotes Neovascularization In Vivo. *Annals of Biomedical Engineering*. 45(6), pp.1387–1398.

Semenza, G.L. 2022. Breakthrough science: hypoxia-inducible factors, oxygen sensing, and disorders of hematopoiesis. *Blood*. 139(16), pp.2441–2449.

Semenza, G.L. 2012. Hypoxia-Inducible Factors in Physiology and Medicine. *Cell*. 148(3), p.399.

Shahin, H., Elmasry, M., Steinvall, I., Söberg, F. and El-Serafi, A. 2020. Vascularization is the next challenge for skin tissue engineering as a solution for burn management. *Burns & Trauma*. 8, p.22.

Shao, H. and Sun, Z. 2024. The recent development of silk fibroin in angiogenesis. *Polymer Bulletin*. 81(5), pp.3759–3779.

Shaya, O., Binshtok, U., Hersch, M., Rivkin, D., Weinreb, S., Amir-Zilberstein, L., Khamaisi, B., Oppenheim, O., Desai, R.A., Goodyear, R.J., Richardson, G.P., Chen, C.S. and Sprinzak, D. 2017. Cell-cell contact area affects Notch signaling and Notch-dependent patterning. *Developmental cell*. 40(5), p.505.

Shi, W., Que, Y., Zhang, X., Bian, L., Yu, X., Tang, X., Yang, G., Dai, Y., Bi, S., Lv, D., Weng, Y., Wu, W., Zhang, Z., Lu, X. and Lu, N. 2021. Functional tissue-engineered bone-like graft made of a fibrin scaffold and TG2 gene-modified EMSCs for bone defect repair. *NPG Asia Materials 2021 13:1*. 13(1), pp.1–18.

Shibuya, M. 2006. Vascular endothelial growth factor receptor-1 (VEGFR-1/Flt-1): a dual regulator for angiogenesis. *Angiogenesis*. 9(4), pp.225–230.

Shibuya, M. 2011. Vascular Endothelial Growth Factor (VEGF) and Its Receptor (VEGFR) Signaling in Angiogenesis: A Crucial Target for Anti- and Pro-Angiogenic Therapies. *Genes & Cancer*. 2(12), p.1097.

Shibuya, M. and Claesson-Welsh, L. 2006a. Signal transduction by VEGF receptors in regulation of angiogenesis and lymphangiogenesis. *Experimental cell research*. 312(5), pp.549–560.

Shibuya, M. and Claesson-Welsh, L. 2006b. Signal transduction by VEGF receptors in regulation of angiogenesis and lymphangiogenesis. *Experimental cell research*. 312(5), pp.549–560.

Shin, M., Beane, T.J., Quillien, A., Male, I., Zhu, L.J. and Lawson, N.D. 2016. Vegfa signals through ERK to promote angiogenesis, but not artery differentiation. *Development (Cambridge, England)*. 143(20), p.3796.

Shoulders, M.D. and Raines, R.T. 2009. Collagen Structure and Stability. *Annual Review of Biochemistry*. 78(1), pp.929–958.

Simons, M., Alitalo, K., Annex, B.H., Augustin, H.G., Beam, C., Berk, B.C., Byzova, T., Carmeliet, P., Chilian, W., Cooke, J.P., Davis, G.E., Eichmann, A., Iruela-Arispe, M.L., Keshet, E., Sinusas, A.J., Ruhrberg, C., Woo, Y.J. and Dimmeler, S. 2015. State-of-the-Art Methods for Evaluation of Angiogenesis and Tissue Vascularization: A Scientific Statement From the American Heart Association. *Circulation research*. 116(11), pp.e99–e132.

Skylar-Scott, M.A., Liu, M.-C., Wu, Y. and Yanik, M.F. 2017. Multi-photon microfabrication of three-dimensional capillary-scale vascular networks. *https://doi.org/10.1117/12.2253520*. 10115, pp.71–80.

Slowey, C. and Nyhan, D. 2022. The Vascular System: Anatomical, Physiological, Pathological, and Aging Considerations. *Anesthesiology clinics*. 40(4), pp.557–574.

Sohn, S., Van Buskirk, M., Buckenmeyer, M.J., Londono, R. and Faulk, D. 2020. Whole Organ Engineering: Approaches, Challenges, and Future Directions. *Applied Sciences 2020, Vol. 10, Page 4277*. 10(12), p.4277.

Sohutskay, D.O., Puls, T.J. and Voytik-Harbin, S.L. 2020. Collagen Self-assembly: Biophysics and Biosignaling for Advanced Tissue Generation. *Studies in Mechanobiology, Tissue Engineering and Biomaterials*. 23, pp.203–245.

Song, H.H.G., Rumma, R.T., Ozaki, C.K., Edelman, E.R. and Chen, C.S. 2018. Vascular tissue engineering: progress, challenges, and clinical promise. *Cell stem cell*. 22(3), p.340.

Sounni, N.E., Paye, A., Host, L. and Noël, A. 2011. MT-MMPS as Regulators of Vessel Stability Associated with Angiogenesis. *Frontiers in Pharmacology*. 2.

Stéphanou, A., Meskaoui, G., Vailhé, B. and Tracqui, P. 2007. The rigidity in fibrin gels as a contributing factor to the dynamics of in vitro vascular cord formation. *Microvascular Research*. 73(3), pp.182–190.

Sun, G., Shen, Y.I., Kusuma, S., Fox-Talbot, K., Steenbergen, C.J. and Gerecht, S. 2011. Functional neovascularization of biodegradable dextran hydrogels with multiple angiogenic growth factors. *Biomaterials*. 32(1), pp.95–106.

Sun, J., Zheng, Q., Wu, Y., Liu, Y., Guo, X. and Wu, W. 2010. Culture of nucleus pulposus cells from intervertebral disc on self-assembling KLD-12 peptide hydrogel scaffold. *Materials Science and Engineering: C*. 30(7), pp.975–980.

Tan, Y., Huang, H., Ayers, D.C. and Song, J. 2018. Modulating Viscoelasticity, Stiffness, and Degradation of Synthetic Cellular Niches via Stoichiometric Tuning of Covalent versus Dynamic Noncovalent Cross-Linking. *ACS Central Science*. 4(8), pp.971–981.

Tran, K.A., Partyka, P.P., Jin, Y., Bouyer, J., Fischer, I. and Galie, P.A. 2020a. Vascularization of self-assembled peptide scaffolds for spinal cord injury repair. *Acta Biomaterialia*. 104, pp.76–84.

Tran, K.A., Partyka, P.P., Jin, Y., Bouyer, J., Fischer, I. and Galie, P.A. 2020b. Vascularization of self-assembled peptide scaffolds for spinal cord injury repair. *Acta Biomaterialia*. 104, pp.76–84.

Traore, M.A. and George, S.C. 2017. Tissue Engineering the Vascular Tree. *Tissue Engineering. Part B, Reviews*. 23(6), p.505.

Unemori, E.N., Ferrara, N., Bauer, E.A. and Amento, E.P. 1992. Vascular endothelial growth factor induces interstitial collagenase expression in human endothelial cells. *Journal of Cellular Physiology*. 153(3), pp.557–562.

Unemoris, E.N., Bouhana, K.S. and Werbq, Z. 1990. THE JOURNAL OF BIOLOGICAL CHEMISTRY Vectorial Secretion of Extracellular Matrix Proteins, Matrix-degrading Proteinases, and Tissue Inhibitor of Metalloproteinases by Endothelial Cells*. *Journal of Biological Chemistry*. 265(1), pp.445–451.

Vajda, J., Milojević, M., Maver, U. and Vihar, B. 2021. Microvascular Tissue Engineering—A Review. *Biomedicines*. 9(6).

Varkey, A., Venugopal, E., Sugumaran, P., Janarthanan, G., Pillai, M.M., Rajendran, S. and Bhattacharyya, A. 2015. Impact of silk fibroin-based

scaffold structures on human osteoblast MG63 cell attachment and proliferation. *International Journal of Nanomedicine*. 10(Suppl 1), p.43.

Vempati, P., Popel, A.S. and Mac Gabhann, F. 2014. Extracellular regulation of VEGF: isoforms, proteolysis, and vascular patterning. *Cytokine & growth factor reviews*. 25(1), p.1.

Wagenbrenner, M., Heinz, T., Horas, K., Jakuscheit, A., Arnholdt, J., Herrmann, M., Rudert, M., Holzapfel, B.M., Steinert, A.F. and Weißenberger, M. 2020. The human arthritic hip joint is a source of mesenchymal stromal cells (MSCs) with extensive multipotent differentiation potential. *BMC Musculoskeletal Disorders*. 21(1).

Wang, C., Li, Y., Yang, M., Zou, Y., Liu, H., Liang, Z., Yin, Y., Niu, G., Yan, Z. and Zhang, B. 2018. Efficient Differentiation of Bone Marrow Mesenchymal Stem Cells into Endothelial Cells in Vitro. *European journal of vascular and endovascular surgery : the official journal of the European Society for Vascular Surgery*. 55(2), p.257.

Wang, J.M., Chen, A.F. and Zhang, K. 2016. Isolation and Primary Culture of Mouse Aortic Endothelial Cells. *Journal of Visualized Experiments : JoVE*. 2016(118), p.52965.

Wang, N., Jin, X. and Zhu, X. 2017. Construction of biomimetic long-circulation delivery platform encapsulated by zwitterionic polymers for enhanced penetration of blood–brain barrier. *RSC Advances*. 7(34), pp.20766–20778.

Wang, X., Bove, A.M., Simone, G. and Ma, B. 2020a. Molecular Bases of VEGFR-2-Mediated Physiological Function and Pathological Role. *Frontiers in Cell and Developmental Biology*. 8, p.599281.

Wang, X., Bove, A.M., Simone, G. and Ma, B. 2020b. Molecular Bases of VEGFR-2-Mediated Physiological Function and Pathological Role. *Frontiers in Cell and Developmental Biology*. 8, p.599281.

Wang, X. and Khalil, R.A. 2018. Matrix Metalloproteinases, Vascular Remodeling, and Vascular Disease. *Advances in pharmacology (San Diego, Calif.)*. 81, p.241.

Wang, Y. and Zhao, S. 2010. Vasculogenesis and Angiogenesis of Human Placenta.

Wang, Z. 2021. Regulation of Cell Cycle Progression by Growth Factor-Induced Cell Signaling. *Cells 2021, Vol. 10, Page 3327*. 10(12), p.3327.

Warren, J.P., Culbert, M.P., Miles, D.E., Maude, S., Wilcox, R.K. and Beales, P.A. 2023. Controlling the Self-Assembly and Material Properties of β-Sheet

Peptide Hydrogels by Modulating Intermolecular Interactions. *Gels 2023, Vol. 9, Page 441*. 9(6), p.441.

Wei, H., Sundararaman, A., Dickson, E., Rennie-Campbell, L., Cross, E., Heesom, K.J. and Mellor, H. 2019. Characterization of the polarized endothelial secretome. *FASEB Journal*. 33(11), pp.12277–12287.

Wei, Z., Lei, M., Wang, Y., Xie, Y., Xie, X., Lan, D., Jia, Y., Liu, J., Ma, Y., Cheng, B., Gerecht, S. and Xu, F. 2023. Hydrogels with tunable mechanical plasticity regulate endothelial cell outgrowth in vasculogenesis and angiogenesis. *Nature Communications 2023 14:1*. 14(1), pp.1–16.

Wein, S., Schemmer, C., Al Enezy-Ulbrich, M.A., Jung, S.A., Rütten, S., Kühnel, M., Jonigk, D., Jahnen-Dechent, W., Pich, A. and Neuss, S. 2024. Fibrin-Based Hydrogels with Reactive Amphiphilic Copolymers for Mechanical Adjustments Allow for Capillary Formation in 2D and 3D Environments. *Gels 2024, Vol. 10, Page 182*. 10(3), p.182.

Weisel, J.W. and Litvinov, R.I. 2017. Fibrin Formation, Structure and Properties. *Sub-cellular biochemistry*. 82, p.405.

Wesche, J., Haglund, K. and Haugsten, E.M. 2011. Fibroblast growth factors and their receptors in cancer. *The Biochemical journal*. 437(2), pp.199–213.

Whitesides, G.M. and Boncheva, M. 2002. Beyond molecules: Self-assembly of mesoscopic and macroscopic components. *Proceedings of the National Academy of Sciences of the United States of America*. 99(8), pp.4769–4774.

Xu, J., Shen, J., Sun, Y.C., Wu, T., Sun, Y., Chai, Y., Kang, Q., Rui, B. and Li, G. 2022. In vivo prevascularization strategy enhances neovascularization of β-tricalcium phosphate scaffolds in bone regeneration. *Journal of orthopaedic translation*. 37, pp.143–151.

Xu, K. and Cleaver, O. 2011. Tubulogenesis during blood vessel formation. *Seminars in cell & developmental biology*. 22(9), p.993.

Xue, X., Hu, Y., Wang, S., Chen, X., Jiang, Y. and Su, J. 2022. Fabrication of physical and chemical crosslinked hydrogels for bone tissue engineering. *Bioactive Materials*. 12, pp.327–339.

Yamada, Y., Fichman, G. and Schneider, J.P. 2021. Serum protein adsorption modulates the toxicity of highly positively charged hydrogel surfaces. *ACS Applied Materials and Interfaces*. 13(7), pp.8006–8014.

Yamamura, N., Sudo, R., Ikeda, M. and Tanishita, K. 2007. Effects of the Mechanical Properties of Collagen Gel on the In Vitro Formation of

Microvessel Networks by Endothelial Cells. *https://home.liebertpub.com/ten*. 13(7), pp.1443–1453.

Yan, C. and Pochan, D.J. 2010. Rheological properties of peptide-based hydrogels for biomedical and other applications. *Chemical Society reviews*. 39(9), p.3528.

Yao, Z., Liu, H., Yang, M., Bai, Y., Zhang, B., Wang, C., Yan, Z., Niu, G., Zou, Y. and Li, Y. 2020. Bone marrow mesenchymal stem cell-derived endothelial cells increase capillary density and accelerate angiogenesis in mouse hindlimb ischemia model. *Stem Cell Research and Therapy*. 11(1), pp.1–11.

Yi, B., Xu, Q. and Liu, W. 2022. An overview of substrate stiffness guided cellular response and its applications in tissue regeneration. *Bioactive Materials*. 15, pp.82–102.

Yin, Z., Kanade, T. and Chen, M. 2012. Understanding the Phase Contrast Optics to Restore Artifact-free Microscopy Images for Segmentation. *Medical Image Analysis*. 16(5), p.1047.

Yokoi, H., Kinoshita, T. and Zhang, S. 2005. Dynamic reassembly of peptide RADA16 nanofiber scaffold. *Proceedings of the National Academy of Sciences of the United States of America*. 102(24), pp.8414–8419.

Yu, C., Guan, G., Glas, S., Wang, L., Li, Z. and Turng, L.S. 2021. A biomimetic basement membrane consisted of hybrid aligned nanofibers and microfibers with immobilized collagen IV and laminin for rapid endothelialization. *Bio-Design and Manufacturing*. 4(2), pp.171–189.

Yu, P., Ma, Y., Zhu, Y., Pei, J., Zheng, G., Liu, Y., Fu, K., Cai, D., Khattab, T. and Zhou, Y. 2024. Transforming growth factor-β1-loaded RADA-16 hydrogel scaffold for effective cartilage regeneration. *Colloids and Surfaces B: Biointerfaces*. 239, p.113959.

Yu, P., Wilhelm, K., Dubrac, A., Tung, J.K., Alves, T.C., Fang, J.S., Xie, Y., Zhu, J., Chen, Z., De Smet, F., Zhang, J., Jin, S.W., Sun, L., Sun, H., Kibbey, R.G., Hirschi, K.K., Hay, N., Carmeliet, P., Chittenden, T.W., Eichmann, A., Potente, M. and Simons, M. 2017. FGF-dependent metabolic control of vascular development. *Nature 2017 545:7653*. 545(7653), pp.224–228.

Yuan, X., Ruan, W., Bobrow, B., Carmeliet, P. and Eltzschig, H.K. 2023. Targeting hypoxia-inducible factors: therapeutic opportunities and challenges. *Nature Reviews Drug Discovery 2023 23:3*. 23(3), pp.175–200.

Zhang, H., Park, J., Jiang, Y. and Woodrow, K.A. 2017. Rational design of charged peptides that self-assemble into robust nanofibers as immune-functional scaffolds. *Acta Biomaterialia*. 55, pp.183–193.

Zhang, P., Moudgill, N., Hager, E., Tarola, N., Dimatteo, C., McIlhenny, S., Tulenko, T. and Dimuzio, P.J. 2011. Endothelial Differentiation of Adipose-Derived Stem Cells from Elderly Patients with Cardiovascular Disease. *Stem Cells and Development*. 20(6), p.977.

Zhao, W., Zhu, J., Hang, J. and Zeng, W. 2022. Biomaterials to promote vascularization in tissue engineering organs and ischemic fibrotic diseases. *MedComm – Biomaterials and Applications*. 1(1), p.e16.

Zhou, B., Lin, W., Long, Y., Yang, Y., Zhang, H., Wu, K. and Chu, Q. 2022. Notch signaling pathway: architecture, disease, and therapeutics. *Signal Transduction and Targeted Therapy 2022 7:1*. 7(1), pp.1–33.

Zhou, H., Li, X., Yin, Y., He, X.T., An, Y., Tian, B.M., Hong, Y.L., Wu, L.A. and Chen, F.M. 2020. The proangiogenic effects of extracellular vesicles secreted by dental pulp stem cells derived from periodontally compromised teeth. *Stem Cell Research and Therapy*. 11(1), pp.1–18.

Zhou, J. and Sun, C. 2020. SENP1/HIF-1α axis works in angiogenesis of human dental pulp stem cells. *Journal of Biochemical and Molecular Toxicology*. 34(3), p.e22436.